

รายงานวิจัยฉบับสมบูรณ์

โครงการ การปลดปล่อยน้ำหอมแบบควบคุม

โดย รศ. คร. ศุภศร วนิชเวชารุ่งเรื่อง และคณะ

### รายงานวิจัยฉบับสมบูรณ์

## โครงการ การปลดปล่อยน้ำหอมแบบควบคุม

### คณะผู้วิจัย

- 1. ศุภศร วนิชเวชารุ่งเรื่อง
- 2. อรพรรณ แสนสุขเจริญผล
- 3. วิเทศ จิวระโมไรย์กุล

### สังกัด

คณะวิทยาศาสตร์ จุฬาลงกรณ์มหาวิทยาลัย คณะวิทยาศาสตร์ จุฬาลงกรณ์มหาวิทยาลัย คณะวิทยาศาสตร์ จุฬาลงกรณ์มหาวิทยาลัย

สนับสนุนโดยสำนักงานกองทุนสนับสนุนการวิจัย

(ความเห็นในรายงานนี้เป็นของผู้วิจัย สกว. ไม่จำเป็นต้องเห็นด้วยเสมอไป)

#### กิตติกรรมประกาศ

โครงการวิจัยนี้สำเร็จลุล่วงด้วยดีด้วยทุนสนับสนุนจาก สำนักงานกองทุนสนับสนุนการวิจัย คณะผู้วิจัยงอแสดง ความงอบคุณอย่างยิ่งไว้ ณ.ที่นี้ นอกจากนี้ งานวิจัยนี้มิอาจสำเร็จได้หากไม่มีนิสิตระดับบัณฑิตศึกษาของภาควิชาเคมี สห สาขาปิโตรเคมีและพอลิเมอร์ และ สหสาขาเทคโนโลยีชีวภาพ คณะวิทยาศาสตร์ จุฬาลงกรณ์มหาวิทยาลัย ซึ่งนอกจากจะทำให้ งานสำเร็จแล้ว ยังทำให้การทำวิจัยเป็นเรื่องสนุกสำหรับทุกๆวันด้วย คณะผู้วิจัยจึงของอบคุณ นายฐาปกรณ์ ตรีอุดม นส. พิมพ์ สิริ ดีมาก นส. ปารมี จิตต์จำนง นส. พฤธินันท์ ช่างหิน นส. พรรณนิภา กฤษฎีไพบูลย์ นาย เทียนชัย ซุปวา และ นส. จิราพร สี หมอก เป็นอย่างยิ่ง

Project Code: BRG5280004

Project Title : การปลดปล่อยน้ำหอมแบบควบคุม

Investigator : รศ. ดร. ศุภศร วนิชเวชารุ่งเรื่อง สังกัด ภาควิชาเคมี คณะวิทยาศาสตร์ จุฬาลงกรณ์

มหาวิทยาลัย

E-mail Address: psupason@chula.ac.th

Project Period : 3 ปี

โครงการนี้ได้สร้างระบบปลดปล่อยน้ำหอมแบบควบคุมขึ้นมาทั้งสิ้น 5 แบบ ได้แก่ 1) แบบที่เป็น อนุพันธ์คูมาริน ซึ่งได้แก่อนุพันธ์คูมารินสองตัวที่นอกจากจะมีกลิ่นเฉพาะตัวแล้ว ยังสามารถดูดกลืนแสงยูวี เอ และปีได้ดี เสถียรต่อแสง และออกซิเจน สามารถใช้เป็นสารกรองรังสียูวีได้ด้วย 2) แบบที่เป็นอนุภาคนา โนของเอธิลเซลลูโลส ผสมกับ เมธิลเซลลูโลส 3) แบบที่เป็นอนุพันธ์ชิฟเบสของซัคซินิลไคโตซาน ซึ่งมีการ ขดตัวเป็นอนุภาคนาโนที่กระจายตัวได้ดีในน้ำ 4) แบบที่เป็นอนุภาคนาโน/ไมโครที่สามารถมีการ ปลดปล่อยที่ตอบสนองต่ออุณหภูมิ และ 5) แบบที่เป็นอนุภาคพอลิซิลเซสควิออกเซนที่นอกจากจะช่วย ควบคุมการปล่อยกลิ่นให้เป็นไปอย่างช้า ๆแล้ว ตัวอนุภาคเองยังทำหน้าที่ดูดกลืนแสงยูวีได้ดีด้วย โดยมีทั้ง แบบที่ดูดกลืนยูวี เอ และแบบที่ดูดกลืนยูวีบี

This project has led to successful fabrication of 5 fragrance controlled release platforms including:

1) fragranced cumarin derivatives that are photostable, and nonreactive to singlet oxygen. The two derivatives absorb UVA/B radiation well and therefore can be used as UV absorber, 2) Fragrance nanocontainer made from the blend of ethylcellulose and methylcellulose, 3) Shiff base derivatives of chitosan which are in the self-assembled water dispersible nanoparticles, 4) Fragrance nano/microcontainers that are thermoresponsive, and 5) polysilsesquioxane particles that not only can control the release of fragrances but also can absorb UVA or UVB radiation.

Keywords : การปลดปล่อยกลิ่น อนุภาคนาโน สารกรองรังสียูวี

## บทน้ำ

สารให้กลิ่น (fragrance) เป็นสารที่สามารถจับกับ receptor ที่ต่อมรับกลิ่นในจมูก และกระตุ้น ให้มีการส่งสันญานรับรู้กลิ่นไปที่สมอง สารให้กลิ่นมักระเหยง่าย หรือมีค่าความดันไอสูง ทำให้มัน หมดไปเร็ว หรือมีการให้กลิ่นได้ไม่ยาวนานพอ การพยายามทำให้สารให้กลิ่นสามารถให้กลิ่นได้ ยาวนานขึ้น เป็นสิ่งที่ได้รับความสนใจมานาน และยังคงมีความพยายามกันอย่างต่อเนื่อง นอกจาก ปัญหาเรื่องกลิ่นที่หมดไปเร็วแล้ว ปัญหาเรื่องความไม่เสถียรของโมเลกุลกลิ่นก็เป็นอีกเรื่องหนึ่ง โมเลกุลกลิ่นมักมีหมู่ฟังก์ชันที่ค่อนข้างว่องไวต่อปฏิกิริยาเคมี เช่น อัลดีไฮด์ คีโตน พันธะคู่ อัลกอ ฮอล์ และอื่นๆ ทำให้มันเกิดปฏิกิริยากับสารข้างเคียงได้ง่าย การได้รับแสง ความร้อน และการ กระทบกับ reactive oxygen species (ROS) จึงทำให้กลิ่นสลายตัวได้ นอกจากนี้ยังสามารถก่อให้เกิด การแพ้ที่ผิวหนังได้ด้วย อีกปัญหาหนึ่งของกลิ่นคือการที่ส่วนใหญ่กลิ่นเป็นโมเลกุลไม่ชอบน้ำ ดังนั้น การนำไปใช้โดยตรงในตัวกลางที่เป็นน้ำจึงทำไม่ได้

การแก้ปัญหาต่างๆข้างต้น แบ่งได้เป็นสองแนวทาง คือการสังเคราะห์อนุพันธ์ของกลิ่น และ การกักเก็บกลิ่นลงในตัวพา การสังเคราะห์อนุพันธ์กลิ่นหมายถึงการสร้างโมเลกุลที่สามารถ เปลี่ยนไปเป็นโมเลกุลกลิ่นได้ ภายใต้สภาวะที่ต้องการ เช่น เมื่อได้รับแสง ค่าความเป็นกรดเบสที่ เหมาะสม โดยที่โมเลกุลดังกล่าวจะมีค่าความดันไอต่ำ ดังนั้นจึงไม่ระเหยไปอย่างรวดเร็ว โดยทั่วไป เรียกอนุพันธ์กลิ่นเหล่านี้ว่า profragrances สำหรับเทคโนโลยีการกักเก็บนั้นมีหลายแบบ ได้แก่ emulsion system, solid lipid nanoparticle, host-guest complexation, coacervation with various polymers, interfacial polymerization, and in situ polymerization แต่ละแบบมีข้อดีข้อเสียต่างกันไป emulsion system มีปัญหาเรื่องความไม่เสถียร solid lipid nanoparticles นั้น แม้จะเสถียรขึ้น แต่ก็ต้อง ระวังเรื่องความร้อน ส่วน host ในกลุ่ม cyclodextrin ก็ราคาแพง และบรรจุได้จำกัด ควบคุมการเข้า ออกไม่ได้ เทคนิค coacervation นั้นได้รับความนิยมมากพอสมควร แต่ยังมีปัญหาเรื่องความจุต่ำ และการต้องใช้สารลดแรงตึงผิว และ stabilizer มากๆ ในขณะที่ระบบ interfacial polymerization นั้น มีปัญหาจากปฏิกิริยากับโมเลกุลกลิ่น หรือไม่ก็การตกค้างของตัวเร่งและมอนอเมอร์ในระบบ ส่วน ระบบ in situ polymerization นั้น การทำให้อยู่ในรูปเป็นอนุภาคเล็กๆที่มีความจุสูงโดยไม่ใช้ ตัวเร่งที่ จะไปทำให้กลิ่นมีการสลายตัวก็ยังต้องพัฒนากันต่อไป

ในโครงการวิจัยนี้ ต้องการสร้างระบบการควบคุมการปลดปล่อยกลิ่นด้วยวิธีต่างๆ ซึ่ง รวมถึงการกักเก็บกลิ่นในอนุภาคนาโนที่เหมาะสม และการสร้าง pro-fragrances ที่เหมาะสม

### การทดลอง

การทดลองในโครงการวิจัยนี้ประกอบด้วย

### 1) การสังเคราะห์อนุพันธ์คูมาริน

ด้วยคูมารินเป็นสารให้กลิ่นที่มีใช้กันมาช้านาน การสร้างอนุพันธ์คูมารินที่เสถียรขึ้น และมีสมบัติ ดูดกลืนแสงยูวีได้ด้วย น่าจะเป็นสิ่งที่น่าสนใจ ดังนั้น ในโครงการนี้จึงได้สังเคราะห์อนุพันธ์คูมาริน ขึ้นมา และทดสอบความเสถียร โดยรายละเอียดการสังเคราะห์มีอยู่ในภาคผนวก ก

### 2) การสร้างระบบนำส่งกลิ่นโดยใช้พอลิเมอร์ในกลุ่มอนุพันธ์เซลลูโลสที่มีอยู่แล้วใน ท้องตลาด

ในที่นี้เน้นการหากระบวนการกักเก็บกลิ่นให้อยู่ในรูปที่ใช้งานง่าย ให้กลิ่นยาวนาน และประยุกต์ ใช้ได้โดยไม่ติดปัญหาเรื่องสารเคมีชนิดใหม่ ดังนั้นจึงได้ทำการตรวจกรองหาพอลิเมอร์ที่เหมาะสม ที่สุด จากพอลิเมอร์ต่างๆที่มีอยู่มากมายในท้องตลาด เพื่อมาใช้เป็น wall material โดยต้องเป็นพอลิ เมอร์ที่ไม่เป็นพิษ เข้ากันได้ดีกับร่างกาย และ รับประทานได้ ซึ่งในที่สุดก็สามารถหาพอลิเมอร์ผสม ของ อนุพันธ์เซลลูโลสได้ รายละเอียดการสร้างระบบกักเก็บกลิ่นด้วยพอลิเมอร์ผสม รวมถึงการ วิเคราะห์ระบบที่ได้แสดงอยู่ในภาคผนวก ข

### 3) การสร้างระบบกักเก็บกลิ่นด้วยไคโตซาน

ด้วยใคโตซานเป็นพอลิเมอร์ที่ได้รับการยอมรับในเรื่องความปลอดภัยแล้วจากนานาประเทศ ประกอบกับประเทศไทยเองก็สามารถผลิตไคโตซานได้เอง ทำให้ผู้วิจัยต้องการสร้างระบบนำส่ง กลิ่นด้วยไคโตซานเป็นอย่างยิ่ง ดังนั้นในโครงการนี้จึงได้ทำการศึกษาถึงความสัมพันธ์ระหว่าง โครงสร้างของไคโตซานที่ถูกปรับเปลี่ยน กับ การนำไปเหนี่ยวนำเป็นอนุภาคตัวพา โดยรายละเอียด มีอยู่ในภาคผนวก ค จากนั้นยังมีการนำไคโตซานมาสร้างเป็นระบบนำส่งกลิ่นสองแบบ คือ แบบที่ เป็น double barrier คือ มีทั้งชั้นที่เป็น physical barrier จาก polymeric matrix และ ชั้นของ chemical barrier ซึ่งทำให้การปลดปล่อยกลิ่นเป็นไปได้อย่างช้าๆ (ดูรายละเอียดในภาคผนวก ง) และแบบที่ เป็น thermoresponsive fragrance carrier คือสามารถเปิดปิดการปลดปล่อยกลิ่นด้วยระดับอุณหภูมิที่ เปลี่ยนไป (ดูรายละเอียดในภาคผนวก จ)

### 4) การสร้างระบบน้ำส่งกลิ่นด้วย พอลิไวนิลแอลกอฮอล์

ในการสร้างระบบนำส่งกลิ่นด้วยพอลิไวนิลแอลกอฮอล์ นั้น การทดลองไม่สามารถกักเก็บกลิ่นได้ดี แต่อย่างไรก็ตาม สามารถทำความเข้าใจเกี่ยวกับประจุของสายพอลิเมอร์และขนาดของอนุภาคที่ เกิดขึ้นได้ โดยมีรายละเอียดแสดงไว้ในภาคผนวก ฉ

### 5) การสร้างระบบกักเก็บกลิ่นที่มีสมบัติดูดกลืนแสงยูวี

ในที่นี้ได้สร้างอนุภาคพอลิซิลซิสควิออกเซน ขึ้น 2 ชนิด คือชนิดที่ดูดกลืนแสงยูวีเอ และชนิดที่ ดูดกลืนแสงยูวีบี โดยเริ่มตั้งแต่การสังเคราะห์มอนอเมอร์ให้ได้โครงสร้างที่มี โครโมฟอร์ที่ ดูดกลืนแสงตามต้องการก่อน ไปจนถึงการทำ polymerization และกักเก็บกลิ่นลงในอนุภาคทั้ง สอง ไปจนถึงการทดสอบการปลดปล่อยกลิ่น (รายละเอียดแสดงในภาคผนวก ช)

# สรุปและวิจารณ์ผลการทดลอง

โครงการนี้ได้สร้างระบบนำส่งกลิ่นหลายแบบ ทั้งแบบที่เป็นการสังเคราะห์อนุพันธ์ (derivatization) และแบบการสร้างตัวพา (encapsulation) โดยในโครงการยังได้มีการศึกษาความสัมพันธ์ด้านโครงสร้าง พอลิเมอร์ และลักษณะการเกิดเป็นอนุภาคในระดับนาโนด้วย โดยสรุปได้ดังนี้

- อนุพันธ์คูมารินที่มีกลิ่นเฉพาะตัว และมีสมบัติคูดกลืนแสงยูวีได้ดี (ดีกว่าอนุพันธ์คูมารินที่ใช้
   อยู่ในท้องตลาด) ทั้งหมด 3 ตัว โดยผลงานส่วนนี้ตีพิมพ์ในวารสารวิจัยนานาชาติ
- อนุภาคนำส่งกลิ่นที่มีความจุสูงและทำจากพอลิเมอร์ที่รับประทานได้ โดยผลงานส่วนนี้ตีพิมพ์
   ในวารสารวิจัยนานาชาติและจดเป็นสิทธิบัตร
- อนุภาคนำส่งกลิ่นแบบ double barrier carrier ที่เริ่มต้นจากไก โตซาน ซึ่งผลงานส่วนนี้นอกจาก ตีพิมพ์ในวารสารวิจัยนานาชาติแล้ว ยังมีการจดสิทธิบัตร และถ่ายทอดเทก โน โลยีให้ ภาคเอกชนแล้ว การขยายสเกลการผลิตทำแล้ว และได้เริ่มจำหน่ายทั้งในและต่างประเทศแล้ว
- อนุภาคนำส่งกลิ่นที่เปิดปิดได้ตามอุณหภูมิ โดยผลงานนี้ตีพิมพ์ในวารสารวิจัยนานาชาติ
- อนุภาคนำส่งกลิ่นที่ดูดกลื่นแสงยูวีได้ โดยมีการตีพิมพ์ในวารสารวิจัยนานาชาติ
   รายละเอียดทั้งหมดอยู่ในภาคผนวก ก-ช

#### **Outputs:**

ผลงานตีพิมพ์ในวารสารวิจัยระดับนานาชาติ

- Jitjumnong P, Wanichwecharungruang SP and Arayachukeat S. Self-Assembly of Negatively Charged Poly(vinyl alcohol) Derivatives. 2010 Macromolecular Research, 18, 730-736.
- 2. Jivaramonaikul W, Rashatasakhon P and **Wanichwecharungruang S**, UVA absorption and photostability of coumarins. 2010 *Photochemical & Photobiological Sciences*, **9**, 1120-1125.
- 3. Deemark P, **Wanichwecharungruang S**, Nonthabenjawan R and Jornjangjun C. Controlling the morphology of self-assemble chitosan through derivatization. 2011 *J. Pol. Res.* **18**: 419.
- Kidsaneepoiboon P, Wanichwecharungruang SP, Chooppawa T, Deephum R and Panyathanmaporn T. Organic-inorganic hybrid polysilsesquioxane nanospheres as UVA/UVB absorber and fragrance carrier. 2011 J. Mater. Chem., 21, 7922-7930 (Inside front cover article).
- 5. Tree-udom T, Wanichwecharungruang SP, Seemork J and Arayachukeat S. Fragrant chitosan

- nanospheres: Controlled release systems with physical and chemical barriers. 2011 Carbohydrate Polymer **86**, 1602–1609.
- 6. Seemork J, Tree-Udom T, Wanichwecharungruang SP\*. Refillable fragrance carrier with a tunable thermal switch. 2012 Flavour and Fragrance Journal, **27**, 386-392.

#### สิทธิบัตร

- นางสาวอรพรรณ แสนสุขเจริญผล นางศุภศร วนิชเวชารุ่งเรื่อง และนางณัฐชนัญ ลีพิพัฒน์
   ไพบูลย์ สิทธิบัตรไทย เรื่อง อนุภาคนาโนและ/หรืออนุภาคไมโครสำหรับควบคุมการ
   ปลดปล่อยสารให้กลิ่น เลขที่คำขอ 0901001254 (ยื่นจดเมื่อ 20 มี.ค. 2552) เจ้าของคำขอ:
   จุฬาลงกรณ์มหาวิทยาลัย
- นางศุภศร วนิชเวชารุ่งเรื่อง และ นาย ฐาปกรณ์ ตรีอุดม สิทธิบัตรไทย เรื่อง ไคโตซานหอม เลขที่คำขอ 1001001511 (ยื่นจดเมื่อ 29 กันยายน 2553) เจ้าของคำขอ: จุฬาลงกรณ์ มหาวิทยาลัย

### การถ่ายทอดเทค โน โลยี

มีการถ่ายทอดเทคโนโลยีไคโตซานหอม ให้กับบริษัทเวท ซุปพีเรีย คอนซัลแตนท์ จำกัด ผ่านทาง สถาบันทรัพย์สินทางปัญญาของจุฬาลงกรณ์มหาวิทยาลัย

#### ภาคผนวก ก

### UVA absorption and photostability of coumarins†

Withet Jivaramonaikul, a,b Paitoon Rashatasakhon and Supason Wanichwecharungruang\*c

Received 13th March 2010, Accepted 3rd June 2010
First published as an Advance Article on the web 14th June 2010
DOI: 10.1039/c0pp00057d

Various substituted 4-methylcoumarin derivatives were synthesized in order to obtain photostable derivatives with UVA absorption property. It was found that substitution positions affected maximum absorption wavelength, whereas types of substituents, whether hydroxy or alkoxy groups, caused no significant effect. Photostability, however, was affected by both the substitution positions and the types of substituents. An acid-catalyzed mechanism through enolization coupled with pre-organization *via* hydrogen bonding between two coumarin moieties is proposed as an explanation for the different extents of the [2+2] cycloaddition (dimerization) amongst different derivatives, which results in a different photostability amongst them. Photostable coumarin derivatives with an absorption maximum in the UVA region are reported.

#### Introduction

Coumarin or benzopyrone is a secondary metabolite found naturally in plants, such as tonka bean, a tropical bean known by the French as *coumarou*. With its distinctive odor, the compound has been used as a food additive and perfume ingredient since the late 1800s. More than 1000 coumarin derivatives from 800 species of plant have been isolated.

Coumarin derivatives such as dicumarol and warfarin can act as blood thinners and have been used medically for this purpose.<sup>2,3</sup> Through a similar anticoagulant mechanism, some coumarin derivatives have been harnessed as pesticides, and chemicals for rodent control.<sup>4</sup> Other bioactivities associated with this class of compounds include antibacterial,<sup>5</sup> anticancer<sup>6</sup> and HIV-1 protease inhibitory activities.<sup>7</sup>

Coumarin derivatives can be synthesized through various methods, including Pechmann,<sup>8</sup> Perkin,<sup>9</sup> Knoevenagel,<sup>10</sup> Reformatsky,<sup>11</sup> Wittig,<sup>12</sup> and lithiation mediated reactions.<sup>13</sup> Due to their inherent photochemical characteristics, reasonable stability, good solubility and relative ease of synthesis, coumarin derivatives have been extensively investigated for electronic and photonic applications, such as fluorescence probes, charge-transfer agents, solar energy collectors and nonlinear optical materials.<sup>14,15</sup> Other applications of coumarins include sensors,<sup>16</sup> dyes and laser dyes,<sup>17–19</sup> liquid crystals,<sup>20</sup> and other functional materials. Light-related applications of coumarin are well recognized in organized media,<sup>21</sup> and solid-state.<sup>22</sup>

As cosmetic ingredients, 6-methylcoumarin is a well-known fragrance material, while 5,7-dimethoxycoumarin and 5-methoxypsoralen have been used as tanning agents.<sup>23</sup> 6,7-Dihydroxycoumarin (esculetin) and its glucoside derivative (esculin), and 4-methyl-6,7-dihydroxycoumarin also are well recognized UVA absorbers, their photooxidation and photosensitizing effect have been reported.<sup>24,25</sup> In order to find a more photostable coumarin with lower photosensitizing effect to be used as a UV absorber, the synthesis of various 4-methylcoumarin derivatives and the evaluation of their light absorption properties and photostability have been carried out and are reported in this paper. Discussion on the relationship between the chemical structure and possible use as UV filter is also included.

#### Results and discussion

Six coumarin derivatives, 7-hydroxy-4-methylcoumarin (H-7), 7-methoxy-4-methylcoumarin (M-7),7,8-dihydroxy-4methylcoumarin (H-78), 5,7-dihydroxy-4-methylcoumarin (H-57), 5,7-dimethoxy-4-methylcoumarin (M-57) and 6,7-dimethoxy-4-methylcoumarin (M-67), were successfully synthesized using the Pechmann reaction between the appropriate phenol derivatives and ethyl acetoacetate with oxalic acid as a catalyst. Two n-octyloxy substituted coumarin derivatives, 4-methyl-7octyloxycoumarin (O-7) and 4-methyl-7,8-dioctyloxycoumarin (O-78), and three 2-ethylhexyl-substituted coumarin derivatives, 7,8-di-2-ethylhexyloxy-4-methyl-coumarin (EH-78),2-ethylhexyloxy-4-methylcoumarin (EH-67) and ethylhexyloxy-4-methylcoumarin (EH-57), were synthesized by reacting H-7, H-78, H-67 or H-57 with n-octylbromide or 2-ethylhexyl bromide using potassium carbonate as a base.

Compared to the unsubstituted coumarin and also to the 4-methylcoumarin, which possess absorption maxima of 274 and 310 nm, respectively, the absorption bands of all the twelve synthesized coumarin derivatives appeared at longer wavelengths (Table 1). Both the hydroxy and the methoxy moieties are auxochrome and so their attachment to the  $\pi$ -system of the chromophore is responsible for the observed red-shift. Substitution at different positions affected the maximum absorption wavelength

<sup>&</sup>lt;sup>a</sup>Program of Petrochemical and Polymer Science, Faculty of Science, Chulalongkorn University, Bangkok, 10330, Thailand

<sup>&</sup>lt;sup>b</sup>National Center of Excellence for Petroleum, Petrochemicals, and Advanced Materials (NCEPPAM), Chulalongkorn University, Bangkok, 10330, Thailand

<sup>&</sup>lt;sup>e</sup>Department of Chemistry, Faculty of Science, Chulalongkorn University, Bangkok, 10330, Thailand. E-mail: psupason@chula.ac.th; Fax: +66 2 2541309; Tel: +66 2 2187634

<sup>†</sup> Electronic supplementary information (ESI) available: Irradiance of UVA and UVB lamps; compounds' characterization; Hyperchem 7 text file of the optimized 3D structure of the EH-67-dimer. See DOI: 10.1039/c0pp00057d

Table 1 UV absorption spectra data of the substituted coumarins in methanol

Compounds	$R_4$	$R_5$	$R_6$	$\mathbb{R}_7$	$R_8$	$\lambda_{\text{max}}/nm$	$\varepsilon/M^{\scriptscriptstyle -1}~cm^{\scriptscriptstyle -1}$
Parent coumarin	Н	Н	Н	Н	Н	274	11 300
4-Methyl-coumarin	methyl	Н	H	H	H	$310^{a}$	$Nd^b$
H-7	methyl	Н	H	hydroxy	H	322	16 300
M-7	methyl	Н	H	methoxy	H	320	15 500
O-7	methyl	Н	H	octyloxy	H	321	16 200
H-78	methyl	Н	H	hydroxy	hydroxy	322	11 800
O-78	methyl	Н	Н	octyloxy	octyloxy	318	15 000
EH-78	methyl	Н	Н	2-ethylhexyloxy	2-ethylhexyloxy	319	14 300
H-57	methyl	hydroxy	H	hydroxy	Н	322	13 300
M-57	methyl	methoxy	H	methoxy	H	318	15 800
EH-57	methyl	2-ethylhexyloxy	H	2-ethylhexyloxy	H	321	16 200
H-67	methyl	Н	hydroxy	hydroxy	H	345	12 000
M-67	methyl	Н	methoxy	methoxy	H	340	11 700
EH-67	methyl	Н	2-ethylhexyloxy	2-ethylhexyloxy	Н	345	11 600

<sup>&</sup>lt;sup>a</sup> From reference 26. <sup>b</sup> Nd = not determined.

 $(\lambda_{max})$  of the compounds. Both the hydroxyl substitution and the alkoxyl substitution gave a similar effect regarding the absorption wavelength, *e.g.*, H-7, M-7 and O-7 possessed a similar maximum absorption wavelength at 320–322 nm, whilst H-57, M-57 and EH-57 also showed a similar absorption maxima to each other at around 318–322 nm. This indicates that the gap between the ground state and the excited state of the coumarin derivatives with a small hydroxy group are similar to those with a bulky alkoxyl substituents.

Mono-substitution at position 7 and di-substitution at positions 6 and 7, with both hydroxy and alkoxy groups, resulted in very similar molar extinction coefficients (ε) for H-67, M-67 and EH-67, and likewise those for H-7, M-7 and O-7 were also similar to each other. This indicates that the big alkoxyl substituents at such positions do not alter the symmetry of the lowest unoccupied molecular orbitals (LUMO) and the highest occupied molecular orbitals (HOMO) of the molecules and so the electronic transition probabilities are not disturbed. However, for di-substitution at either positions 5 and 7 or 7 and 8, there was an approximately 20% increase in the  $\varepsilon$  value when the hydroxy group was changed to an alkoxy group, e.g., H-57 versus that of M-57, and EH-57 and H-78 versus that of O-78 and EH-78, respectively. This implies that the changes in the molecular structure affects the symmetry of the LUMO and HOMO in such a way that makes electronic transition more probable.

Therefore, it can be concluded that the reactivity of the hydroxy-substituted coumarin derivatives could be reduced, while still preserving the absorption wavelength, by replacing the reactive hydroxy group with the more inert alkoxy group. Assessment of the photostability of the 12 synthesized coumarin derivatives revealed that H-78 was the most photostable (Fig. 1). It should, however, be noted here that when the two hydroxy groups of H-78 were replaced with alkoxy groups (O-78 and EH-78) the photostability of the materials decreased. This is also true for the

5,7-disubstituted derivatives (H-57, M-57 and EH-57). However, the opposite was observed for H-7 and H-67, *i.e.*, M-7 and O-7 were more photostable than H-7, whilst M-67 and EH-67 were more photostable than H-67. Previous studies have suggested that the loss in UV absorbance was partly due to the photodimerization caused by the [2+2] cycloaddition of two coumarin molecules.<sup>27</sup> The dimer formed contributed to the observed decrease in the photostability.

The experiment also showed that all derivatives were more photostable in hexane than in methanol. To explain the solvent effect on dimerization, a plausible mechanism of photodimerization upon UV irradiation of coumarin is proposed (Fig. 2). In polar media, the keto form (I) tautomerizes into a more polar enol form (II). 28,29 The latter is then protonated and undergoes a [2+2] cycloaddition. It is likely that the dimer structure of the two enol forms (V) is more stable than that of the two keto forms (VI) because of the H-bonding between the hydroxy groups from the two coumarin moieties. H-Bonding between the two enol molecules also helps to pre-organize the two molecules to undergo the [2+2] cycloaddition. To verify this hypothesis, the 3D structure of the EH-67 dimer was optimized and calculated for the distance between the hydrogen and the oxygen from the two hydroxy groups using Hyper Chem 7. The result showed that the length was 2.465 Å, a distance within the H-bonding range (Fig. 2), thus supporting pre-organization through enolization coupled with hydrogen bonding, and explaining why dimerization of coumarin derivatives in a polar solvent (methanol) is more pronounced than that in a less polar solvent (hexane) (Fig. 3). It should be mentioned here that the configuration of the dimer is not a focus here, however, the syn head-to-head configuration depicted in Fig. 2 was the most stable configuration obtained from the optimization process. This syn head-to-head was also reported previously as the major product of photodimerization. 30,31 NMR analysis of the irradiated samples confirmed the presence of the

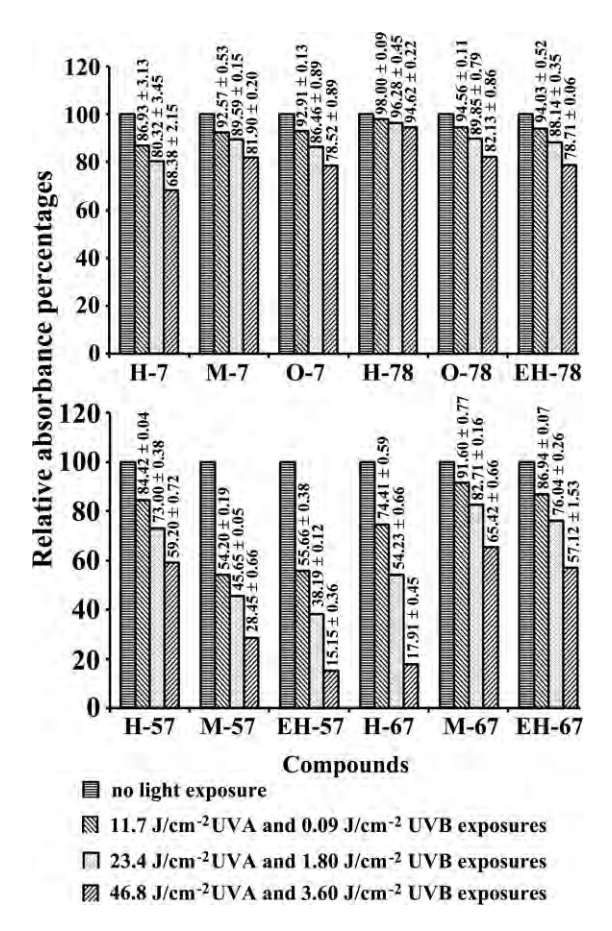
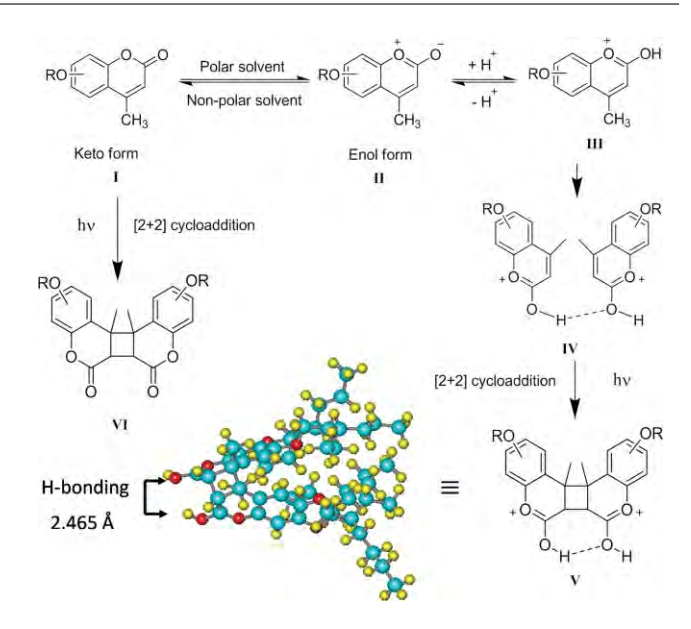


Fig. 1 Photostability of all substituted 4-methylcoumarins at a concentration of  $5.7 \times 10^{-5}$  M in methanol. The results are shown as relative absorbance percentages of samples after various exposures to broadband UVA/B.

proposed dimer (resonance peaks at 3.7–3.9 ppm). To verify the importance of the enolization step, photostability of EH-67 in neutral and in acidic media was compared. The result indicated lower photostability in acidic polar media where enolization could take place more easily (Fig. 3), thus supporting the proposed acid-catalyzed mechanism *via* the formation of a charged enol.

It should be noted here that enolization of coumarin in polar media is well known while the formation of excimer intermediate during the dimerization of coumarin was also mentioned previously.<sup>30</sup> If the concept of pre-organization proposed here is linked to the previously mentioned excimer intermediate formation, it is possible that H-bonding during the pre-organization could be between the excited intermediate and the ground state molecule.

The proposed mechanism could be used to explain the low photostability and easily dimerized characteristic of the 5,7-disubstituted coumarin derivatives (H-57, M-57 and EH-57). In this series of compounds, the protonated enol form could be well stabilized through the delocalization of the positive charge to the 5- and 7-substituents (Fig. 4). Such double stabilization shifts the tautomerization equilibrium towards the enol form. The formed enol molecules then pair up (pre-organize) through hydrogen bonding, as previously proposed, into the configuration from which the [2+2] cycloaddition could easily take place.



**Fig. 2** Proposed dimerization mechanism through an acid-catalyzed formation of a charged enol and the H-bond-assisted pre-organization. The optimized 3D structure of the dimer of EH-67 is shown, showing the close proximity between the two hydroxyl groups.

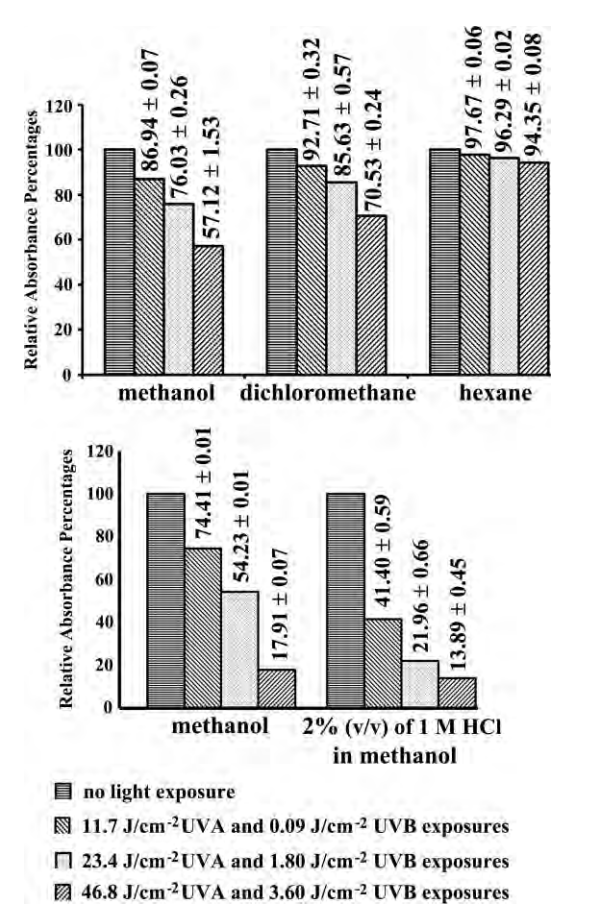


**Fig. 3** Photostability of EH-67 (at  $5.7 \times 10^{-5}$  M) in three different solvents (top) and H-67 under neutral (methanol) and acidic (2% (v/v) of 1 M HCl in methanol) conditions (bottom).

In contrast, H-78 was the most photostable compound amongst the twelve synthesized coumarin derivatives. It is likely that the

**Fig. 4** Charge stabilization of the enol form from alkoxyl substitution at the 5 and 7 positions (left) and intramolecular hydrogen bonding in 8-hydroxy substituted coumarin (right).

enolization of compound H-78 was inhibited by the intramolecular H-bonding (Fig. 4). With less enol formation, the preorganization could not take place, thus minimizing dimerization and maximizing photostability.

To better understand the excitation of the coumarin derivatives, the photostability of EH-67 was evaluated in the presence and in the absence of oxygen. The result showed only ~1% difference between the two conditions (Fig. 5), and so upon light exposure EH-67 was probably excited to the singlet excited state. Accordingly, the process involves either an insignificant amount of the triplet excited state or a very short-lived triplet state. This speculation agrees with a previous study which indicated that the initially formed excited state of coumarin and its derivatives were in a singlet state,  $^{30}$  and although the formed singlet excited state could undergo an intersystem crossing into a triplet excited state, it was reported that the quantum yield of the intersystem crossing was very low ( $\Phi_{\rm isc} \sim 0.05$  for 6-methylcoumarin in methanolic solution).  $^{31}$ 

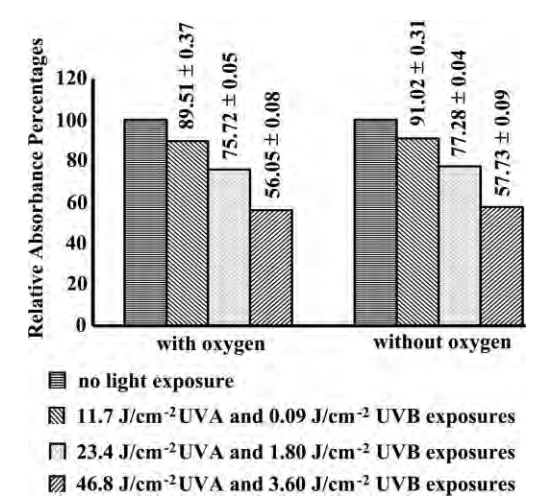


**Fig. 5** Photostability of EH-67 at a concentration of  $5.7 \times 10^{-5}$  M in methanol under air-filled (with oxygen) and nitrogen-filled (without oxygen) conditions.

Amongst the twelve synthesized coumarin derivatives, the series with substitution at positions 6 and 7 (H-67, M-67, EH-67) gives the most pronounced red-shift to the mid UVA region of around 340–345 nm, while other compounds show absorption in the far

UVA (~320 nm). As a result, M-67 and EH-67 may have a possible use as organic UVA filter. The facts that they are quite photostable, the reactive hydroxyl functionality is not present in their structures, and they are not good oxygen photosensitizers, make them more interesting for further study in their safety. In fact, here it was clearly shown that M-67 and EH-67 were significantly more photostable than H-67, a commercially used UVA filter (Fig. 1). As it is known that oxidation into orthoquinone is a problem of H-67,<sup>25</sup> replacement of the two hydroxy groups with more inert alkoxy groups should also help minimizing such reaction.

#### **Experimental**

#### Materials and instruments

3-Methoxyphenol, 3,5-dihydroxyphenol, 3,5-dimethoxyphenol, 4,5-dimethoxyphenol, 4-methylesculetin, 1-bromobutane, 1-bromooctane and 2-ethylhexyl bromide were purchased from Acros Organics (Geel, Belgium). 2,3-Dihydroxyphenol, 3-hydroxyphenol and ethyl acetoacetate were purchased from Merck (Merck AG, Darmstadt, Germany). All other chemicals were reagent grade and used without additional purification.

The <sup>1</sup>H and <sup>13</sup>C NMR analyses were performed using a Varian Mercury spectrometer, operated at 400.00 MHz for <sup>1</sup>H and 100.00 MHz for <sup>13</sup>C nuclei (Varian Company, Palo Alto, CA, USA) in CDCl<sub>3</sub>, DMSO-d<sub>6</sub> or D<sub>2</sub>O. Mass spectra were acquired on a Water Micromass Quatto micro API ESCi (Waters, MA, USA). UV absorption spectra were acquired with a UV 2500 UV-vis spectrophotometer (Shimadzu Corporation, Kyoto, Japan) using a quartz cell with a 1 cm path length. FT-IR spectra were obtained using a Nicolet Fourier transform infrared spectrophotometer, model Impact 410 (Nicolet Instruments Technologies, Inc., Madison, WI, USA). UVB (280-320 nm) and UVA (320-400 nm) were generated by a FSX24T12/UVB/HO lamp (National Biological Corporation, OH, USA) and a F24T12/BL/HO (PUVA) lamp, respectively. UVA and UVB irradiances were measured using UVA-400C and UVB-500C power meters (National Biological Corporation, OH, USA), respectively.

### Preparation of various hydroxy and methoxy substituted coumarin derivatives

The synthesis (Scheme 1) was carried out according to the method described by Kokare et al.32 In short, the phenol derivative (10 mmol), ethyl acetoacetate (10 mmol) and oxalic acid (10 mol%) were heated together at 110 °C (oil bath temperature) until a complete reaction was observed on TLC (~1-2 h). Then, the reaction was allowed to cool to room temperature (~25 °C) and poured into iced water. The precipitate was collected by filtration, washed with water and air dried. The dry product was recrystallized in absolute ethanol. Phenol derivatives used for the synthesis of 7-hydroxy-4-methylcoumarin (H-7), 7-methoxy-4-methylcoumarin (M-7), 7,8-dihydroxy-4-methylcoumarin (H-78), 5,7-dihydroxy-4-methylcoumarin (H-57), 5,7-dimethoxy-4-methylcoumarin (M-57) and 6,7dimethoxy-4-methylcoumarin (M-67), were 3-hydroxyphenol, 3-methoxyphenol, 2,3-dihydroxyphenol, 3,5-dihydroxyphenol, 3,5-dimethoxyphenol and 2,3-dimethoxyphenol, respectively.

 $R = n-C_8H_{17}, C_2H_5(C_2H_5)C_4H_9$ 

Scheme 1 Synthesis of coumarin derivatives.

#### Preparation of n-octyloxy-substituted coumarin derivatives

n-Octyloxy substituted coumarin derivatives were prepared by reaction of the appropriate hydroxyl-substituted coumarin derivatives (10 mmol) with n-octyl bromide (20 mmol) in DMF (20 mL) using potassium carbonate (10 mmol) as a base. After refluxing for 12 h, 20 mL of aqueous HCl (1 M) was added to the mixture and the product was extracted by ethyl acetate. The crude product was purified by silica gel column chromatography.

Two n-octyloxy substituted coumarin derivatives, 4-methyl-7-octyloxycoumarin (O-7) and 4-methyl-7,8-dioctyloxycoumarin (O-78) were synthesized from 7-hydroxy-4-methylcoumarin (H-7) and 7,8-dihydroxy-4-methylcoumarin (H-78), respectively.

**4-Methyl-7,8-dioctyloxycoumarin** (O-78). 75%. White wax. M.p. 47–48 °C.  $R_{\rm f}$  0.70 (SiO<sub>2</sub>, hexane–EtOAc, 70:30). ε 14970 M<sup>-1</sup> cm<sup>-1</sup>. ATR-FTIR (neat, cm<sup>-1</sup>); 2956, 2918, 2844 (–C–H str.), 1710 (C=O str.), 1602 (C=C str.), 1510 (C=C str.), 1386 (C–O str. of ether), 1299 (C–O str. of ether) and 1092 (C–O str. of ester). <sup>1</sup>H NMR (CDCl<sub>3</sub>, δ, ppm); 7.25 (d, J = 9.8 Hz, 1H, Ar–H), 6.84 (d, J = 9.2 Hz, 1H, Ar–H), 6.12 (s, 1H, =CH), 4.06 (m, 4H, 2 × –OCH<sub>2</sub>C<sub>7</sub>H<sub>15</sub>), 2.37 (s, 3H, –CH<sub>3</sub>) and 1.89–0.80 (m, 30H, 2 × –C<sub>7</sub>H<sub>15</sub>); <sup>13</sup>C NMR (CDCl<sub>3</sub>, δ, ppm); 160.9, 155.2, 152.6, 148.1, 135.7, 119.1, 114.6, 112.2, 109.0, 74.2, 69.2, 31.9, 31.8, 30.2, 29.5, 29.3, 29.3, 29.2, 26.0, 25.9, 22.7, 22.6, 18.8, 14.1 and 14.0. MS m/z: 417.373 [obtained M+1]<sup>+</sup>, 416.593 [M cal].

#### Preparation of 2-ethylhexyloxy substituted coumarin derivatives

Three 2-ethylhexyloxy-substituted coumarin derivatives were synthesized using a similar procedure to that described for the noctyloxy coumarin derivatives, except that octyl bromide was replaced with 2-ethylhexyl bromide.

7,8-Di-2-ethylhexyloxy-4-methyl-coumarin (EH-78), 6,7-di-2-ethylhexyloxy-4-methylcoumarin (EH-67) and 5,7-di-2-ethylhexyloxy-4-methylcoumarin (EH-57) were synthesized from 7,8-dihydroxy-4-methylcoumarin (H-78), 6,7-dihydroxy-4-methylcoumarin (H-67) and 5,7-dihydroxy-4-methylcoumarin (H-57), respectively.

**7,8-Di-2-ethylhexyloxy-4-methyl-coumarin** (EH-78). 68%. Yellow liquid.  $R_{\rm f}$  0.57 (SiO<sub>2</sub>, hexane–EtOAc, 70:30).  $\epsilon$  14255 M<sup>-1</sup> cm<sup>-1</sup>. ATR-FTIR (neat, cm<sup>-1</sup>); 2956, 2920, 2872, 2856 (–C–H str.), 1734 (C=O str.), 1602 (C=C str.), 1509 (C=C str.), 1243 (C–O str. of ether), 1201 (C–O str. of ether) and 1085 (C–O str. of ester). <sup>1</sup>H NMR (CDCl<sub>3</sub>,  $\delta$ , ppm); 7.22 (d, J = 8.8 Hz,

1H, Ar–H), 6.84 (d, J = 8.8 Hz, 1H, Ar–H), 6.09 (s, 1H, =CH), 3.94 (m, 4H,  $2 \times -\text{OCH}_2\text{CH}(\text{C}_2\text{H}_5)\text{C}_4\text{H}_9$ ), 2.35 (s, 3H, -CH<sub>3</sub>), 1.76 (m, 2H,  $2 \times -\text{OCH}_2\text{CH}(\text{C}_2\text{H}_5)\text{C}_4\text{H}_9$ ) and 1.68–0.83 (m, 28H,  $2 \times -\text{OCH}_2\text{CH}(\text{C}_2\text{H}_5)\text{C}_4\text{H}_9$ ); <sup>13</sup>C NMR (CDCl<sub>3</sub>,  $\delta$ , ppm); 160.8, 155.4, 152.5, 148.0, 135.9, 119.0, 114.5, 112.2, 108.8, 76.5, 71.4, 40.4, 39.5, 30.4, 30.3, 29.2, 29.0, 23.7, 23.6, 23.1, 23.0, 18.7, 14.1, 14.1, 11.1 and 11.1. MS m/z: 417.449 [obtained M+1]<sup>+</sup>, 416.593 [M call.

**6,7-Di-2-ethylhexyloxy-4-methylcoumarin (EH-67).** 70%. Yellow liquid.  $R_f$  0.61 (SiO<sub>2</sub>, hexane–EtOAc, 70:30). ε 11586 M<sup>-1</sup> cm<sup>-1</sup>. ATR-FTIR (neat, cm<sup>-1</sup>); 2949, 2923, 2872, 2855 (–C–H str.), 1712 (C=O str.), 1612 (C=C str.), 1509 (C=C str.), 1272 (C–O str. of ether), 1233 (C–O str. of ether) and 1066 (C–O str. of ester). <sup>1</sup>H NMR (CDCl<sub>3</sub>, δ, ppm); 6.92 (s, 1H, Ar–H), 6.79 (s, 1H, Ar–H), 6.12 (s, 1H, =CH), 3.86 (m, 4H, 2 × –OCH<sub>2</sub>CH(C<sub>2</sub>H<sub>5</sub>)C<sub>4</sub>H<sub>9</sub>), 2.38 (s, 3H, –CH<sub>3</sub>), 1.78 (m, 2H, 2 × –OCH<sub>2</sub>CH(C<sub>2</sub>H<sub>5</sub>)C<sub>4</sub>H<sub>9</sub>) and 1.59–0.84 (m, 28H, 2 × –OCH<sub>2</sub>CH(C<sub>2</sub>H<sub>5</sub>)C<sub>4</sub>H<sub>9</sub>); <sup>13</sup>C NMR (CDCl<sub>3</sub>, δ, ppm); 161.7, 153.3, 152.5, 149.4, 146.2, 112.2, 111.8, 107.3, 100.7, 72.3, 71.4, 39.6, 39.2, 30.6, 30.5, 29.1, 29.0, 23.9, 23.8, 23.0, 23.0, 18.9, 14.1, 14.0, 11.2 and 11.1. MS m/z: 417.372 [obtained M+1]<sup>+</sup>, 416.593 [M cal].

**5,7-Di-2-ethylhexyloxy-4-methylcoumarin (EH-57).** 71%. Yellow liquid.  $R_{\rm f}$  0.72 (SiO<sub>2</sub>, hexane–EtOAc, 70:30).  $\epsilon$  16239 M<sup>-1</sup> cm<sup>-1</sup>. ATR-FTIR (neat, cm<sup>-1</sup>); 2953, 2928, 2871, 2852 (–C–H str.), 1729 (C=O str.), 1601 (C=C str.), 1444 (C=C str.), 1169, 1107 (C–O str. of ether), 1076 (C–O str. of ester). <sup>1</sup>H NMR (CDCl<sub>3</sub>,  $\delta$ , ppm); 6.41 (s, 1H, Ar–H), 6.29 (s, 1H, Ar–H), 5.93 (s, 1H, =CH), 3.87 (m, 4H,  $2 \times$  –OCH<sub>2</sub>CH(C<sub>2</sub>H<sub>5</sub>)C<sub>4</sub>H<sub>9</sub>), 2.55 (s, 3H, –CH<sub>3</sub>), 1.74 (m, 2H,  $2 \times$  –OCH<sub>2</sub>CH(C<sub>2</sub>H<sub>5</sub>)C<sub>4</sub>H<sub>9</sub>) and 1.55–0.86 (m, 28H,  $2 \times$  –OCH<sub>2</sub>CH(C<sub>2</sub>H<sub>3</sub>)C<sub>4</sub>H<sub>9</sub>); <sup>13</sup>C NMR (CDCl<sub>3</sub>,  $\delta$ , ppm); 162.5, 161.2, 158.7, 157.0, 154.4, 111.0, 104.6, 96.2, 93.7, 71.2, 70.8, 39.4, 39.2, 30.7, 30.4, 29.0, 29.0, 24.7, 24.1, 23.7, 23.0, 23.0, 14.1, 14.0, 11.1 and 11.1. MS m/z: 417.461 [obtained M+1]<sup>+</sup>, 416.593 [M cal].

It should be noted here that amongst the twelve synthesized compounds, only O-78, EH-78, EH-57 and EH-67 are reported here for the first time and therefore their characterization data are presented above. Characterization data of the other 8 derivatives are reported in the ESI.†

#### **Photostability**

The photostability of all synthesized coumarin derivatives was tested in methanol under normal oxygenated atmosphere. A  $5.7 \times$ 10<sup>-5</sup> M solution was irradiated with 13.0 mW cm<sup>-2</sup> broadband UVA and 1.0 mW cm<sup>-2</sup> broadband UVB at room temperature for 0, 15, 30 or 60 min which corresponds to 0, 11.70, 23.40 and 46.80 J cm<sup>-2</sup> UVA, respectively, and 0, 0.90, 1.80 and 3.60 J cm<sup>-2</sup> UVB, respectively. The irradiated solution was then analyzed by a UV/VIS spectrophotometer. The photostability of each compound was expressed as the relative absorbance (as A%) at the maximum absorption wavelength of the compound and calculated as follows:

%relative absorbance =  $100 \times \frac{\text{Absorbance after } t \text{ min of irradiation}}{\text{Absorbance of the unirradiated sample}}$ 

To evaluate the solvent effect, solutions of tested compounds in dichloromethane and hexane were subjected to similar experimental procedures.

The light source was a combination of broadband UVB (280-315 nm) and UVA (315-400 nm) radiation, as to imitate natural UV radiation (see their spectral profiles in the ESI†).

#### Oxygen effect

To evaluate the influence of oxygen, a sample solution (5.7  $\times$ 10<sup>-5</sup> M) in methanol was divided into two equal portions. A first portion was saturated with nitrogen gas while the other was saturated with air. Both samples were then subjected to the UV irradiation and analysis as described above.

#### Photostability under acidic conditions

To evaluate the photostability of compounds in acidic and neutral media, a sample solution  $(5.7 \times 10^{-5} \text{ M})$  was prepared in methanol (neutral media) and 2% (v/v) of 1 M HCl in methanol (acidic media). Both samples were then subjected to the UV irradiation and analysis as described above.

All the results (Fig. 1, 3 and 5) are shown as relative absorbance percentages of the samples after being exposed to various radiations. Data are shown on each bar as the mean  $\pm$  1 S.D., and are derived from 3 replications.

#### Computational modeling

Hyper Chem 7 was used to determine the most stable conformation of coumarin derivatives. Three-dimensional structures of coumarin derivatives were optimized using a semi-empirical method with PM3 parameter.

#### Conclusion

A series of 4-methylcoumarin derivatives was synthesized via the Pechmann reaction. Selective alkylations of the remaining hydroxy groups with alkyl bromides (n-octyl bromide or 2-ethylhexyl bromide) led to additional coumarin derivatives. The substitution position affected the maximum absorption wavelength  $(\lambda_{max})$ , whereas the type of substituents, whether hydroxy or alkoxy groups, caused no significant effect. The substitution position also significantly affected photostability of the materials. An acid-catalyzed mechanism through enolization coupled with preorganization via hydrogen bonding between the two coumarin moieties was proposed as an explanation for the different extents of photostability amongst the different derivatives.

Amongst the twelve derivatives, H-78 was the most photostable derivative with far-UVA ( $\lambda_{max} \sim 320 \text{ nm}$ ) absorption property, while M-67 and EH-67 were the most photostable mid-UVA ( $\lambda_{max}$  ~ 340 nm) absorptive derivatives. In facts, M-67 and EH-67 were significantly more photostable than H-67, a compound being used as UVA filter.

#### Acknowledgements

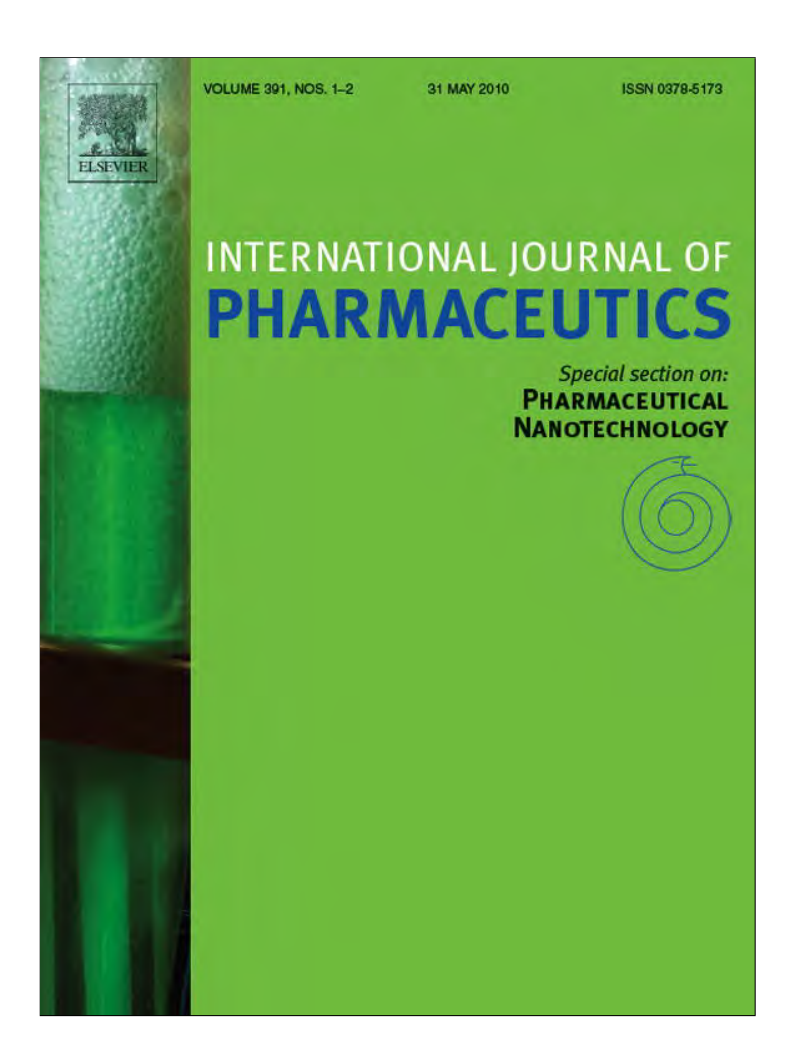
The authors thank the Thailand Research Fund (BRG52) and the Chulalongkorn University Graduate Thesis Grant for the financial support.

#### References

- 1 J. J. Yourick and R. L. Bronaugh, J. Appl. Toxicol., 1997, 17, 153.
- 2 K. P. Link, Circulation, 1959, 19, 97.
- 3 K. Von Resag, G. Nelzer and R. E. Nitz, Arzneim.-Forsch., 1976, 26,
- 4 T. O. Soine, J. Pharm. Sci., 1964, 53, 231.
- 5 V. Dadák and K. Hoďák, Experientia, 1966, 22, 38.
- 6 A. Lorico and B. H. Long, Eur. J. Cancer, 1993, 29, 1985.
- 7 A. S. Bourinbaiar, X. Tan and R. Nagorny, Acta Virol., 1993, 37, 241.
- 8 R. Adams and J. W. Mecorney, J. Am. Chem. Soc., 1944, 66, 802.
- 9 B. J. Donnelly, D. M. X. Donnelly and A. M. O'Sullivan, Tetrahedron, 1968. **24**. 2617
- 10 B. E. Hoogenboom, M. S. El-Faghi, S. C. Fink, P. J. Ihrig, A. N. Langsjoen, C. J. Linn and K. L. Maehling, J. Org. Chem., 1975, 40,
- 11 G. Brufola, F. Fringuelli, O. Piermatti and F. Pizzo, Heterocycles, 1996, **43**. 1257
- 12 I. Yavari, R. Hekmat-Shoar and A. Zonouzi, Tetrahedron Lett., 1998, **39** 2391
- 13 R. G. Harvey, C. Cortez, T. P. Ananthanarayan and S. Schmolka, J. Org. Chem., 1988, 53, 3936.
- 14 M. Schadt, H. Seiberle and A. Schuster, *Nature*, 1996, **381**, 212.
- 15 R. Jakubiak, T. J. Bunning, R. A. Vaia, L. V. Natarajan and V. P. Tondiglia, Adv. Mater., 2003, 15, 241.
- 16 N. Saleh, Y. A. Al-Soud and W. M. Nau, Spectrochim. Acta A, 2008, **71**. 818.
- 17 K. H. Drexhage, Laser Focus, 1973, 9, 35-39.
- 18 B. H. Winters, H. I. Mandelberg and W. B. Mohr, Appl. Phys. Lett., 1974, 25, 723-725.
- 19 G. A. Reynolds and K. H. Drexhage, Opt. Commun., 1975, 13, 222.
- 20 M. Obi, S. Morino and K. Ichimura, Chem. Mater., 1999, 11, 656.
- 21 V. B. Kovalska, K. D. Volkova, A. V. Manaev, M. Y. Losytskyy, I. N. Okhrimenko, V. F. Traven and S. M. Yarmoluk, Dyes Pigm., 2010, 84,
- 22 S. Hartner, H. C. Kim and N. Hampp, J. Photochem. Photobiol., A, 2007, 187, 242
- 23 S. Makki, P. Treffel, P. Humbert and P. Agache, J. Chromatogr., 1991, **563**, 407.
- 24 B. C. Lee, S. Y. Lee, H. J. Lee, G. S. Sim, J. H. Kim, Y. H. Cho, D. H. Lee, H. B. Pyo, T. B. Choe, D. C. Moon, Y. P. Yun and J. T. Hong, Arch. Pharm. Res., 2007, 30, 1293.
- 25 B. M. Hausen and M. Schmieder, Contact Dermatitis, 1986, 15, 157.
- 26 J. Preat, D. Jacquemin and E. A. Perpète, Chem. Phys. Lett., 2005, 415, 20.
- 27 G. S. Hammond, C. A. Stout and A. A. Lamola, J. Am. Chem. Soc., 1964, 86, 3103.
- 28 B. N. Mattoo, Trans. Faraday Soc., 1956, 52, 1184.
- 29 R. H. AbuEittah and B. A. H. El-Tawil, Can. J. Chem., 1985, 63, 1173.
- 30 X. Yu, D. Scheller, O. Rademacher and T. Wolff, J. Org. Chem., 2003, **68** 7386
- 31 T. Wolff and H. Görner, Phys. Chem. Chem. Phys., 2004, 6, 368.
- 32 N. D. Kokare, J. N. Sangshetti and D. B. Shinde, Chin. Chem. Lett., 2007, 18, 1309.

Provided for non-commercial research and education use.

Not for reproduction, distribution or commercial use.



This article appeared in a journal published by Elsevier. The attached copy is furnished to the author for internal non-commercial research and education use, including for instruction at the authors institution and sharing with colleagues.

Other uses, including reproduction and distribution, or selling or licensing copies, or posting to personal, institutional or third party websites are prohibited.

In most cases authors are permitted to post their version of the article (e.g. in Word or Tex form) to their personal website or institutional repository. Authors requiring further information regarding Elsevier's archiving and manuscript policies are encouraged to visit:

http://www.elsevier.com/copyright

### Author's personal copy

International Journal of Pharmaceutics 391 (2010) 267-273

EISEVIED

Contents lists available at ScienceDirect

### International Journal of Pharmaceutics

journal homepage: www.elsevier.com/locate/ijpharm



Pharmaceutical Nanotechnology

### High loading fragrance encapsulation based on a polymer-blend: Preparation and release behavior

Aurapan Sansukcharearnpon <sup>a,c</sup>, Supason Wanichwecharungruang <sup>b,\*</sup>, Natchanun Leepipatpaiboon <sup>b</sup>, Teerakiat Kerdcharoen <sup>d</sup>, Sunatda Arayachukeat <sup>a</sup>

- <sup>a</sup> Program of Petrochemistry and Polymer Science, Chulalongkorn University, Bangkok 10330, Thailand
- <sup>b</sup> Department of Chemistry, Faculty of Science, Chulalongkorn University, Payatai Road, Patumwan, Bangkok 10330, Thailand
- c National Center of Petroleum, Petrochemicals and Advanced Materials, Chulalongkorn University, Bangkok 10330, Thailand
- d Department of Physics, Center of NANO, Faculty of Science, Mahidol University, Bangkok 10400, Thailand

#### ARTICLE INFO

Article history:
Received 24 November 2009
Received in revised form 6 January 2010
Accepted 10 February 2010
Available online 17 February 2010

Keywords: Nanoparticles Fragrance Encapsulation Controlled release TGA Essential oil

#### ABSTRACT

The six fragrances, camphor, citronellal, eucalyptol, limonene, menthol and 4-tert-butylcyclohexyl acetate, which represent different chemical functionalities, were encapsulated with a polymer-blend of ethylcellulose (EC), hydroxypropyl methylcellulose (HPMC) and poly(vinyl alcohol) (PV(OH)) using solvent displacement (ethanol displaced by water). The process gave  $\geq$ 40% fragrance loading capacity with  $\geq$ 80% encapsulation efficiency at the fragrance to polymer weight ratio of 1:1 and at initial polymer concentrations of 2000–16,000 ppm and the obtained fragrance-encapsulated spheres showed hydrodynamic diameters of less than 450 nm. The release profile of the encapsulated fragrances, evaluated by both thermal gravimetric and electronic nose techniques, indicated different release characteristics amongst the six encapsulated fragrances. Limonene showed the fastest release with essentially no retention by the nanoparticles, while eucalyptol and menthol showed the slowest release.

© 2010 Elsevier B.V. All rights reserved.

#### 1. Introduction

Components in essential oils are secondary metabolites with unique odors. They are used worldwide not only in folk medicine, spa, cosmetics and toiletries, but also in many scented household and occupational products. Scientific studies on the biological actions of these essential oils have already started to accumulate (Fukumoto et al., 2006; Moretti et al., 2002; Morita et al., 2003). These unique odorous molecules are being synthesized or isolated from natural sources and used as fragrance components in various industries. However, many of these fragrance molecules are unstable due to their reactive functionalities, such as aldehyde, ketone and terpenes. Degradation not only causes changes in their sensory characteristics, but also, in many cases, creates allergenic products (Karlberg et al., 1992; Matura et al., 2005, 2006). It has been known that control of the volatilization rate and degradation is the heart of prolonging the sensory characteristics of fragrance materials. One way of doing so is encapsulation, which provides both stabilization and a controlled release of the entrapped materials. Other benefits of encapsulation include ease of handling (e.g. a stable solid encapsulated product instead of an unstable volatile liquid), improved

safety (e.g. reduced flammability) and an increased applicability to various products (e.g. water dispersible essential oil-encapsulated spheres can be easily applied in water based formulations). However, the fragrance release properties are the key issue in selecting a particular encapsulation technology.

The existing fragrance encapsulation technologies includes double emulsion preparation (Edris and Bergnståhl, 2001), molecular inclusion into a host, such as cyclodextrin (Wang and Chen, 2005), incorporation into solid lipid nanoparticles using appropriate lipids and surfactants (Lai et al., 2006), coacervation with various carbohydrates with and without the use of crosslinking agents (Soper et al., 2000; Chang and Dobashi, 2003), interfacial polymerization based on various polymers, such as polyurethane-urea (PUU) and phenol–formaldehydes (Ouall and Lahoussine, 2006; Scarfato et al., 2007; Hwang et al., 2006a,b; Rodrigues et al., 2008) and *in situ* polymerization, such as the synthesis of fragrance-encapsulated mesoporous silica spheres (Wang et al., 2008). Amongst these, interfacial polymerization and complex coacervation are the two most popular choices.

Partial solubility in water of many essential oils' components usually causes instability in the microencapsulation by interfacial reactions because of the change in the hydrolytic stability of the particle during polymerization reaction. Moreover, side reactions between the monomers with several reactive functionalities of the essential oil's components can lead to some alteration of the

<sup>\*</sup> Corresponding author. Tel.: +66 2 218 7634; fax: +66 2 254 1309. E-mail address: psupason@chula.ac.th (S. Wanichwecharungruang).

Fig. 1. The chemical structure of the six fragrance molecules.

encapsulated products, especially in the PUU system. To avoid such drawbacks, the environmental unfriendly phenol-formaldehyde (melamine-formaldehyde) has been used. The system is neither biocompatible nor biodegradable which limits its applications.

Complex coacervation has been reported and patented by several authors as a method for fragrance prolongation (Soper et al., 2000; Bachtsi and Kiparissides, 1996; Jean-Pierre et al., 1998; Markus and Linder, 2004). However, the coacervated products generally have a weak mechanical resistance, due to water solubility of the polymer, making them inappropriate for many applications where a long shelf-life and a good mechanical strength are required. The use of crosslinking agents to improve the stability, although it has been demonstrated, possesses the drawbacks of side reactions between the encapsulated material and the residues of the crosslinking agents.

For fragrance-encapsulated polymeric microspheres, the release of the fragrance component(s) incorporated in the polymer is controlled by the initial loading of the fragrance(s) in the polymer and the ability of the fragrance molecules to diffuse through the polymeric barrier into the surrounding environment. Interactions between fragrance molecules and the polymer matrix, together with the vapor pressure of the volatile substances on each side of the matrix, are the major driving forces influencing diffusion. The characteristics of the encapsulated fragrance-blend are the result of the release rates of each component. Thus, it is essential to understand the release profile of each component in order to predict the change of odorous note throughout the application.

To the best of our knowledge, biocompatible polymeric nanocarriers which can encapsulate fragrance molecules effectively without the use of crosslinking agents and also give highly stable encapsulated products with a satisfying long lasting controlled release property, are very rare, if ever reported. In this paper, we, therefore, demonstrate the fragrance encapsulation process using a blend of non-toxic, biocompatible and biodegradable polymers. Six common fragrance molecules of different chemical functionalities, camphor (ketone), citronellal (aldehyde), eucalyptol (ether), limonene (unsaturated hydrocarbon), menthol (alcohol) and 4-tertbutylcyclohexyl acetate (ester) (Fig. 1), were encapsulated and their release profiles were investigated.

#### 2. Materials and methods

Hydroxypropyl methylcellulose (HPMC; Mn 90,000; D.S. methoxy 1.10–1.60; M.S. propylene oxide 0.10–0.30), poly(vinyl alcohol) (PV(OH); Mw 124,000–186,000, 87–89% deacetylated), ethylcellulose (EC; Mn 175,000; ethoxy content 48%), 4-tert-butylcyclohexyl acetate or Vertenex, and (1R)–(+)-camphor or (R)–1,7,7-trimethylbicyclo[2.2.1]heptan-2-one were purchased from Aldrich (Steinheim, Germany). (3R)–

citronellal or (R)-3,7-dimethyloct-6-en-1-al, p-limonene or (R)-4-isopropenyl-1-methylcyclohexene (1R, 2S, 5R)-menthol or (1R, 2S, 5R)-2-(2-propyl)-5-methylcyclohexanol, and eucalyptol or 1,3,3-trimethyl-2-oxabicyclo[2,2,2]octane were purchased from Acros Organics (Geel, Belgium). Dialysis tubing cellulose membranes (MWCO) 12,400 Da, size  $76 \, \mathrm{mm} \times 49 \, \mathrm{mm}$  were purchased from Sigma–Aldrich (Steinheim, Germany).

<sup>1</sup>H nuclear magnetic resonance (NMR) analyses were performed using a Varian Mercury spectrometer, which operated at 400.00 MHz for <sup>1</sup>H in deuterated chloroform (CDCl<sub>3</sub>) with tetramethylsilane (TMS) as an internal standard (Varian Company, Palo Alto, CA, USA). Centrifugation was performed on Allegra 64R et Avanti 30 (Beckman Coulter, Inc., Fullerton, CA, USA). Thermal gravimetric analysis (TGA) was carried out on a simultaneous thermal analysis Model STA490C (NETZSCH, Selb, Germany).

#### 2.1. Self-assembling of the polymer-blend

Self-assembling of polymer-blend into particles was induced by solvent displacement (water displacement of ethanol). A solution of the polymer-blend (HPMC:PV(OH):EC at a w/w/w ratio of 1:1:6) was prepared at 70 °C using 75% (v/v) aqueous ethanol to obtain the solution of the appropriate concentration. The mixture (20 mL) was then placed into a dialysis bag and dialyzed against water ( $5 \times 1000 \, \text{mL}$ ). The final volume of the obtained suspension was adjusted to 50 mL by adding water. This self-assembly of the polymer-blend into nanoparticles was carried out at initial polymer concentrations of 2000, 4000, 8000, 12,000, 16,000, 18,000, 24,000 and 28,000 ppm. The final volume of the suspension usually doubled the volume of the polymer solution used at the beginning so the final concentrations of the polymer in the obtained suspension were adjusted to 1000, 2000, 4000, 6000, 8000, 9000, 12,000 and 14,000 ppm, respectively, by adding water. The particle size distribution and zeta potential of the obtained suspensions were acquired by dynamic light scattering (DLS) using a Mastersizer S and Zetasizer nanoseries (Mulvern Instruments, Worcestershire, UK) equipped with a He-Ne laser beam at 632.8 nm (scattering angle of 173°). Each measurement was carried out in triplicate and an average value is reported.

Morphology and approximate sizes were characterized using scanning electron microscopy (SEM), transmission electron microscopy (TEM) and atomic force microscopy (AFM). The photographs of SEM were obtained using JSM-6400 (JEOL, Ltd., Japan). A drop of the nanoparticle suspension was placed on a glass slide and dried overnight. The sample was coated with a gold layer under vacuum at 15 mA for 90 s. The coated sample was then mounted on an SEM stud for visualization. The accelerating voltage used was 15 kV. TEM photographs were obtained using JEM-2100 (JEOL, Ltd., Japan) with an accelerating voltage of 120 kV in conjunction with selected area electron diffraction (SAED). The AFM photographs were acquired with Nano Scope IV (Veeco Metrology Group, CA, USA). A glass slide was dipped into the obtained suspension to gain the dried smooth film of nanoparticles on surface of the glass slide.

#### 2.2. Fragrance encapsulation

#### 2.2.1. Particles with various fragrance contents

Camphor was encapsulated into the polymer-blend at camphor to polymer weight ratios of 1:1 and 2:1. For each composition, 80 mg of the polymer-blend were dissolved in 20 mL of 75% (v/v) aqueous ethanol at 70 °C. Then the desired amount of camphor (80 and 160 mg) was added to the cool solution and the mixture was placed into a dialysis bag and dialyzed against distilled water (5 × 500 mL) in a tightly closed container with no void volume between the dialysate and the lid. The final volume of the resulting colloidal suspension (suspension in the dialysis bag) was

adjusted to 40 mL with water. Ten milliliters of the obtained suspension were filtering centrifuged (centrifugal-filtering devices with MWCO 100000, Amicon Ultra-15, Millipore, Ireland) and the obtained solid was dissolved in 5 mL ethanol. The ethanol solution was quantified for camphor using headspace analysis in combination with gas chromatography/mass spectroscopic detector (headspace-GC/MS) with the aid of a calibration standard curve. Calibration standards were freshly prepared in ethanol with the final volume of 5 mL. The encapsulation efficiency percentage (% EE), loading capacity (% loading) and yield of the process (% yield) were each determined as follows:

$$\% \ EE = \left[ \frac{weight \ of \ encapsulated \ fragrance}{weight \ of \ fragrance \ used \ initially} \right] \times 100 \tag{1}$$

$$\% \, loading = \left[ \frac{weight \, of \, encapsulated \, fragrance}{weight \, of \, fragrance - \, encapsulated \, particles} \right] \times 100 \end{20}$$

$$\% \ yield = \left[\frac{weight \ of \ fragrance - encapsulated \ particles}{weight \ of \ polymer \ and \ fragrance \ used \ initially}\right] \times 100 \end{2pt}$$

Similar processes were repeated for the other five fragrances which included citronellal, eucalyptol, limonene, menthol and 4-tert-butylcyclohexyl acetate. The aqueous suspensions of fragrance-encapsulated nanoparticles so obtained were subjected to a morphological analysis by SEM, TEM, AFM and DLS.

Part of the fresh aqueous suspension was centrifuged at  $45,000 \times g$  for 30 min and the obtained white solid was air-dried at room temperature (overnight). The freshly dried particles were dissolved in deuterated chloroform and subjected to  $^1$ H NMR analysis in order to confirm the presence of the encapsulated fragrance. The freshly dry samples were subjected to a controlled release study using the e-nose and TGA.

### 2.2.2. Headspace-gas chromatography in conjunction with mass spectroscopic detector (headspace-GC/MS)

Headspace-GC/MS analysis was carried out on the Agilent 6890N/5975i GC/MS equipped with a headspace oven of Agilent 7694 (Agilent Technologies, Wilmington, DE, USA). The headspace sample (ethanol solutions of the centrifuged fragranceencapsulated spheres and the calibration standards) was loaded in a 20 mL capped flat bottom headspace vial with headspace aluminum crimp caps with PTFE/silicone septa (Agilent technologies, USA), and heated in a headspace oven at 85 °C for 20 min before the headspace gas was automatically transferred into the GC system. The transfer line was held at 110 °C for 0.4 min, before being flushed into a GC system for 2 min. A Restex 10624 Stabilwax column (30 m  $\times$  0.32 mm ID  $\times$  0.25  $\mu$ m) (Restex Corp., Pennsylvania, USA) was used. The carrier gas was helium under a constant flow rate of 1 mL/min. The initial GC oven temperature was 40 °C which was held for 3 min and was then ramped by 6 °C/min to 220 °C and held for 2 min. The inlet temperature was 260 °C. The mass spectrometer was operated in an electron impact (EI) mode, using the total ion scan mode with scanning from mass 50 to 500 Da. One mL of the headspace gas from each sample was injected with the auto-sampler into the above GC/MS.

### 2.2.3. Citronellal-encapsulated particles prepared at various concentrations

The appropriate amount of polymer-blend (80, 120, 160, 320 and 640 mg) was dissolved in 20 mL of 75% (v/v) aqueous ethanol. The mixture was then stirred and heated at  $70\,^{\circ}$ C until a clear solution was obtained and citronellal (same amount to the

polymer-blend) was added. The mixture was then placed into a dialysis bag and dialyzed against water. The final volume of the suspension was adjusted to 40 mL with water. The % EE, % loading and % yield were determined as described above. The obtained citronellal-encapsulated particles were subjected to morphological analysis by SEM and DLS.

#### 2.3. Determination of the release profiles

The release profiles of the centrifuged-air-dried particles were acquired by quantitating the amount of fragrances remained in samples which had been left uncovered for specified times. Quantification was carried out using the electronic nose and thermal gravimetric analysis.

#### 2.3.1. Electronic nose (e-nose)

Electronic nose analysis was carried out using a home-made instrument (Fig. 2) consisting an array of eight commercial gas sensors which respond to various kinds of volatile organic compounds such as alcohol, aldehyde, ketone acid and hydrocarbon. This range of chemical sensitivity should be sufficient to detect most volatile components in aroma oil. Seven 50 mg-samples were left in open containers (20 mL flat bottom headspace vial, 0.D.  $\times$  H. 20 mm  $\times$  70 mm) at 30 °C. At the specified collection time, each vial was capped and subjected to e-nose analysis. Release profile was compared to the corresponding unencapsulated fragrance sample.

Unencapsulated camphor sample was prepared by adding 20.5 mg of camphor into a vial and the polymer-blend (in this case 29.5 mg) was added to make the total weight of 50 mg. The sample was thoroughly mixed. The other five unencapsulated fragrance samples were prepared similarly but the amounts of fragrance added into the vials were 19.9, 22.1, 8.0, 21.0 and 21.0 mg for citronellal, eucalyptol, limonene, menthol and 4-tert-butylcyclohexyl acetate samples, respectively. Amounts of polymer-blend added were adjusted accordingly, as to get the final weight of 50 mg. Seven vials were prepared for each fragrance and they were left opened at 30 °C. At the specified collection time, each vial was capped and subjected to e-nose analysis.

Analysis was carried out by putting the sample vial into the chamber for analysis, with a blank vial (containing only polymerblend) in the reference chamber. It is necessary that during the measurement, switching between a reference and a sample line must be performed. Four electrically controlled solenoid valves were used for this system (Fig. 2). When a pair of two solenoid valves is open, another pair will be automatically closed. This guarantees there is no mixing of the gas from the reference and sample

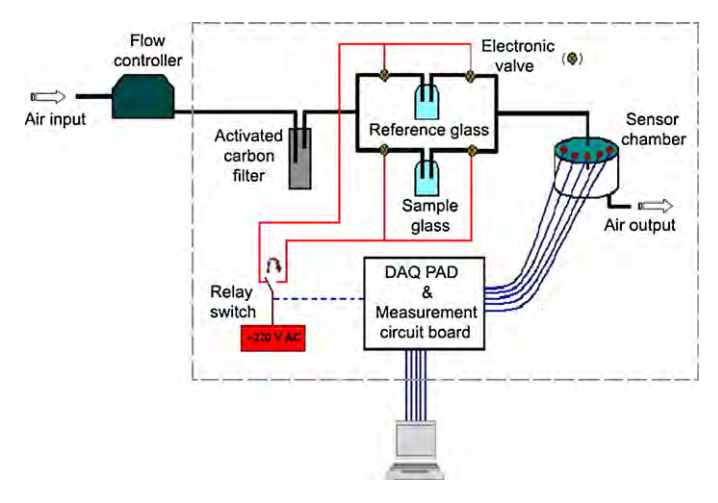
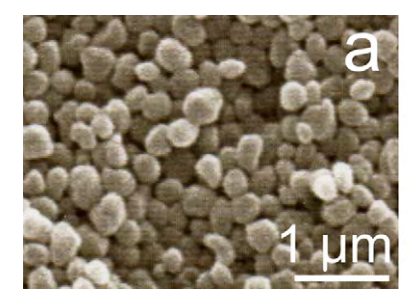
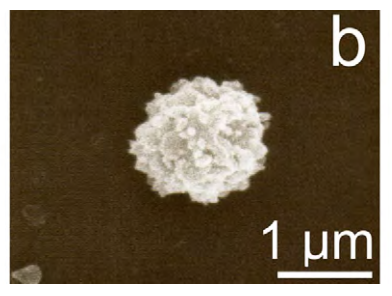


Fig. 2. Diagram showing the working principle of the e-nose system.

A. Sansukcharearnpon et al. / International Journal of Pharmaceutics 391 (2010) 267–273







**Fig. 3.** Representative SEM and TEM images of spheres obtained with the starting polymer concentrations of (a) 2000–16,000 ppm, (b) 18,000 ppm and (c) 24,000–28,000 ppm. The figures are representative of products from at least three independent preparations.

lines. Then, the gas from the reference or sample flows to the sensor chamber. In the experiment, the reference lines were measured for 5 min in the first stage. Then, the gas from headspace of the sample vial was presented into the sensor chamber for 1 min. In each experiment, the measurement of reference and sample was iterated at least five times. The data acquisition was carried out on an USB-DAQ-Card National Instruments NI USB-6008 and the measurement program was written using LabVIEW version 8.0.29. The  $\Delta R/R0$  values of the sensors were recorded for each combination of above variations. The sensors response (sensitivity of sensors) was plotted by % (R/R0) with time.

#### 2.3.2. Thermal gravimetric analysis (TGA)

TGA was used to determine the weight loss related to the release of fragrance from the sample. The centrifuged and air-dried samples (or unencapsulated fragrance samples prepared similarly to those used in the e-nose experiment) were kept in open containers at 30°C and a specific amount (30 mg) was taken to TGA analysis at appropriate times. For particles encapsulated with citronellal, limonene and 4-tert-butylcyclohexyl acetate, the thermal programs were started with heating from room temperature to 100 °C at a constant heating rate of 50 °C/min and the temperature was held at 100 °C for 30 min in order to evaporate the water molecules out from the samples. Then, the temperature was increased at a heating rate of 5 °C/min from 100 °C to 200 °C and held at 200 °C for 40 min before being ramped at the same heating rate to 300 °C. The thermal programs for particles encapsulated with camphor, eucalyptol menthol and fresh powder, were started by ramping from ambient temperature to 100 °C at heating rate of 50°C/min and held for 15 min as above, and then increasing from 100 °C to 150 °C at a heating rate of 5 °C/min and held for 20 min before being increased from 150 °C to 300 °C at a heating rate of 10°C/min.

#### 3. Results and discussion

#### 3.1. Self-assembly of the polymer-blend

When ethanol in the polymer-blend solution was displaced by water, the formation of milky white aqueous particle suspension was observed. SEM analyses of the dry particles and the aqueous suspension revealed similar results of spherical particles in which their sizes varied with the initial concentration of the polymer solution used. At starting polymer concentrations of 2000–16,000 ppm, smooth surface-spherical particles with diameters less than 400 nm were obtained (Fig. 3a), while at starting polymer concentrations of 18,000 ppm, jagged spherical particles with diameters  $\sim\!\!1\,\mu\mathrm{m}$  were observed (Fig. 3b). Increasing the initial polymer concentration to 24,000–28,000 ppm resulted in  $\sim\!\!2\,\mu\mathrm{m}$  particles being created (Fig. 3c). Higher still polymer concentrations (32,000 ppm) resulted in the significant formation of precipitates.

Amongst the three polymers used in the blend (EC, HPMC and PV(OH)), EC is the only polymer that is insoluble in water, thus upon slow displacement of ethanol by water, EC chains self-assembled into spheres with probably most of the hydrophobic ethoxyl moieties oriented away from the surrounding water medium and with most of the hydroxyl groups of the sugar units oriented outwards to have a maximum interaction with water molecules. During such self-assembling process, some PV(OH) and HPMC chains could be trapped along with the EC molecules through entanglements, thus making the spherical walls being composed of the polymer-blend. Some of the PV(OH) and HPMC chains must also be left in the aqueous medium because of their good water solubility. In this stage they act as stabilizers for the polymer-blend-spheres. Upon drying, these two polymers also cover up the surface of the spheres, making them readily dispersible in water.

All the obtained particles showed no morphological change after either heat treatment at  $100\,^{\circ}\text{C}$  for  $30\,\text{min}$  or strong mechanical agitation by stirring at 2400 rpm, indicating both the relative thermal and the mechanical stabilities of the polymerblend-particles. Although some settling of the microspheres in suspensions prepared from initial polymer concentrations of  $\geq 20,000\,\text{ppm}$  was observed, they could easily be redispersed by agitation.

Fine-tuning of the particles' size could be achieved through adjusting the starting polymer concentration (Table 1). All particles of sizes 250–360 nm showed a similar zeta potential of approximately –30 mV, indicating acceptable stability. Thus, it was concluded that a likely stable aqueous suspensions of the polymer-

**Table 1**Particle sizes and zeta potential of the nanoparticles prepared at different initial polymer concentrations.

Starting polymer concentration (ppm)	Hydrodynamic diameter of the empty particles (nm)	Zeta potential of the empty particles (mV)
2000	$253.0 \pm 1.3  \text{nm}  (\text{PDI} = 0.08)$	-30.11
4000	$267.7 \pm 2.8  \text{nm}  (\text{PDI} = 0.14)$	-33.24
6000	$362.9 \pm 3.7  \text{nm}  (\text{PDI} = 0.20)$	-26.32
8000	$357.9 \pm 0.7  \text{nm}  (\text{PDI} = 1.48)$	-32.87
12,000	$363 \pm 4.3  \text{nm}  (\text{PDI} = 1.68)$	-26.53
16,000	$358 \pm 3.9  \text{nm}  (\text{PDI} = 1.83)$	-27.19

Data are shown as the mean + S.D. and are derived from 3 repeats.

**Table 2**The encapsulation efficiency (at a fragrance:polymer weight ratio of 1:1) and the properties of the encapsulated fragrances prepared from a starting polymer concentration of 4000 ppm.

Fragrance	Vapor pressure of the fragrance (mm Hg at 25 °C)	Boiling point of the fragrance (°C)	% EE (suspension)	% Loading (suspension)	% Loading (after centrifuged and air-dried)	Diameter of the fragrance-encapsulated spheres (nm)
Camphor	0.65	204	$85.7 \pm 0.8$	$46.2\pm0.2$	41.1 ± 4.3	$287 \pm 3.1$
Citronellal	0.28	203	$92.3 \pm 1.6$	$48.0\pm0.4$	$39.7 \pm 4.9$	$278 \pm 3.6$
Eucalyptol	1.65	177	$84.0 \pm 2.1$	$45.6\pm0.6$	$44.3 \pm 3.2$	$295\pm2.6$
Limonene	1.98	176	$79.7\pm3.4$	$44.4 \pm 1.1$	$16.2 \pm 5.2$	$280 \pm 2.9$
Menthol	0.0323	212	$85.2 \pm 1.1$	$46.0\pm0.3$	$41.8 \pm 4.4$	$279 \pm 3.2$
4-tert-butylcyclohexyl acetate	0.0498	229	$84.2 \pm 1.5$	$45.7\pm0.4$	$42.3\pm4.7$	$298 \pm 3.1$

blend-particles could be prepared up to a maximum concentration of 8000 ppm (starting polymer concentration of 16,000 ppm).

#### 3.2. Encapsulation

Six fragrances were carefully selected for encapsulation so as to encompass molecules of different chemical functionalities. They consisted of camphor (ketone), citronellal (aldehyde), eucalyptol (ether), menthol (alcohol), limonene (unsaturated hydrocarbon) and 4-tert-butylcyclohexyl acetate (ester).

First, the encapsulation was carried out at a starting polymer concentration of 4000 ppm using two weight ratios between fragrance and polymer, i.e., 1:1 and 2:1. It should be mentioned here that a special closed container was used during dialysis in which neither air nor void volume was allowed in the system in order to avoid partition of fragrance molecules into the void space. It was found that dialysis in this air-free condition gave a suspension with no precipitation, while in contrast a significant amount of precipitate was found (especially at high polymer concentrations) when there was an air-contact to the surface of the dialysis bag (data not shown). We speculate that the air-contact interfered with the self-assembly through solvent evaporation and favoring precipitate formation at the air-interface. Encapsulation efficiency and loading capacity were then obtained through analysis of the obtained particle suspensions. Encapsulation efficiency was >80% at 1:1 fragrance to polymer ratio (Table 2). However, the 2:1 fragrance to polymer ratio resulted in observable non-dispersible floating fragranced gum which complicated the determination of loading capacity and encapsulation efficiency. Thus, the maximum fragrance to polymer ratio was limited to 1:1 in all further studies. Satisfyingly, all six fragrances could be loaded into the nanospheres at a fragrance:polymer ratio up to 1:1 and the obtained spheres possessed fragrance loading of  $\geq$ 44%.

SEM images indicated a similar spherical shape amongst the six fragrance-encapsulated polymeric spheres (see an example of menthol-encapsulated spheres in Fig. 4a). TEM pictures showed particles with obvious core (Fig. 4b), while the AFM photographs

of the encapsulated nanoparticles indicated soft and not rigid polymeric spheres (Fig. 4c).

When ethanol was displaced by water, self-assembling of the water-insoluble EC, likely with some entanglements with HPMC and PV(OH) occurred as described previously. With the presence of fragrance molecules, self-assembly occurred together with the entrapment of the water-insoluble fragrance molecules. The stability of the fragrance-loaded spheres is then a result of the hydrophobic interactions between the fragrance molecules and the ethoxy moieties of the EC chains. The amount of HPMC and PV(OH) was probably more prominent towards the rim of the sphere. All the six fragrances could be entrapped well into the spheres, indicating a wide window of encapsulation capability of the polymer-blend-spheres.

Confirmation of the successful encapsulation was carried out by sonicating the dry fragrance-encapsulated spheres in  $CDCl_3$  (5 min at 40 kHz, 25 °C) and then subjected the resulting solution to  $^1H$  NMR analysis. Resonance of protons from fragrance molecules could be observed clearly for all encapsulated products (data not shown), confirming the presence of fragrances in the spheres. In addition, no degradation was observed for all six fragrances.

To investigate if fragrance-encapsulated spheres could be prepared at other concentrations, encapsulation at a citronellal:polymer weight ratio of 1:1 was evaluated using starting polymer concentrations of 2000, 4000, 6000, 8000, 12,000, 16,000 and 32,000 ppm. SEM and TEM images of the products indicated that citronellal-encapsulated nanospheres (diameter between 200 and 450 nm) were formed at starting polymer concentrations of ≤16,000 ppm while at 32,000 ppm citronellalencapsulated microparticles (diameter around 1-2 µm) were obtained together with some non-dispersible polymeric masses mixed with citronellal oil (gum-like material). Quantitative analysis of the encapsulated products indicated  $88 \pm 1.8$ ,  $85 \pm 1.6$ ,  $84 \pm 2.2$ ,  $86\pm2.1,~83\pm2.0$  and  $80\pm2.8\%$  EE for particles prepared at the starting polymer concentrations of 2000, 4000, 6000, 8000, 12,000 and 16,000 ppm, respectively. However, at the starting polymer concentration of 32,000 ppm, only  $51 \pm 5.6\%$  EE was obtained. The

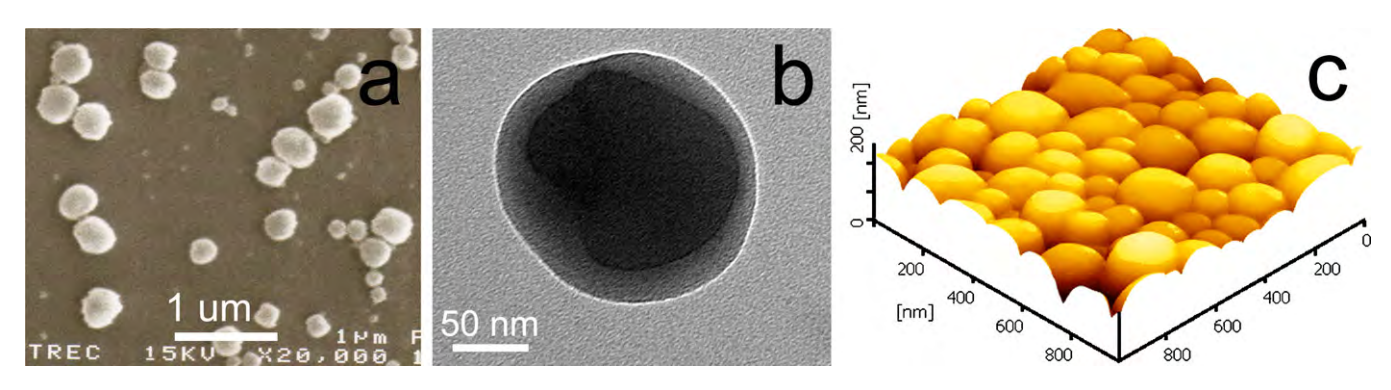


**Fig. 4.** Representative (a) SEM, (b) TEM and (c) AFM images of menthol-encapsulated polymeric nanoparticle suspension prepared at the starting polymer concentration of 4000 ppm and with a 1:1 menthol to polymer weight ratio. Images are representative of 5 independent samples.

low encapsulation efficiency at high polymer concentration agreed well with a significant formation of a non-dispersible polymeric mass observed.

All the above results clearly indicated that the polymer-blend of HPMC:PV(OH):EC at a (w/w/w) ratio of 1:1:6 could effectively nanoencapsulate all six fragrances with different chemical functionalities through solvent displacement of the ethanol by water and gave fragrance-encapsulated nanospheres with excellent water dispersibility. The process could be carried out at initial polymer concentrations of up to 16,000 ppm (with a similar concentration of fragrance) to give a % EE of  $\ge 80\%$ .

#### 3.3. Release behavior

In this work dry fragrance-encapsulated particles was obtained through centrifugation and air-drying. Fragrance lost during the drying process was noticed. Ethanol dissolution of the dry fragrance-encapsulated particles was carried out and the fragrance contents were determined using headspace-GC-MS analysis. Results indicated that the lost varied with drying time (data not shown). Also different fragrance gave different lost. Although the six suspensions (camphor, citronellal, eucalyptol, limonene,

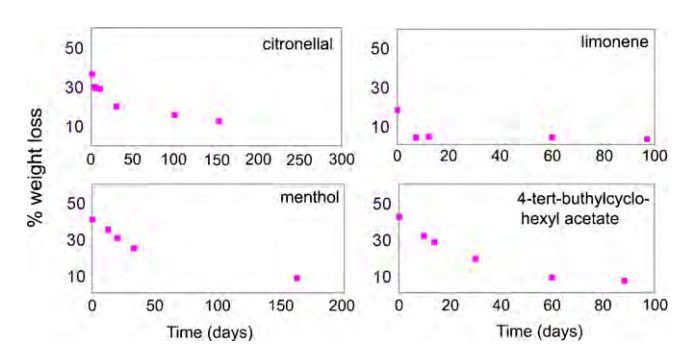


**Fig. 5.** The release of various fragrances from the dry polymeric nanospheres (prepared at an initial polymer concentration of 4000 ppm and a fragrance:polymer weight ratio of 1:1) as analyzed by TGA. Each point is the average value of two data points that are within 10% of each other. Initial fragrance loading of the dry samples was  $40\pm4.9$ ,  $16\pm5.2$ ,  $42\pm4.4$  and  $42\pm4.7\%$  for citronellal, limonene, menthol and 4-tert-butylcyclohexyl acetate-encapsulated particles, respectively.

menthol and 4-*tert*-butylcyclohexyl acetate) initially contained comparable fragrance loading (Table 2), the dry particles contained different fragrance loading, i.e.,  $41\pm4.3$ ,  $40\pm4.9$ ,  $44\pm3.2$ ,  $16\pm5.2$ ,  $42\pm4.4$  and  $42\pm4.7\%$  loading for camphor, citronellal,

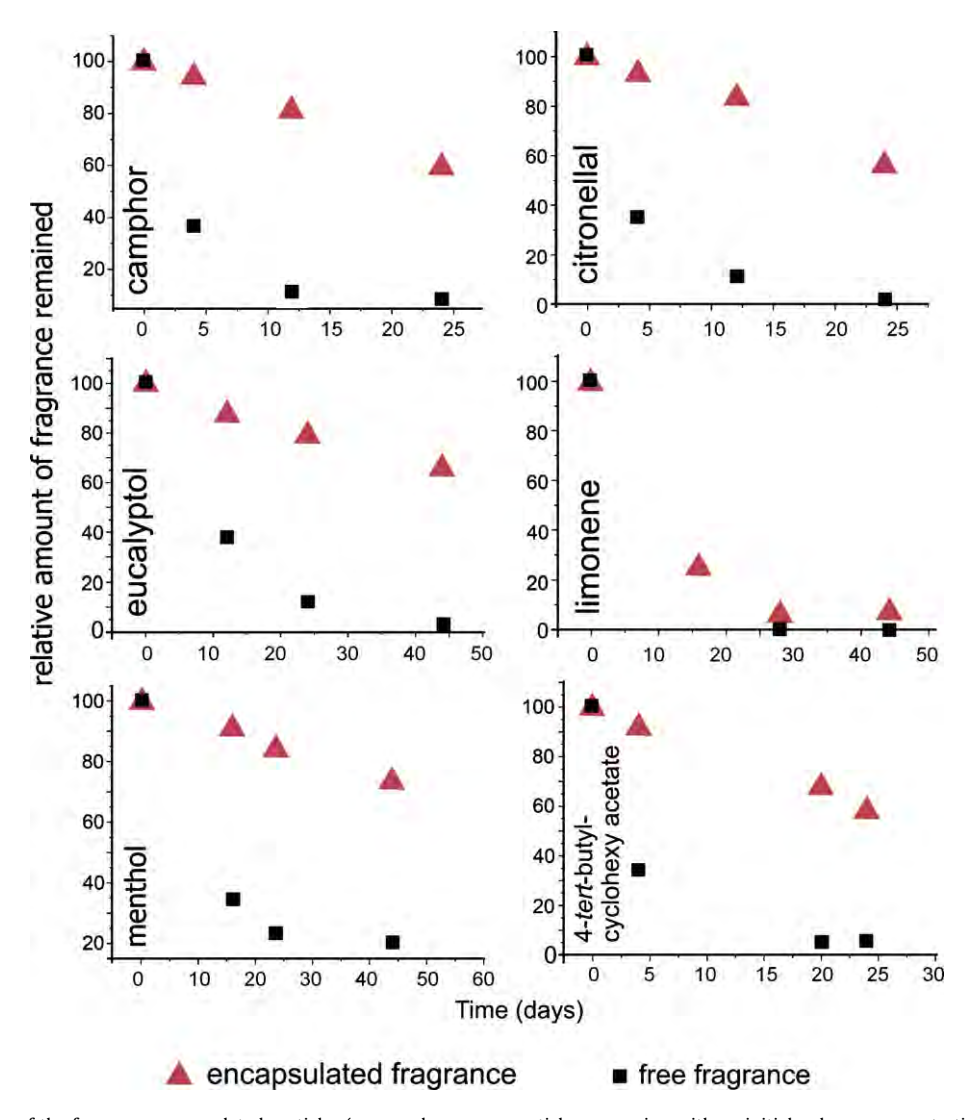


**Fig. 6.** The release profiles of the fragrance-encapsulated particles (prepared as a nanoparticle suspension with an initial polymer concentration of 4000 ppm and a fragrance:polymer weight ratio of 1:1 and subjected to centrifugation and air-drying), compared to the unencapsulated fragrances. The profiles are shown as amount of fragrance remained in the sample relative to amount of fragrance found in the sample on day 0 of the same sample. Initial fragrance loading of the dry samples was  $41\pm4.3$ ,  $40\pm4.9$ ,  $44\pm3.2$ ,  $16\pm5.2$ ,  $42\pm4.4$  and  $42\pm4.7\%$  for camphor, citronellal, eucalyptol, limonene, menthol and 4-tert-butylcyclohexyl acetate-encapsulated particles, respectively. Data are present as average values of two experimental data points which are within 15% of each other.

eucalyptol, limonene, menthol and 4-tert-butylcyclohexyl acetate-encapsulated particles, respectively.

For the centrifuged-air-dried samples, the TGA analysis, based upon the weight loss from the solid sample, where the reduction of the amount of fragrances remaining in the samples corresponds to the fragrance release behavior of the sample (Fig. 5), revealed that three (citronellal, menthol and 4-tert-buthylcyclo-hexyl acetate) of the four tested fragrances showed delayed release kinetics, but that limonene did not. Since the TGA analysis relies on getting the dry sample weight (initial weight after water evaporation), samples in which the fragrance significantly co-volatilizes out with water during the preheating period, such as camphor- and eucalyptol-encapsulated spheres, cannot be analyzed by this technique. However, the e-nose can be used to monitor the release of all six encapsulated products (Fig. 6). For the four common fragrances analyzed, the TGA and e-nose results agreed well and indicated that limonene-encapsulated particles gave the most significant burst at the beginning and only a very small percentage of limonene remained to be released at later times. Therefore, it was concluded that encapsulation of limonene into the polymer-blendparticles could not effectively help in prolonging the release of this fragrance. However, release behaviors of all other five fragrances could be prolonged by this polymeric encapsulation but to different extents. It should be pointed out here that each release profile of the unencapsulated fragrance shown in Fig. 5 was obtained from the mixture of fragrance and polymer-blend, not from the pure fragrance (see details in Section 2). Interactions between fragrance molecules and polymer matrix could delay the volatilization of the fragrance. It was noticed that after being encapsulated, the vapor pressure and boiling point of the fragrance were no longer the major factors determining the release rate. Rather the release characteristics are likely to be governed by the ability of the fragrance to diffuse through the polymer matrix, and different fragrance molecules possess different chemical interactions with the polymer-blend-shell, and thus diffusion rates.

#### 4. Conclusion

We have successfully demonstrated that a blend of HPMC, PV(OH) and EC can be used to encapsulate five (out of six) diverse fragrances with different functional groups and act as fragrance reservoirs for a more sustained controlled release. Through solvent displacement (in this case, water displacing ethanol), fragrance encapsulation with a ≥80% EE was obtained at a fragrance:polymer ratio of 1:1 to give an aqueous suspension of the fragranceencapsulated nanospheres (diameter of less than 450 nm) at a maximum concentration of 16,000 ppm or 1.6% (w/v) suspension. The process was applicable to all six tested fragrances, representative of compounds with different chemical functionalities, but one, limonene (an unsaturated hydrocarbon), showed no significant retention in the nanoparticles. Smaller particles could be prepared at lower polymer concentrations, while preparation at higher polymer concentrations (32,000 ppm) gave microparticles (diameter > 1000 nm), but at the encapsulation efficiency of  $\sim$ 51%. Different fragrance molecules showed different release characteristic from the polymeric spheres, i.e., limonene showed the fastest release while eucalyptol and menthol showed the slowest release, and the release rate of the encapsulated fragrance was independent of the fragrance's vapor pressure.

#### Acknowledgements

The authors thank the Commission of Higher Education-Thailand Research Fund (BRG5280004) and the Ratchadaphisek-somphot endowment fund from Chulalongkorn University for financial support.

#### References

- Bachtsi, A.R., Kiparissides, C., 1996. Synthesis and release studies of oil-containing poly(vinyl alcohol) microcapsules prepared by coacervation. J. Control. Release 38. 49–58.
- Chang, C.P., Dobashi, T., 2003. Preparation of alginate complex capsules containing eucalyptus essential oil and its controlled release. Colloids Surf. B: Biointerfaces 32, 257–262.
- Edris, A., Bergnståhl, B., 2001. Encapsulation of orange oil in a spray dried double emulsion. Nahrung 45, 133–137.
- Fukumoto, S., Sawasaki, E., Okuyama, S., Miyake, Y., Yokogoshi, H., 2006. Flavor components of monoterpenes in citrus essential oils enhance the release of monoamines from rat brain slices. Nutr. Neurosci. 9, 73–80.
- Hwang, J.S., Kim, J.N., Wee, Y.J., Yun, J.S., Jang, H.G., Kim, S.H., Ryu, H.W., 2006a. Preparation and characterization of melamine–formaldehyde resin microcapsules containing fragrant oil. Biotechnol. Bioprocess Eng. 11, 332–336.
- Hwang, J.S., Kim, J.N., Wee, Y.J., Jang, H.G., Kim, S.H., Ryu, H.W., 2006b. Factors affecting the characteristics of melamine resin microcapsules containing fragrant oils. Biotechnol. Bioprocess Eng. 11, 391–395.
- Jean-Pierre, B., Joel, R., Curtis, T., 1998. Method for preparing microcapsules of active substances coated with a polymer and novel microcapsules in particular resulting from the method. WO 98/13136 A1.
- Karlberg, A.T., Magnusson, K., Nilsson, U., 1992. Air oxidation of p-limonene (the citrus solvent) creates potent allergens. Contact Dermatitis 26, 332–340.
- Lai, F., Wissing, S.A., Müller, R.H., Fadda, A.M., 2006. Artemisia arborescens L essential oil-loaded solid lipid nanoparticles for potential agricultural application: preparation and characterization. AAPS PharmSciTech 7 (1), article no. 2.
- Markus, A., Linder, C., 2004. Encapsulated essential oils. WO 2004/098767 A1.
- Matura, M., Sköld, M., Börje, A., Andersen, K.E., Bruze, M., Frosch, P., Goossens, A., Johansen, J.D., Svedman, C., White, I.R., Karlberg, A.T., 2005. Selected oxidized fragrance terpenes are common contact allergens. Contact Dermatitis 52, 320–328.
- Matura, M., Sköld, M., Börje, A., Andersen, K.E., Bruze, M., Frosch, P., Goossens, A., Johansen, J.D., Svedman, C., White, I.R., Karlberg, A.T., 2006. Not only oxidized R-(+)-but also S-(-)-limonene is a common cause of contact allergy in dermatitis patients in Europe. Contact Dermatitis 55, 274–279.
- Moretti, M.D., Sanna-Passino, G., Demontis, S., Bazzoni, E., 2002. Essential oil formulations useful as a new tool for insect pest control. AAPS PharmSciTech 3 (2), article no. 13.
- Morita, T., Jinno, K., Kawagishi, H., Arimoto, Y., Suganuma, H., Inakuma, T., Sugiyama, K., 2003. Hepatoprotective effect of myristicin from nutmeg (Myristica fragrans) on lipopolysaccharide/p-galactosamine-induced liver injury. J. Agric. Food Chem. 51, 1560–1565.
- Ouall, L., Lahoussine, D., 2006. Process for production nano-capsules containing a fragrance. WO 2006/027664 A2.
- Rodrigues, S.N., Fernandes, I., Martins, I.M., Mata, V.G., Barreiro, F., Rodrigues, A.E., 2008. Microencapsulation of limonene for textile application. Ind. Eng. Chem. Res. 47. 4142–4147.
- Scarfato, P., Avallone, E., Iannelli, P., De Feo, V., Aderno, D., 2007. Synthesis and characterization of polyurea microcapsules containing essential oils with antigerminative activity. J. Appl. Polym. Sci. 105, 3568–3577.
- Soper, J.C., Kim, Y.D., Thomas, M.T., 2000. Method of encapsulating flavours and fragances by controlled water transport into microcapsules. US Patent 6,106,875. Wang, C.X., Chen, S.L., 2005. Fragrance-release property of  $\beta$ -cyclodextrin inclusion
- compounds and their application in aromatherapy. J. Ind. Text. 34, 157–166. Wang, P., Zhu, Y., Yang, X., Chen, A., 2008. Prolonged-release performance of perfume encapsulated by tailoring mesoporous silica spheres. Flavour Frag. J. 23, 29–34.

#### ORIGINAL PAPER

# Controlling the morphology of self-assemble chitosan through derivatization

Pimsiree Deemak · Supason Wanichwecharungruang · Rutchanee Nonthabenjawan · Chotiros Jornjangjun

Received: 14 October 2009 / Accepted: 25 March 2010 © Springer Science+Business Media B.V. 2010

**Abstract** Twenty chitosan derivatives with systematic variations in their chemical functionalities were prepared, by grafting phthaloyl groups, various cinnamoyl derivatives, and poly(ethylene oxide) moieties onto the chitosan backbones and then their self-assembled architectures were investigated. Derivatives with a high level of 2,4,5-trimethoxycinnamoyl substitution gave rod-shape and/or planar-shape architectures through solvent displacement, whilst the other derivatives gave spheres. Transformation of self-assembled architectures was also observed in derivative with an appropriate level of 2,4,5-trimethoxycinnamoyl substitution.

**Keywords** Chitosan · Self-assembly · Nanosphere · Nanorod · Cinnamate

**Electronic supplementary material** The online version of this article (doi:10.1007/s10965-010-9432-2) contains supplementary material, which is available to authorized users.

P. Deemak · C. Jornjangjun Program of Petrochemistry and Polymer Science, Chulalongkorn University, Bangkok 10330, Thailand

P. Deemak National Center of Petroleum, Petrochemicals and Advanced Materials, Chulalongkorn University, Bangkok 10330, Thailand

Published online: 07 April 2010

S. Wanichwecharungruang (☒) · R. Nonthabenjawan Sensor Research Unit, Department of Chemistry, Faculty of Science, Chulalongkorn University, Bangkok 10330, Thailand e-mail: psupason@chula.ac.th

#### Introduction

A diverse variety of amphiphilic polymeric materials have been synthesized and self-assembled into numerous supramolecular architectures [1–4]. Noncovalent interactions amongst the polymer chains themselves and with the surrounding molecules, play an important role in determining their self-assembled architectures [5, 6]. Such a delicate balance is a function of several variables, such as the polymer structural composition and concentration [7], ionic strength [8], and solvent molecules [9, 10]. Understanding of these interactions can lead to not only a good design of synthetic nanoscale-assemblies, but also help facilitate an understanding of how nature shapes various organelles and biological components into their specific morphologies starting from biomolecules and biopolymers [3, 11–15].

Reports of self-assembling block copolymers have involves the effects of changes in the molecular weight or in the ratio between the hydrophobic and hydrophilic blocks [16–18]. Micelle-type polymeric nanospheres have been used as drug carriers and nanosize-reaction-containers. For these applications to be successful, association amongst nanoparticles must be prevented. We, however, are looking at the system in the opposite direction; that is where association amongst nanoparticulates is being encouraged and investigated. In facts, such transformation has been speculated for amphiphilic block copolymers [1, 7, 9], whilst the only report that has captured such coupling was the self-assembling of metal-coordination polymers, where the cubical suprastructures were demonstrated to be a result of the association amongst rod-shape-suprastructures [19]. To our best knowledge, this type of investigation on grafted



polymer has, however, never been reported, thus in this paper, associations amongst self-assembled architectures of grafted chitosan polymer coupled with morphological transformations at room temperature in water was investigated. In addition, we demonstrate that fine-tuning of the grafted functional groups on the polymeric structure can be used to control the morphology of the self-assembled entities.

#### **Experimental**

#### Materials

Chitosan (Mw 110,000) was from Seafresh Chitosan (Lab), Co., Thailand. Methoxy poly(ethylene glycol) methyl ether (PEO) of nominal Mw 5,000 was from Fluka Chemical Company (Buchs, Switzerland). 1-Ethyl-3(3-dimethyl-aminopropyl)carbodiimide (EDCI), 4-methoxycinnamic acid and 1-hydroxy benzotriazole (HOBt) were from Acros Organics (New Jersey, USA). Phthalic anhydride was from Carlo Erba Reagent (Val de Reuil, France).

#### Synthesis of chitosan derivatives

Twenty chitosan derivatives were synthesized by the grafting of phthaloyl moieties, various cinnamoyl derivative moieties and PEO onto chitosan chains (Scheme 1). Cinnamoyl derivatives used were cinnamoyl, 4-methoxycinnamoyl and 2,4,5-trimethoxycinnamoyl moieties. Substitution degrees were determined using <sup>1</sup>H NMR data and C/N weight ratios from elemental analysis [20]. Synthetic and characterization details of each derivative could be found in the supporting information.

#### Self-assembly

The self-assembly of each polymer into nanoparticulates was induced by solvent displacement. For this, 24 mg of the polymer were dissolved in 40 mL of DMF and then dialyzed against water (5×1000 mL) using a regenerated cellulose tubular membrane (CelluSep T4, MWCO 12000–14000, 75 mm flat width, 17.9 mL/cm volume capacity, Membrane Filtration Products, Seguin, TX, USA). After dialysis, the suspension in the dialysis bag was periodically sampled (0.5 ml) for SEM and TEM analysis.

#### SEM and TEM analysis

TEM and SEM photographs were acquired on a transmission electron microscope (JEM-2100, JEOL, Japan) with an

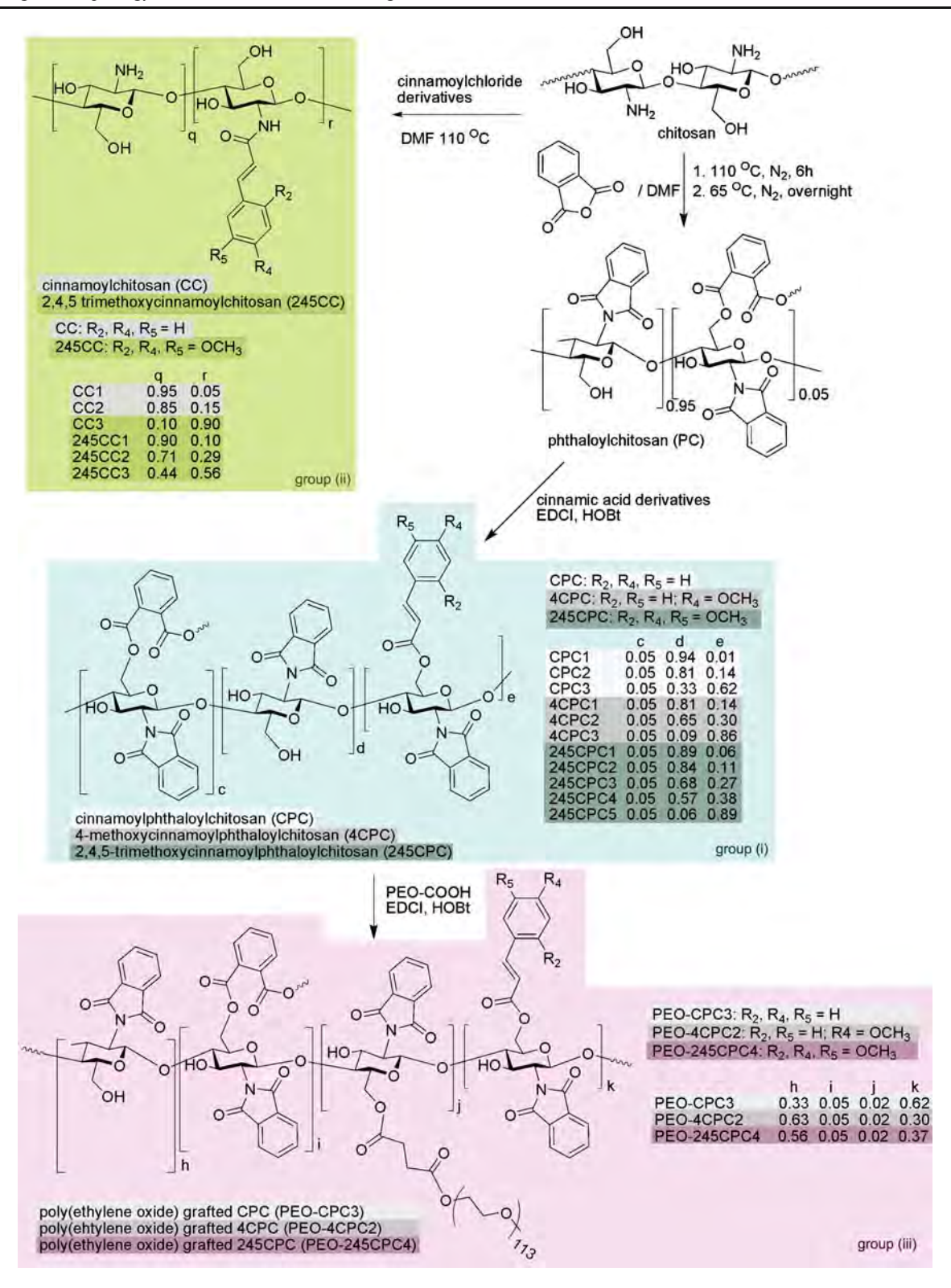
accelerating voltage of 100–120 kV in conjunction with selected area electron diffraction (SAED) and scanning electron microscope (JSM-6400, JEOL, Japan), respectively. A drop of the nanoparticle suspension was placed on a glass slide, dried and coated with a gold layer under vacuum at 10–15 kV for 60–90 s. Visualization was done at the accelerating voltage of 15 kV.

#### Results and discussion

The twenty chitosan derivatives were successfully prepared and their structures were characterized through spectroscopic analysis together with elemental analysis (see supporting information for characterization details). The synthesized derivatives can be grouped by the grafted functionalities into (i) chitosan grafted with phthaloyl and cinnamoyl derivatives (three cinnamoylphthaloylchitosans (CPC), three 4-methoxycinnamoylphthaloylchitosans (4CPC), and five 2,4,5-trimethoxycinnamoylphthaloylchitosans (245CPC)), (ii) chitosan grafted with cinnamoyl derivatives (three cinnamovlchitosans (CC) and three 2,4,5-trimethoxycinnamoylchitosans (245CC)) and (iii) chitosan grafted with phtaloyl, cinnamoyl derivative and poly(ethylene oxide) or PEO moieties (PEO-grafted cinnamoylphthaloylchitosan (PEO-CPC), PEO-grafted 4methoxycinnamoylphthaloylchitosan (PEO-4CPC) and PEO-grafted 2,4,5-trimethoxycinnamoylphthaloylchitosan (PEO-245CPC)) (see Scheme 1). They were allowed to self-assemble into suprastructures by solvent displacement. SEM photographs of 245CPC5 (DS of 2,4,5trimethoxycinnamoyl moiety=0.89) showed the presence of connected 200 nm spheres (Fig. 1a). Interestingly, after the suspension was left for a few days, flexible long rods (Fig. 1b-c) were detected, totalling about 80% and after a few weeks coral-shaped architectures (Fig. 1d-f) were predominated in the same suspension, totalling approximately 70% of the total mass. This indicated a slow shape transformation of the 245CPC5-self-assembled structures. By repeating the experiments at similar concentration (self-assembly of 245CPC5 polymer by dialysis with periodically sampling to SEM analysis), it could be confirmed that spheres, rods and coral shapearchitecures could always be observed in a similar sequence.

Within the group (i) derivatives, 245CPC4 (DS of 2,4,5-trimethoxycinnamoyl moiety=0.38), uniform nanorods were observed (Fig. 2a), whilst 245CPC3 (DS of 2,4,5-trimethoxycinnamoyl moiety=0.27) produced 50 nm spherical micelles (totalling about 90% of the shapes seen, Fig. 2b). Aggregation of the 245CPC3 spheres into straight microrods was also observed (totalling about 20% of the shape seen, Fig. 2c). Magnification at the surface of some





Scheme 1 Synthesis of the twenty chitosan derivatives

of the microrods implied that their walls were made of associated nanospheres (Fig. 2d and e). In facts, this observation implied shape association of the suprastructures. Other group (i) derivatives (245CPC2 and 245CPC1,

DS of 2,4,5-trimethoxycinnamoyl moiety of 0.11 and 0.06, respectively) were observed to self-assemble into only spherical particles. For group (ii) derivatives, self-assembly of 245CC2 and 245CC3 (chitosan grafted with 2,4,5-



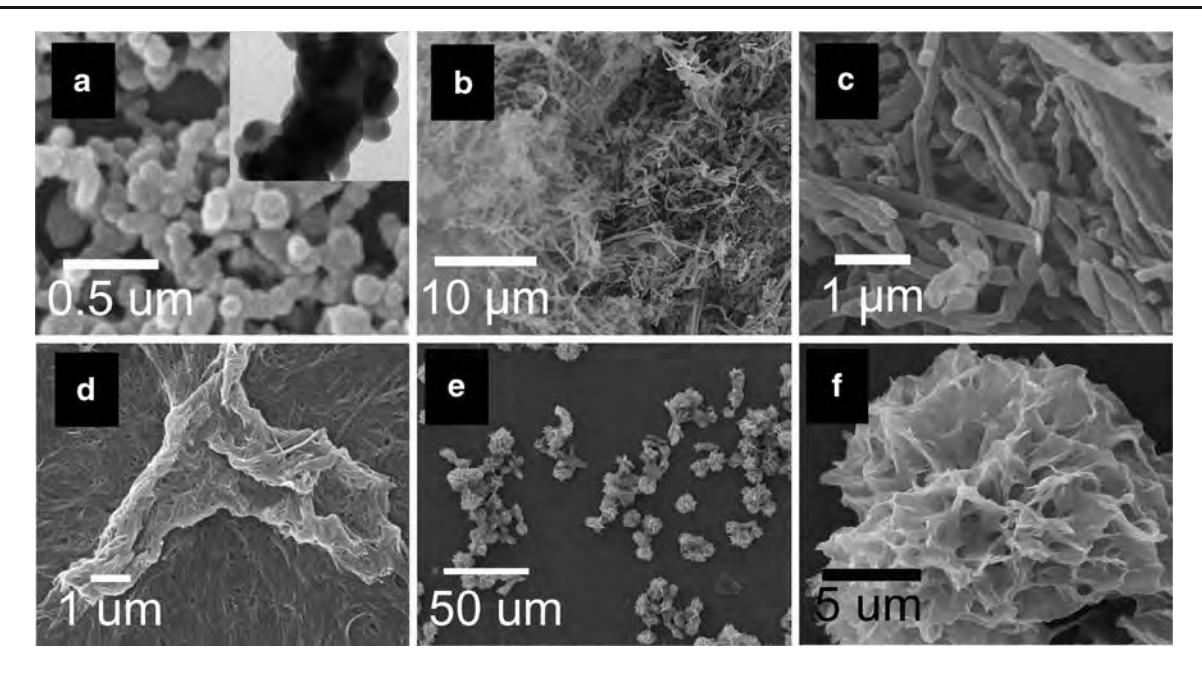
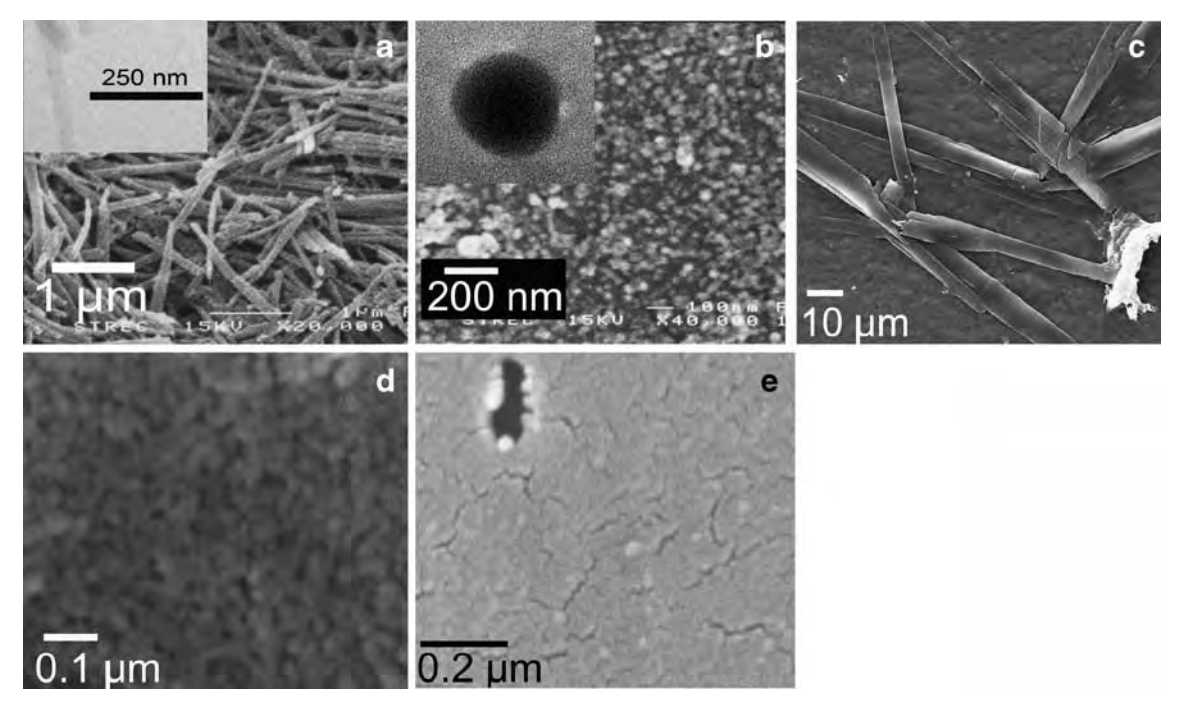


Fig. 1 Representative SEM photographs showing the morphological transformation of 245CPC5. (a) SEM images of the freshly prepared self-assembled structures. After aging at 25°C, (b and c) the line-up-

particles then transformed into rod-like architectures and (d-f) then the rods associated into coral shapes. TEM image of the freshly prepared structures is shown as an inset of a

trimethoxycinnamoyl groups at DS values of 0.29 and 0.56) resulted in a mixture of spheres and rods. (Fig. 3) while 245CC1(DS of 2,4,5-trimethoxycinnamoyl moiety=0.10) gave only spheres.

SEM monitoring of suspensions obtained from the solvent-displacement processes of other chitosans derivatives from both group (i) and group (ii) (CC1, CC2, CC3, 245CC1, CPC1, CPC2, CPC3, 4CPC1, 4CPC2 and

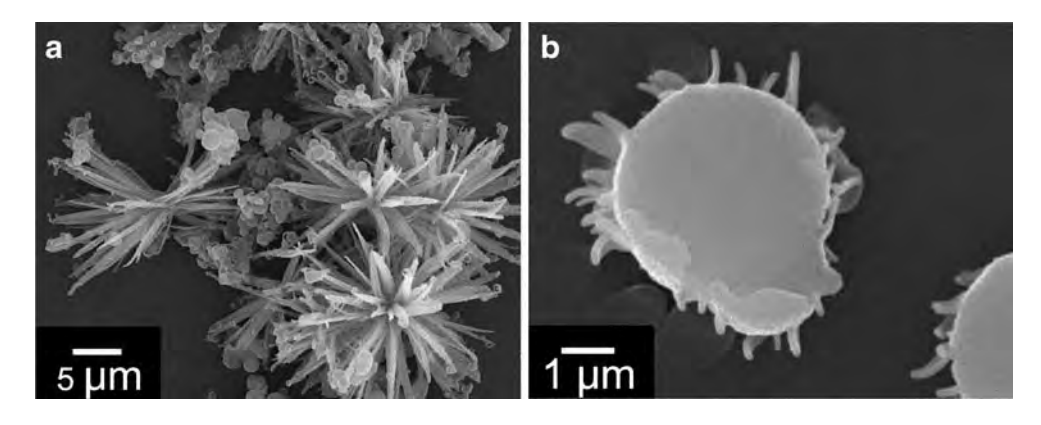


**Fig. 2** Representative SEM photographs showing self-assembled particulates obtained by displacing DMF with water from 600 ppm polymer solutions of (a) 245CPC4 and (b–e) 245CPC3 where **d** and **e** 

are the magnifications at the surface of the microrods shown in  $\boldsymbol{c}$ . TEM photographs are shown as insets



Fig. 3 Representative SEM photographs showing self-assembled particulates obtained by displacing DMF with water from 600 ppm polymer solutions of (a) 245CC3 and (b) 245CC2



4CPC3) revealed only nanospheres regardless of cinnamoyl substitution degree.

Since all cinnamoylchitosan and 4-methoxycinnamoylchitosan derivatives gave spheres while 2,4,5-trimethoxycinnamoylchitosan derivatives with a DS of ≥0.27 (245CPC3, 245CPC4, 245CPC5, 245CC2 and 245CC3), gave either rod- or coral-shaped architectures, it was concluded that the presence of the 2,4,5-trimethoxycinnamoyl moieties was responsible for the deviations away from spherical structures.

The previously proposed theory, based on works with block copolymers, has stated that the ratio of hydrophobic to hydrophilic contents of amphiphilic polymers was one of the critical factors that determines the shape of selfassembled suprastructures [16] and with higher hydrophobic to hydrophilic ratio, planar of bilayer assembly and rod shape were more likely to be found. The results here, however, showed that chitosan derivatives with cinnamovl or 4-methoxycinnamoyl substitutions gave only spherical self-assembled suprastructures regardless of the substituion degree. This indicates that the hydrophobic to hydrophilic ratio is not the only critical factor influencing the shape of the self-assembled structures. Rod-shaped-assembled architectures were found in 245CPC3 while a hybrid of planar bilayer and rod (coral shape) was observed in 245CPC5. It is speculated that the steric 2,4,5-trimethoxycinnamoyl moieties probably affect the chain topology in a way that reduces the conformational entropy, increases the chain stiffness, and encourages a more rigid but less compact molecular packing of the hydrophobic part, and thus encourages planar and rod-shape formation over spherical micellar particles. The steric bulkiness of the 2,4,5-trimethoxyeinnamoyl group probably causes a very slow shuffling amongst the various interactions between the associated selfassembled structures. It should be noted here that the high stiffness of the 2,4,5-trimethoxycinnamoyl moities, comparing to 4-methoxycinnamoyl moities, is consistent with the fact that trans/cis photoisomerization of 4-methoxycinnamoyl group can occur more easily than that of 2,4,5-trimethoxyeinnamoyl group [21]. This would explain why slow shape transformation was witnessed in 245CPC5.

All the above discussed molecular structures of the polymer were not directly observed but rather speculated through the morphology observed by the SEM and TEM. In addition, cryogenic technique was not employed in this study, thus all the observed morphology must be stable at room temperature and must be able to withstand the SEM process. Up to this point, it is appropriate to say that the shape transformation observed in this work (for 245CPC5) is a result of a very slow transformation at room temperature. No shape transformation observed for other derivatives, was probably a result of a fast equilibrium achivement of their morphological shapes at room temperature.

It can, therefore, be concluded that both the hydrophobic to hydrophilic ratio of the polymer structure and the steric bulkiness of the grafted moieties, are the two critical factors determining shapes of the self-assembled structures.

All three derivatives with attached PEO chains, PEO-CPC3, PEO-4CPC2 and PEO-245CPC4, gave nanospheres with much better water dispersability compared to their corresponding derivatives with no PEO attached, CPC3, 4CPC2 and 245CPC4, respectively. Since no permanent agglomerated pieces could be detected, it was confirmed that with enough hydrophilic corona around the spheres, merging amongst spheres was unlikely because of the increased stability of each sphere.

#### Conclusion

Here we report a phenomena where different self-assembled architectures were observed from chitosan grafted with different functionalities. Amongst twenty grafted chitosan derivatives with systematic variation of the grafted moieties, only those grafted with enough 2,4,5-trimethoxycinnamoyl moieties gave planar and/or rod-shape assembly while other gave spheres. In addition, with the right 2,4,5-trimethoxycinnamoyl substitution degree, shape transformation of the self-assembled suprastructures could also be observed.



**Acknowledgements** We thank the Commission on Higher Education-Thailand Research Fund (BRG5280004) and the Graduate School of Chulalongkorn University for financial support.

#### References

- 1. Kinning DJ, Winey KI, Thomas EL (1988) Macromolecules 21:3502
- 2. Zhang L, Eisenberg A (1995) Science 268:1728
- Ringsdorf H, Schlarb B, Venzmer J (1988) J Angew Chem-Int Edit 27:113
- 4. Szostak JW, Bartel DP, Luisi PL (2001) Nature 409:387
- Ilhan F, Galow TH, Gray M, Clavier G, Rotello VM (2000) J Am Chem Soc 122:589
- 6. Bhattacharya S, De S (1999) Langmuir 15:3400
- 7. Yu Y, Eisenberg A (1997) J Am Chem Soc 119:8383

- 8. Zhang L, Eisenberg A (1996) Macromolecules 29:8805
- 9. Ding J, Liu G (1999) Macromolecules 32:8413
- 10. Peng X, Zhang L (2007) Langmuir 23:10493
- Kadler KE, Holmes DF, Trotter JA, Chapman JA (1996) Biochem J 316:1
- 12. Koch K, Ensikat HJ (2008) Micron 39:759
- Sunde M, Kwan AHY, Templeton MD, Beever RE, Mackay JP (2008) Micron 39:773
- 14. Zhao X, Pan F, Lu JR (2008) Progress Natural Sci 18:653
- Yi H, Wu LQ, Bentley WE, Ghodssi R, Rubloff GW, Culver JN, Payne GF (2005) Biomacromolecules 6:2881
- 16. Zhang L, Eisenberg A (1998) Polym Adv Technol 9:677
- 17. Zhang L, Eisenberg A (1999) Macromolecules 32:2239
- 18. Jain S, Bates FS (2003) Science 300:460
- 19. Jung S, Oh M (2008) J Angew Chem-Int Edit 47:2049
- Anumansirikul N, Wittayasuporn M, Klinubol P, Tachaprutinun A, Wanichwecharungruang SP (2008) Nanotechnology 19:205101
- Monhaphol T, Albinsson B, Wanichwecharungruang SP (2007) J Pharm Pharmacol 59:279

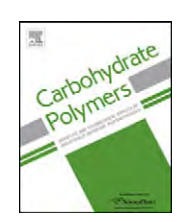


ELSEVIER

Contents lists available at ScienceDirect

### Carbohydrate Polymers

journal homepage: www.elsevier.com/locate/carbpol



# Fragrant chitosan nanospheres: Controlled release systems with physical and chemical barriers

Thapakorn Tree-udom  $^{a,b}$ , Supason P. Wanichwecharungruang  $^{c,*}$ , Jiraporn Seemork  $^a$ , Sunatda Arayachukeat  $^d$ 

- <sup>a</sup> Program of Petrochemistry and Polymer Science, Faculty of Science, Chulalongkorn University, Bangkok 10330, Thailand
- <sup>b</sup> National Center of Petroleum, Petrochemicals and Advanced Materials, Chulalongkorn University, Bangkok 10330, Thailand
- <sup>c</sup> Department of Chemistry, Faculty of Science, Chulalongkorn University, Bangkok 10330, Thailand
- <sup>d</sup> Program of Macromolecular Science, Faculty of Science, Chulalongkorn University, Bangkok 10330, Thailand

#### ARTICLE INFO

#### Article history: Received 18 May 2011 Received in revised form 23 June 2011 Accepted 26 June 2011 Available online 6 July 2011

Keywords: Chitosan Fragrance Controlled release Nanospheres Imine Profragrance

#### ABSTRACT

Existing fragrance controlled release systems are either based on a physical barrier, such as entrapment of the fragrant molecules inside the micro- or nano-spheres, or a chemical barrier, such as labile chemical bonds. Here, we propose a system with a combination of the two approaches but fabricated *via* a simple surfactant free one step process using biodegradable chitosan polymer. The fabrication process involves a chemical reaction to covalently link the fragrant aldehydes with the amine functionalities of the N-succinylchitosan (NS-chitosan) carriers that simultaneously leads to an ultrasonic aided reorganization of the spheres in such a way that the grafted entities are at the particles' core. Localization of the grafted mine moieties at the core of the imine-NS-chitosan particles was confirmed by X-ray photoelectron spectroscopy (XPS) analysis. The obtained fragrant chitosan nanospheres not only showed up to 85-fold fragrance prolongation but also dispersed well in water.

© 2011 Elsevier Ltd. All rights reserved.

#### 1. Introduction

Current fragrance controlled release systems can be categorized into two groups, those that use (i) a physical barrier system in which the diffusion of the fragrant molecules are controlled by entrapping them into a polymeric matrix (carrier), and (ii) a chemical barrier system in which the fragrances are modulated *via* chemical derivatization into more robust forms but where this is reversible so that the fragrant molecules can be regenerated in a controllable manner (Herrmann, 2007). Both strategies have been employed in the flavor & fragrance industry.

Various labile chemical bonds (chemical barriers) have been employed for the controlled release of a range of fragrant molecules, such as (a) the controlled release of alcohol using neighboring-group-assisted ester hydrolysis (De Saint Laumer, Frerot, & Herrmann, 2003), (b) the use of Schiff bases to help control the release of aldehydes and ketones (Kamogawa, Mukai, Nakajima, & Nanasawa, 1982; Turin, 2006; Muzzarelli & Ilari, 1994), (c) the use of Norrish type-II photofragmentation to control the delivery of alkenes and acetophenones (Levrand & Herrmann, 2002), car-

bonyl compounds (Levrand & Herrmann, 2007) and aldehydes and ketones (Rochat, Minardi, De Saint Laumer, & Herrmann, 2000), (d) the use of aminal (Godin, Levrand, Trachsel, Lehn, & Herrmann, 2010) or acetal (Morinaga, Morikawa, Wang, Sudo, & Endo, 2009) groups for the controlled release of aldehydes, (e) the use of hydrazone for the delivery of aldehydes and ketones (Levrand, Fieber, Lehn, & Herrmann, 2007; Levrand, Ruff, Lehn, & Herrmann, 2006), (f) the photo-assisted release of aldehydes from  $\alpha$ -acetoxy ethers (Robles & Bochet, 2005) and (g) the slow release of enones through a Retro-Michael addition reaction (Fehr & Galindo, 2005).

Examples of physical barrier used in the prolongation of fragrances include double emulsion system (Edris & Bergnståhl, 2001), cyclodextrin host (Wang & Chen, 2005a, 2005b), mesoporous silica spheres (Wang, Zhu, Yang, & Chen, 2008), solid lipid nanoparticles (Souto & Müller, 2008), multi-arm star block copolymer (Ternat et al., 2007), various other synthetic polymers formed by miniemulsion polymerization (Landfester, 2009) and in situ polymerization (Lee, Lee, Cheong, & Kim, 2002), amphipilic crosslinked polymer network (Brown, Bergquist, Ferm, & Wooley, 2005) and various carbohydrates (Hambleton, Fabra, Debeaufort, Dury-Brun, & Voilley, 2009; Korus, Tomasik, & Lii, 2003; Paula, Sombra, Cavalcante, Abreu, & De Paula, 2011; Quellet, Schudel, & Ringgenberg, 2001). Fragrance prolongation technology for personal care and household product applications should not only

<sup>\*</sup> Corresponding author. Tel.: +662 2187634; fax: +662 2541309. E-mail address: psupason@chula.ac.th (S.P. Wanichwecharungruang).

provide long lasting fragrance but also possess no harm to the environment. The use of non-biodegradable non-biocompatible melamine-formaldehyde microspheres may pose environmental problem considering that they are now being used in many household products including laundry detergents and fabric softeners. However, reported systems based on biodegradable carbohydrates, such as alginate, starch and chitosan, in the form of water dispersible nanoparticles or microparticles neither provide enough physical stability nor show satisfactory fragrant prolongation.

Here, for the first time, we demonstrate the fabrication of long lasting fragrance controlled release systems which contain both chemical and physical barriers, based on the biocompatible biodegradable non-toxic chitosan polymer. The fabricated materials are double barrier nanospheres in which fragrant aldehyde molecules are chemically linked to the N-succinylchitosan (NS-chitosan) and at the same time embedded in the particles' core.

#### 2. Materials and methods

#### 2.1. Materials

Chitosan with a degree of deacetylation of 85% ( $M_v = 30,000$  Da) was obtained from Seafresh Chitosan (Lab) Co., Ltd. (Bangkok, Thailand). Succinic anhydride, vanillin, citral and citronellal were purchased from Acros organics (Geel, Belgium). Cinnamaldehyde was purchased from Aldrich (Steinheim, Germany). All other chemicals were analytical grade reagents and were obtained locally.

#### 2.2. Synthesis of N-succinvlchitosan (NS-chitosan) (Scheme 1)

NS-chitosan was synthesized based on the previously described method (Zhu, Yuan, & Lu, 2007), with a slight modification. Chitosan (2.01 g) was dissolved in 70 ml of 2% (v/v) acetic acid. Then succinic anhydride (0.25 g) in 10 ml of acetone was dropped into the chitosan solution and the mixture was stirred at room temperature overnight before being precipitated, and repeatedly washed (after filtration) with an excess amount of acetone. The product was dried in desiccators at room temperature. The dry product was analyzed by attenuated total reflectance-Fourier transform infrared spectroscopy (ATR-FTIR; Nicolet 6700 FT-IR spectrometer, Thermo Electron Corporation, Madison, WI, USA), [1H]-NMR in D<sub>2</sub>O (400 MHz Varian mercury spectrometer, Variance Inc., Palo Alto, USA), X-ray diffraction spectrometry (XRD), using a Cu Kα radiation source and operating at 40 kV and 30 mA (Rigaku DMAX 2200/Ultima<sup>+</sup> diffractometer, Rigaku International Corporation, Tokyo, Japan) and UV-Vis spectroscopy in a one centimeterpath-length-quartz cell, thermostated at 25 °C (UV 2500 UV-Vis spectrophotometer, Shimadzu Corporation, Kyoto, Japan).

N-succinylchitosan (NS-chitosan). White powder. 75% yield. Degree of succinyl grafting: 0.18. [ $^1$ H]-NMR (D $_2$ O, 400 MHz,  $\delta$ , ppm): 2.01 (H of acetyl groups), 2.42–2.50 (methylene protons of the succinyl moiety), 2.80 (H2 of glucosamine, GlcN), 3.50–3.92 (H2′ of N-acetylglucosamine, GlcNAc, H3, H4, H5 and H6 of Glc-NAc and GlcN) and 4.54 (H1 of GlcNAc and GlcN). ATR-FTIR (cm $^{-1}$ ): 3282 (N–H stretching and O–H stretching vibration), 2864 (C–H stretching vibration), 1652 (amide I (C=O stretching)), 1555 (amide II), 1406 (symmetric stretching vibration of COO $^-$  and amide III), 1319 (amide III (C–N stretching)), 1143 (C–O–C stretching vibration) and 1027 (C–O stretching vibration). UV–Vis (distilled water, 25 °C)  $\lambda_{max}$ : 252 nm,  $\varepsilon$ : 0.0278 M $^{-1}$  cm $^{-1}$  per monomeric unit.

#### 2.3. Characterization of the self-assembled NS-chitosan

A transparent colloidal suspension of NS-chitosan was easily obtained by simply dispersing the NS-chitosan in water: it was dried in desiccators at room temperature. The dry sample was

subjected to the following analyses: scanning electron microscopy (SEM; ISM-6400 scanning electron microscope, IEOL, Tokyo, Japan), following gold coating under vacuum at 15 kV for 90 s and visualization at an accelerating voltage of 15 kV; atomic force microscopy (AFM; Nanoscope IV scanning probe microscope operated in tapping mode, Veeco Metrology Group, California, USA); transmission electron microscopy (TEM; JEM-2100, JEOL, Tokyo, Japan) operated at 100–120 kV; X-ray photoelectron spectroscopy (XPS; Kratos AXIS Ultra DLD instrument, Kratos, Manchester, England) using a monochromatic Al K\alpha X-ray source at 1486.6 eV and operated at 150 W, 15 kV and 10 mA with a base pressure in the XPS analysis chamber of  $5 \times 10^{-8}$  Torr. High resolution spectra (C1s and N1s) were acquired using a pass energy of 20 eV and 0.1 eV energy steps. All binding energies (BEs) were referenced to the hydrocarbon C1s peak at 285 eV. In addition, an aqueous suspension of NS-chitosan was used to evaluate the hydrodynamic diameter and zeta potential values (Zetasizer nanoseries model S4700, Malvern Instruments, Worcestershire, UK).

#### 2.4. Synthesis of imine-NS-chitosan (Scheme 1)

NS-chitosan nanospheres were allowed to react with aldehyde at a 1:3 (w/w) ratio of aldehyde: NS-chitosan. The procedure involved adding 4 ml of alcoholic solution of 20% (v/v) aldehyde drop-wise to the aqueous NS-chitosan particle suspension (16 ml, 60 mg) under ultrasonic conditions. The mixture was further ultrasonicated (40 kHz at 30 °C) for 4h. The product was dried in desiccators at room temperature and subjected to ATR-FTIR, SEM, AFM, TEM and XPS analyses.

*N*,*N'*-vanillidene-succinylchitosan nanospheres. Degree of vanillin substitution: 0.34. ATR-FTIR (cm<sup>-1</sup>): 3282 (N–H stretching and O–H stretching vibration), 2867 (C–H stretching vibration), 1635 (C=N stretching vibration), 1592 and 1512 (C=C stretching vibration of aromatic), 1555 (amide II), 1143 (C–O–C stretching vibration) and 1027 (C–O stretching vibration).

*N*,*N'*-cinnamylidene-succinylchitosan nanospheres. Degree of cinnamaldehyde substitution: 0.29. ATR-FTIR (cm<sup>-1</sup>): 3282 (N-H stretching and O-H stretching vibration), 2867 (C-H stretching vibration), 1632 (C=N stretching vibration), 1592 (C=C stretching vibration of aromatic), 1552 (amide II), 1147 (C-O-C stretching vibration) and 1024 (C-O stretching vibration).

*N,N'-citronellalidene-succinylchitosan nanospheres.* Degree of citronellal substitution: 0.38. ATR-FTIR (cm<sup>-1</sup>): 3282 (N–H stretching and O–H stretching vibration), 2870 (C–H stretching vibration), 1638 (C=N stretching vibration), 1612 (C=C stretching vibration), 1552 (amide II), 1147 (C–O–C stretching vibration) and 1024 (C–O stretching vibration).

*N,N'-citralidene-succinylchitosan nanospheres.* Degree of citral substitution: 0.38. ATR-FTIR (cm<sup>-1</sup>): 3282 (N–H stretching and O–H stretching vibration), 2874 (C–H stretching vibration), 1638 (C=N stretching vibration), 1612 (C=C stretching vibration), 1555 (amide II), 1143 (C–O–C stretching vibration) and 1027 (C–O stretching vibration).

#### 2.5. Synthesis of imine-chitosan

N-vanilidenechitosan was synthesized via the Schiff reaction carried out with a 3:1 (w/w) ratio of chitosan to vanillin. Briefly, 20 mg of vanillin in 4 ml of ethanol was added drop-wise into a 16 ml of a 0.75% (w/v) aqueous chitosan solution in 2% (v/v) acetic acid. The mixture was continuously stirred without heat for 4 h and then the obtained product was dried in desiccators at room temperature and the dry product was subjected to ATR-FTIR and XPS analyses.

*N-vanillidenechitosan.* ATR-FTIR (cm<sup>-1</sup>): 3289 (N-H stretching and O-H stretching vibration), 2877 (C-H stretching vibration),

Scheme 1. Synthesis and structural details of NS-chitosan and imine-NS-chitosan from chitosan.

1635 (C=N stretching vibration), 1592 and 1512 (C=C stretching vibration of aromatic), 1150 (C-O-C stretching vibration) and 1027 (C-O stretching vibration).

### 2.6. Critical aggregation concentration (CAC) determination by steady-state fluorescence spectroscopy

One ml of pyrene solution ( $10\,\mu\text{M}$  in methanol) was placed in a test tube and the methanol was removed by evaporation under a nitrogen atmosphere. To this,  $10\,\text{ml}$  of an aqueous solution of NS-chitosan of various concentrations (0.05, 0.10, 0.15, 0.20, 0.25, 0.30, 0.35, 0.40, 0.45, 0.50, 0.55 and  $0.6\,\text{mg/ml}$ ) was added into the test tube to obtain a  $1\,\mu\text{M}$  final concentration of pyrene. The mixture was left at room temperature overnight for equilibration before being subjected to spectrofluorometric analysis ( $\lambda_{\text{excite}}$  =  $334\,\text{nm}$ , the emission recorded from 350 to 450 nm, Varian Cary Eclipse spectrofluorometer, Varian Optical Spectroscopy Instruments, Mulgrave, Victoria, Australia). The emission spectra for imine-NS-chitosan were acquired using the same procedure as described above. All experiments were carried out in triplicate.

#### 2.7. Determination of the release profiles

For each of the Schiff base nanoparticle aqueous dispersions (pH of 5.5, prepared from 37.5 mg NS-chitosan and 12.5 mg aldehyde), 5 ml were loaded in a 20 ml flat bottom-headspace-vial (seven vials for each sample). The vials were left uncovered at 32 °C (room temperature in Bangkok). Due to water evaporation, 20% (v/v) ethanol–water was added to each vial everyday to maintain a near constant volume throughout the 16-day experiment. At the indicated times (0, 1, 2, 5, 8, 12 and 16 days), one of the seven initial

vials per sample was pH adjusted to 1.0 with 1 M HCl, filled with 15 ml of hexane and then capped with headspace aluminum crimp caps with PTFE/silicone septa. The hexane layer was then subjected to aldehyde quantification using UV–Vis spectroscopy with the aid of a calibration graph constructed from freshly prepared standard aldehyde solutions. The release of each free aldehyde was similarly tested using a sample vial containing 12.5 mg of aldehyde in 20% (v/v) ethanol–water.

The release of perfumery aldehydes was also evaluated in dry samples at  $40\,^{\circ}\text{C}$ . Here  $10\,\text{ml}$  of the freshly prepared imine-NS-chitosan nanoparticle suspensions (prepared at final concentration of aldehyde of  $2500\,\text{ppm}$ ) were left in the uncapped  $20\,\text{ml}$  flat bottom-headspace-vial for 60 days. Under this condition the samples became dry after 20 days, as no water was added into the vials, and the dry samples were kept at the same condition until the 60-day period was reached. Control samples were solutions of corresponding aldehydes at  $2500\,\text{ppm}$  (in  $20\%\,(\text{v/v})$  ethanol–water). Then after  $60\,\text{days}$ , each sample vial was filled with  $15\,\text{ml}$  of  $50\%\,(\text{v/v})$  ethanol–water, the sample was kept  $24\,\text{h}$ , and the ethanol–water phase was subjected to aldehyde quantification as described above.

#### 3. Results and discussion

### 3.1. Chemical structure of N-succinylchitosan (NS-chitosan) (Scheme 1)

Successful grafting of the succinyl group onto the chitosan chain was confirmed through (i) the [¹H]-NMR spectrum of the product with the appearance of the resonance peaks at 2.42–2.50 ppm from the methylene protons of the grafted succinyl moiety (Fig. 1),

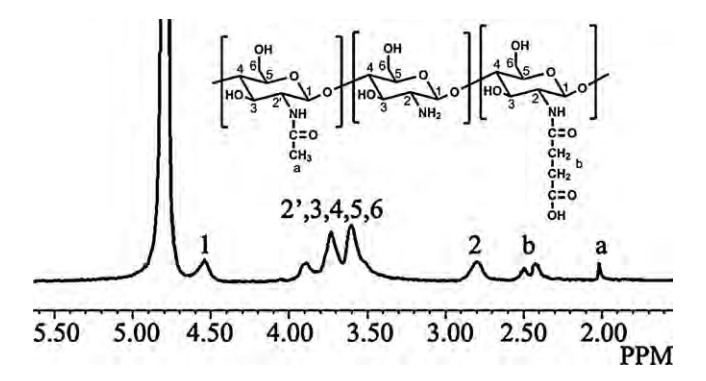


Fig. 1. [1H]-NMR spectrum of NS-chitosan.

and (ii) the FT-IR spectrum of the product with the appearance of the strong absorption peak at  $1555\,\mathrm{cm^{-1}}$  which corresponded to amide II, an evident decrease of the peak at  $1588\,\mathrm{cm^{-1}}$  (-NH<sub>2</sub> bending), and an appearance of the new absorption peak at  $1406\,\mathrm{cm^{-1}}$  corresponding to the symmetric stretching vibration of COO<sup>-</sup> and amide III (Fig. 2). The degree of grafting or succinyl substitution was estimated from the [ $^1$ H]-NMR spectrum using the ratio between the integrated area of the resonance peaks of the methylene protons of the grafted succinyl group,  $I_{\rm succinyl}$  (-C(O)CH<sub>2</sub>CH<sub>2</sub>C(O)-, 2.42–2.50 ppm) and that of the resonance peaks from hydrogen atoms at C2 in glucosamine units,  $I_{\rm H2}$  (H2 of the Gln, 2.80 ppm). Taking into account the degree of deacetylation of 0.85 for the starting chitosan, the degree of succinyl grafting was approximated to be 0.18.

Chitosan is insoluble in water at a pH >6.5 because of its compact crystalline structure and strong intra- and inter-molecular H-bondings. The XRD pattern of chitosan possesses a distinct  $2\theta$  at  $11^\circ$  and  $20^\circ$  while that of the NS-chitosan shows a broad  $2\theta$  peak at  $20^\circ$  (Fig. 3). This information implied that NS-chitosan was significantly less crystalline than chitosan, which corresponds to the change in polymer packing structure and is ascribed to the disruption of H-bondings in the chitosan chains upon succinylation, and results in the freedom of NS-chitosan chains to self-assemble into particular suprastructures, as discussed below.

#### 3.2. Morphology of NS-chitosan nanoparticles

A transparent colloidal suspension of NS-chitosan could easily be obtained by simply dispersing the NS-chitosan in water. The SEM  $\,$ 

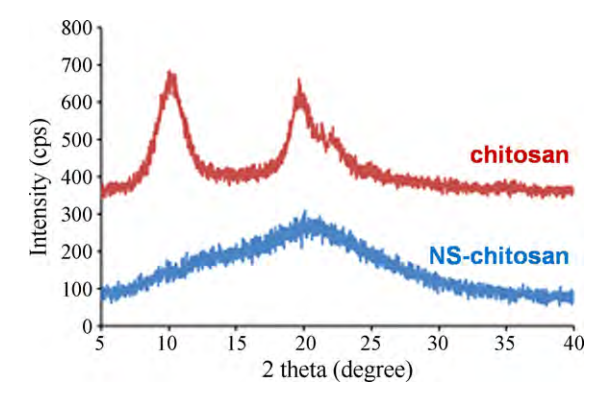


Fig. 3. X-ray powder diffraction patterns of chitosan and NS-chitosan.

and TEM images of the dried NS-chitosan preparation (Fig. 4) confirmed their spherical morphology when dry. The hydrodynamic diameter and zeta potential of the hydrated (aqueous suspension) NS-chitosan nanoparticles were  $46.3\pm0.24\,\mathrm{nm}$  (PDI of 0.1850) and  $22.3\pm2.6\,\mathrm{mV}$ , respectively (Fig. 4c).

The NS-chitosan aggregates are equilibrium structures that result from a balance of electrostatic repulsion, hydrophobic interactions and hydrogen bonding of functional groups in the NS-chitosan structures and water molecules. The hydrophilic functional groups of the NS-chitosan include the carboxylic acid, amide and free amino and hydroxy moieties on the GlcN units, while the hydrophobic functionalities include the diethylene (-CH<sub>2</sub>CH<sub>2</sub>-) units of the grafted succinyl moieties and the methylene groups of the sugar units.

#### 3.3. Synthesis and characterization of imine-NS-chitosan

The objective of this work was to convert the obtained NS-chitosan nanospheres into double barrier carriers for the controlled release of perfumery aldehydes. Here, the chemical barrier could be successfully created *via* a Schiff base formation between the NS-chitosan nanospheres and the aldehydes by directly reacting the amino groups on the NS-chitosan spheres with the aldehydes. Four perfumery aldehydes consisting of two aromatic (vanillin and cinnamaldehyde) and two aliphatic (citral and citronellal) aldehydes were used and the products obtained were N,N'-vanillidene-succinylchitosan (van-NS-chitosan), N,N'-cinnamylidene-succinylchitosan (cin-NS-chitosan), N,N'-cinnamylidene-succinylchitosan (cin-NS-chitosan), N,N'-

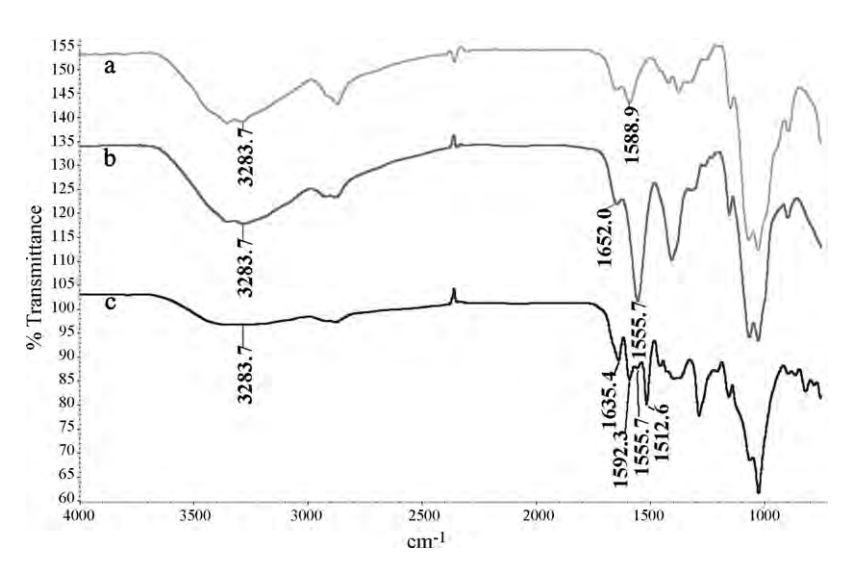


Fig. 2. ATR-FTIR spectra of (a) chitosan, (b) NS-chitosan and (c) van-NS-chitosan.

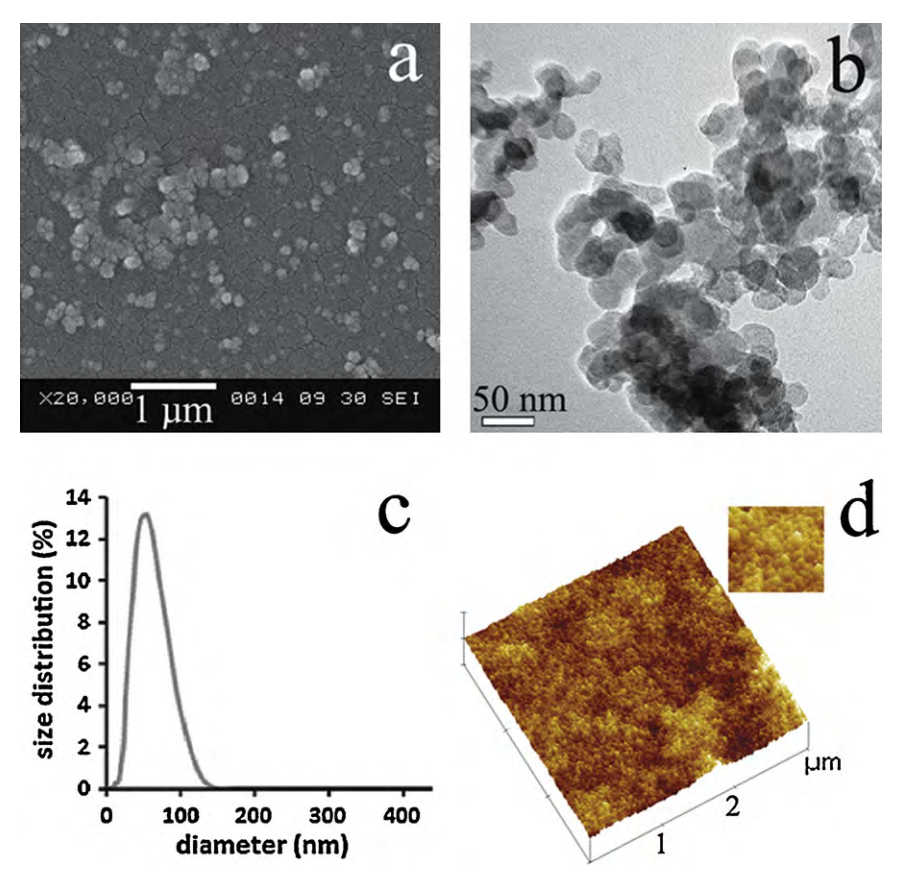


Fig. 4. (a) SEM image, (b) TEM image, (c) size distributions of NS-chitosan nanoparticles. (d) AFM image of van-NS-chitosan spheres.

citronellalidene-succinylchitosan (citro-NS-chitosan) and N,N'-citralidene-succinylchitosan (citral-NS-chitosan), respectively. Characterization of the product was carried out by FT-IR analysis: for the van-NS-chitosan product, new absorption peaks at  $1635 \,\mathrm{cm}^{-1}$ , and  $1592 \,\mathrm{and}\, 1512 \,\mathrm{cm}^{-1}$ , corresponding to the C=N stretching of imine (Schiff base) and the C=C stretching vibration of the aromatic ring, respectively, together with the disappearance of the absorption peak at 1665 cm<sup>-1</sup> that corresponds to the characteristic stretching vibration of the aryl aldehyde group, confirmed the successful synthesis and verified that no aldehyde functionality was left in the system (Fig. 2). Other Schiff base products based on cinnamaldehyde, citronellal and citral could also be successfully synthesized (see their FT-IR spectra in supplementary data). The experiment was carried out to obtain maximum mole ratio between aldehyde and NS-chitosan. Under the obtained condition, all aldehyde molecules were used up in the reaction (no aldehyde was detected in all four products, see details in supplementary data), thus it could be estimated that all four imine-NS-chitosan products possessed a degree of imine substitution in the range of approximately 0.29-0.38 (Scheme 1). To confirm this, each product was subjected to acid hydrolysis followed with quantitative analysis of the recovered aldehydes and the result agreed well with our estimation above. AFM images of the Schiff base products indicated a spherical morphology (Fig. 4d and more in supplementary data). AFM images of the Schiff base products clearly show undeformed spheres. The hydrodynamic diameter increased from 50 nm for NS-chitosan particles to 80-165 nm for the Schiff base NS-chitosan particles. The imine-NS-chitosan nanoparticles exhibited a higher zeta potential value than the NS-chitosan particles (Table 1). Comparing between aromatic aldehydes (vanillin and cinnamaldehyde) and aliphatic aldehydes (citral and citronellal), the former gave Schiff base spheres with larger diameters. This was not surprising because all four Schiff

base products possessed a similar imine substitution degree but the two aromatic imine moieties are larger than the two aliphatic ones. The size of the spheres thus corresponded to the polymer chemical structures.

#### 3.4. Critical micellar concentration

The critical aggregation concentration (CAC) of NS-chitosan and citro-NS-chitosan was determined using fluorescence spectroscopy by monitoring the assembly of the polymer in the presence of pyrene as the fluorescent probe and the results suggested the values in water of  $\approx\!0.2\,\text{mg/ml}$  for NS-chitosan and citro-NS-chitosan, respectively (see supplementary data for more details). The CAC values were more than ten folds lower than the concentrations of the two materials in the reaction, thus confirming their aggregation state in the reaction.

### 3.5. Surface characterization by X-ray photoelectron spectroscopy (XPS)

We hypothesized that the grafted hydrophobic imine moieties should try to position themselves into the spherical cores,

**Table 1**Characters of the imine-NS-chitosan particles.

Nanospheres	Hydrodynamic siz	Zeta potential	
	nm	PDI	mV
Van-NS-chitosan	163.4 ± 2.1	0.177	48.8 ± 1.7
Cin-NS-chitosan	$130.9 \pm 4.9$	0.333	$57.3 \pm 4.6$
Citro-NS-chitosan	$109.6 \pm 1.6$	0.198	$38.3\pm2.4$
Citral-NS-chitosan	$80.9 \pm 1.7$	0.166	$42.4 \pm 0.65$
NS-chitosan	$46.3 \pm 0.24$	0.185	$22.3 \pm 2.6$

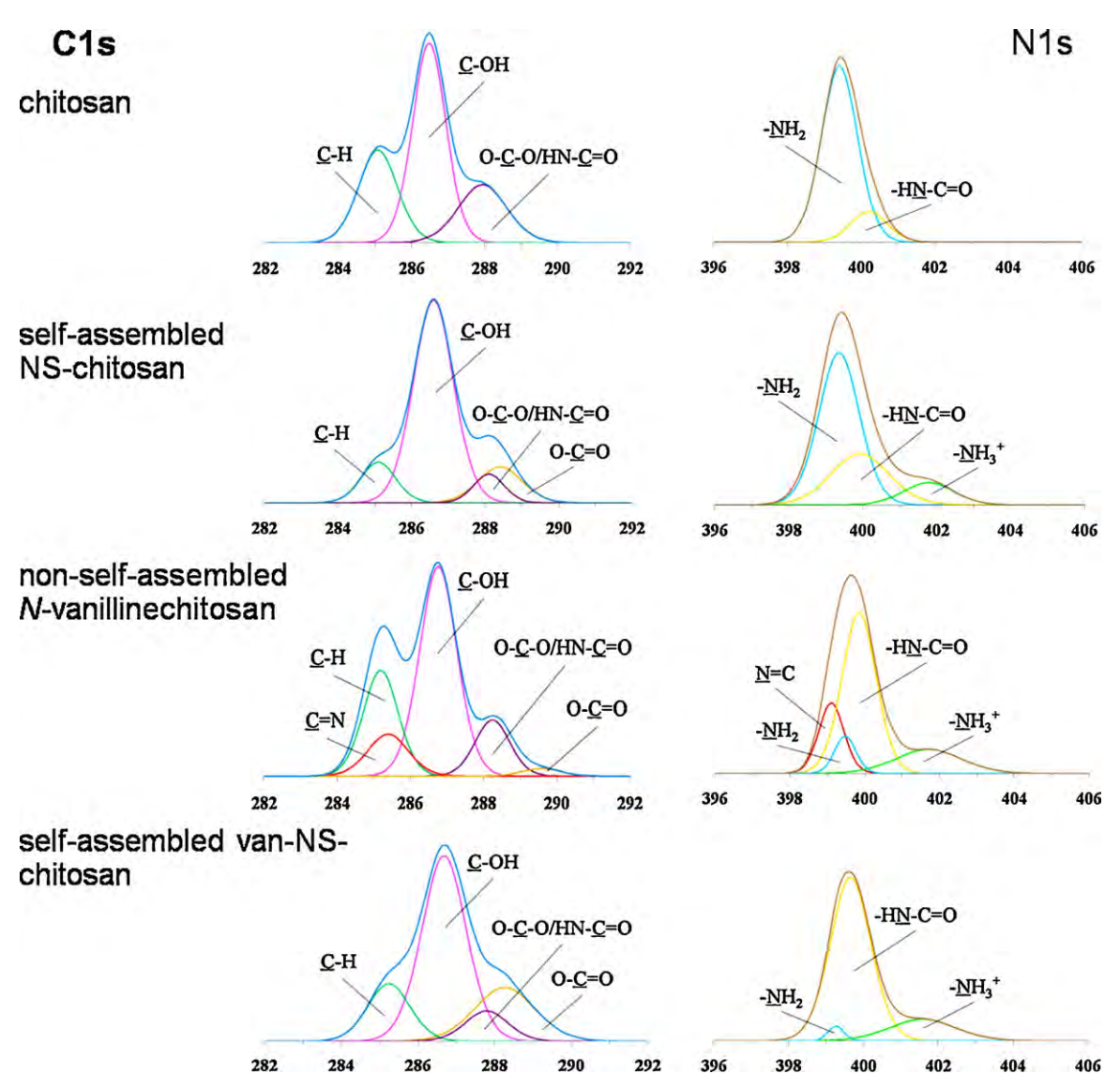


Fig. 5. XPS high resolution spectra of chitosan, self-assembled NS-chitosan, non-self-assembled N-vanillinechitosan and self-assembled van-NS-chitosan.

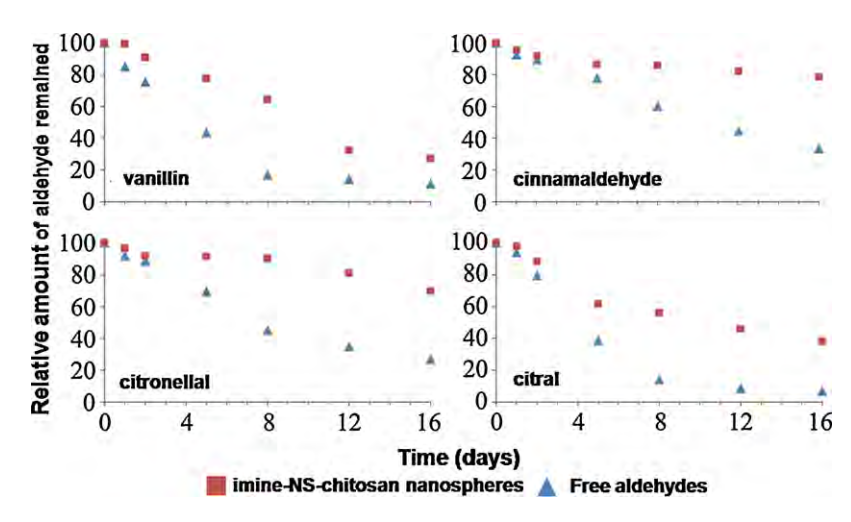


Fig. 6. The release of aldehydes from imine-NS-chitosan nanospheres in an aqueous suspension compared to the free aldehydes. The remaining unrelated imine moieties were quantified by UV-absorption analysis after acid hydrolysis. Data are shown as the mean + 1 SD.

away from being in direct contact with polar water medium. If this hypothesis is correct, a double barrier-carrier, in which the imine linkage was the chemical barrier and the polymeric matrix wall was the physical barrier, would have been successfully generated. Therefore, we investigated the location of the grafted imine groups in the obtained imine-NS-chitosan spheres. Here the XPS technique, which usually gives chemical composition data at the surface layer up to a thickness of approximately 8 nm, was employed.

Comparing to the NS-chitosan particles, X-ray photoelectron (XPS) analysis revealed more than 90% decrease in the amino functionality (relative to amide functionality) at the van-NS-chitosan particles' surface, but with no appearance of the C=N functionality (Fig. 5). Since the IR spectrum of the van-NS-chitosan particles showed prominent C=N functionality (1635 cm<sup>-1</sup>), the C=N moieties were likely to be at the inside of the particles, more than 8 nm dept from the surface. This implied that, all the grafted perfumery moieties were at the core of the dry particles. Although the XPS analysis was performed on the dry particles (prepared through freeze-drying by quickly freezing the aqueous particle suspension at -80°C and subjecting to high vacuum removal of water), the result should also represent the particles' structure in water too. This was because the reshuffling of the moieties in the particles during the freeze-drying, should be minimized. More importantly, since the air is much less polar than water, if the shuffling during the drying was to occur, it should be in the direction that the less polar moieties (the grafted imines) were shuffled up to the surface. But the result showed no imine on the particles' surface.

The localization of the grafted hydrophobic imine moieties at the particles' core occurred because of the drive towards the minimum free energy of the local equilibrium around the spheres. In other words, thermodynamically such organization took place in order to maximize hydrophobic interactions amongst the grafted hydrophobic moieties and to minimize contact between the polar medium (water) and the non-polar imine moieties. Kinetically the ultrasonication helped the system to be able to cross the chemical interactions within the NS-chitosan particles, and organized into the more thermodynamically stable architectures. It was possible that as the reaction was taking place firstly between the amino groups at the particles' surface and the incoming aldehyde molecules (XPS analysis of NS-chitosan particles showed abundant of amino functionality at the surface), simultaneously and continuously with the aid of ultrasonication, the particles reorganized to localize the grafted hydrophobic imine to the core, this then exposing more amino groups towards the surface of the particles and thus more imine could be formed, and finally all the formed imine moieties were shuffled into the core of the particles (no detection of imine functionality at the surface by XPS analysis but obvious imine peak in the FTIR spectrum).

With no succinyl moiety on the chitosan backbone, the obtained N-vanillidenechitosan could not self-assemble into spherical architecture (confirmed through AFM, TEM and SEM). With no self-organization, some of the imine functionality (C=N) should be observable by XPS as they should remain at the surface. The C1s and N1s spectra of this non-self-assembled N-vanillidenechitosan showed evident peaks of the imine bond (C=N) at 285.4 eV and 399.1 eV, in the N1s and C1s high resolution XPS spectra, respectively, indicating that the grafted imine moieties were not all covered by polymeric matrix, but rather significant amounts of them were at the surface of the material (see ESI). This result assured that the XPS technique could clearly detect the C=N functionality in a chitosan derivative and that the undetection of C=N functionality for the imine-NS-chitosan particles was because they were not at the particles' surface.

Therefore, it is most likely that the proposed double barrier-carrier was successfully fabricated through a one step pro-

cess in which the formation of imine linkages between the amino groups and aldehydes of the NS-chitosan nanospheres occurred in concerted with the localization of the grafted imine moieties at the particles' core.

#### 3.6. Release of aldehydes

Since the imine-NS-chitosan nanospheres were designed to be double barrier fragrance controlled release systems in which the imine bond was a chemical barrier while the polymer shell was a physical barrier, the aldehyde release behavior of the four water suspension products was monitored by quantification amounts of the grafted imine that remained in the sample after incubation at 32 °C for up to 16 days. The remaining imine moieties were quantified by subjecting each sample to an acid-based imine hydrolysis to generate aldehydes and the generated aldehydes were then extracted with hexane and quantified by UV absorption spectroscopy. The prolonged release of aldehyde molecules could be observed both in the freeze-dry sample and in the aqueous suspension of the samples. The aqueous suspension system showed evident slow down release (Fig. 6). The release of the fragrant aldehydes from the dry samples was evaluated after being kept at 40 °C for 60 days. Hydrolysis of the samples followed with aldehyde quantification indicated (mean  $\pm$  SD) 2.88  $\pm$  0.20, 0.77  $\pm$  0.02,  $4.52 \pm 0.31$  and  $1.31 \pm 0.10$  mg of vanillin, cinnamaldehyde, citronellal and citral in the corresponding imine-NS-chitosan samples, which was significantly higher (79.9-, 85.4-, 20.1- and 29.1-fold, respectively) than the free aldehyde levels in the control samples at  $0.036 \pm 0.001$ ,  $0.009 \pm 0.002$ ,  $0.225 \pm 0.092$  and  $0.045 \pm 0.002$  mg of vanillin, cinnamaldehyde, citronellal and citral, respectively. Note that each imine-NS-chitosan particles were prepared using 25 mg aldehyde and 25 mg of each corresponding aldehyde was used for the free aldehyde control sample. Comparing the release characteristic of the dry to that of the aqueous suspension samples, it was evident that the prolonged release of the double barrier systems was much more pronounced in the dry state. This was because the imine hydrolysis needs water molecules and there was much less availability of the water molecules for the dry samples.

#### 4. Conclusion

Here a novel double barrier–carrier for fragrance aldehyde molecules was successfully created from biocompatible biodegradable chitosan polymer. The system contained a chemical barrier, in which the fragrance aldehydes were linked to the NS-chitosan *via* imine linkages, and a physical barrier, in which the grafted imine moieties were buried inside the chitosan matrix. Prolonged release of perfumery aldehydes was demonstrated both in a water suspension and, especially, in the dry state.

#### Acknowledgements

The authors thank the Development and Promotion of Science and Technology talents project (DPST), the Commission of Higher Education-Thailand Research Fund (BRG5280004), the Special Task Force for Activating Research (STAR) from the centenary academic development project, Chulalongkorn University, and the Thai Government Stimulus Package 2 (TKK2555) under the Project for Establishment of Comprehesive Center for Innovative Food, Health Products and Agriculture, for financial support. The authors also thank Professor Masayuki Yamaguchi and Mr. Murakami Tatsuya (School of Material Science, Japan Advanced Institute of Science and Technology, Japan) for the XPS analysis.

#### Appendix A. Supplementary data

Supplementary data associated with this article can be found, in the online version, at doi:10.1016/j.carbpol.2011.06.074.

#### References

- Brown, G. O., Bergquist, C., Ferm, P., & Wooley, K. L. (2005). Unusual, promoted release of guests from amphiphilic cross-linked polymer networks. *Journal of the American Chemical Society*, 127, 11238–11239.
- De Saint Laumer, J. Y., Frerot, E., & Herrmann, A. (2003). Controlled release of perfumery alcohols by neighboring-group participation. Comparison of the rate constants for the alkaline hydrolysis of 2-acyl-, 2-(hydroxymethyl)-, and 2carbamoylbenzoates. *Helvetica Chimica Acta*, 86, 2871–2899.
- Edris, A., & Bergnståhl, B. (2001). Encapsulation of orange oil in a spray dried double emulsion. *Die Nahrung*, 45, 133–137.
- Fehr, C., & Galindo, J. (2005). Aldols by Michael addition: Application of the retro-Michael addition to the slow release of enones. *Helvetica Chimica Acta*, 88, 3128–3136.
- Godin, G., Levrand, B., Trachsel, A., Lehn, J. M., & Herrmann, A. (2010). Reversible formation of aminals: A new strategy to control the release of bioactive volatiles from dynamic mixtures. *Chemical Communications*, 46, 3125–3127.
- Hambleton, A., Fabra, M. J., Debeaufort, F., Dury-Brun, C., & Voilley, A. (2009). Interface and aroma barrier properties of iota-carrageenan emulsion-based films used for encapsulation of active food compounds. *Journal of Food Engineering*, 93, 80–88.
- Herrmann, A. (2007). Controlled release of volatiles under mild reaction conditions: From nature to everyday products. *Angewandte Chemie International Edition*, 46, 5836–5863.
- Kamogawa, H., Mukai, H., Nakajima, Y., & Nanasawa, M. (1982). Chemical release control – Schiff bases of perfume aldehydes and aminostyrenes. *Journal of Polymer Science – Polymer Chemistry Edition*, 20, 3121–3129.
- Korus, J., Tomasik, P., & Lii, C. Y. (2003). Microcapsules from starch granules. *Journal of Microencapsulation*, 20, 47–56.
- Landfester, K. (2009). Miniemulsion polymerization and the structure of polymer and hybrid nanoparticles. Angewandte Chemie International Edition, 48, 4488–4508.
- Lee, H. Y., Lee, S. J., Cheong, I. W., & Kim, J. H. (2002). Microencapsulation of fragrant oil via in situ polymerization: Effects of pH and melamine-formaldehyde molar ratio. *Journal of Microencapsulation*, 19, 559–569.
- Levrand, B., & Herrmann, A. (2002). Light induced controlled release of fragrances by Norrish type II photofragmentation of alkyl phrnyl ketones. *Photochemical and Photobiological Sciences*, 1, 907–919.

- Levrand, B., Ruff, Y., Lehn, J. M., & Herrmann, A. (2006). Controlled release of volatile aldehydes and ketones by reversible hydrazone formation "classical" profragrances are getting dynamic. *Chemical Communications*, 2965–2967.
- Levrand, B., Fieber, W., Lehn, J. M., & Herrmann, A. (2007). Controlled release of volatile aldehydes and ketones from dynamic mixtures generated by reversible hydrazone formation. *Helvetica Chimica Acta*, 90, 2281–2314.
- Levrand, B., & Herrmann, A. (2007). Controlled light-induced release of volatile aldehydes and ketones by photofragmentation of 2-oxo-(2-phenyl) acetates. *Chimia*, 61. 661–664.
- Morinaga, H., Morikawa, H., Wang, Y., Sudo, A., & Endo, T. (2009). Amphiphilic copolymer having acid-labile acetal in the side chain as a hydrophobe: controlled release of aldehyde by thermoresponsive aggregation – dissociation of polymer micelles. *Macromolecules*, 42, 2229–2235.
- Muzzarelli, R. A. A., & Ilari, P. (1994). Chitosans carrying the methoxyphenyl functions typical of lignin. Carbohydrate Polymers, 23, 155–160.
- Paula, H. C. B., Sombra, F. M., Cavalcante, R. D. F., Abreu, F. O. M. S., & De Paula, R. C. M. (2011). Preparation and characterization of chitosan/cashew gum beads loaded with Lippia sidoides essential oil. *Materials Science and Engineering C*, 31, 173–178.
- Quellet, C., Schudel, M., & Ringgenberg, R. (2001). Flavors & fragrance delivery systems. Chimia, 55, 421–428.
- Robles, J. L., & Bochet, C. G. (2005). Photochemical release of aldehydes from α-acetoxy nitroveratryl ethers. Organic Letters, 7, 3545–3547.
- Rochat, S., Minardi, C., De Saint Laumer, J. Y., & Herrmann, A. (2000). Controlled release of perfumery aldehydes and ketones by Norrish type-II photofragmentation of  $\alpha$ -keto esters in undegassed solution. *Helvetica Chimica Acta*, 83, 1645–1671.
- Souto, E. B., & Müller, R. H. (2008). Cosmetic features and applications of lipid nanoparticles (SLN®, NLC®). International Journal of Cosmetic Science, 30, 157-165.
- Ternat, C., Kreutzer, G., Plummer, C. J. G., Nguyen, T. Q., Herrmann, A., Ouali, L., et al. (2007). Amphiphilic multi-arm star-block copolymers for encapsulation of fragrance molecules. *Macromolecular Chemistry and Physics*, 208, 131–145.
- Turin, L. (2006). WO Patent 2006/012215. Flexitral Inc. [Chem. Abstr. 2006, 144, 176961].
- Wang, C. X., & Chen, S. L. (2005a). Aromachology and its application in the textile field. Fibres and Textiles in Eastern Europe, 13, 41–44.
- Wang, C. X., & Chen, S. L. (2005b). Fragrance-release property of ß-cyclodextrin inclusion compounds and their application in aromatherapy. *Journal of Industrial Textiles*. 34. 157–166.
- Wang, P., Zhu, Y., Yang, X., & Chen, A. (2008). Prolonged-release performance of perfume encapsulated by tailoring mesoporous silica spheres. *Flavour and Fragrance Journal*. 23. 29–34.
- Zhu, A., Yuan, L., & Lu, Y. (2007). Synthesis and aggregation behavior of N-succinyl-o-carboxymethylchitosan in aqueous solutions. Colloid and Polymer Science, 285, 1535–1541.

### **Supplementary Information for CARBPOL-D-11-00765-R1**

# Fragrant chitosan nanospheres: Controlled release systems with physical and chemical barriers.

Thapakorn Tree-udom, Supason P. Wanichwecharungruang\*, Jiraporn Seemork and Sunatda Arayachukeat

#### 1. Finding the optimum ratio between NS-chitosan nanoparticles and aldehyde

Five weight ratios of **NS-chitosan** to vanillin (5:1, 4:1, 3:1 2:1 and 1:1) were experimented using the optimized reaction time of 4 h. From the ATR-FTIR spectra of the products, both imine (1635 cm<sup>-1</sup>) and aldehyde (1665 cm<sup>-1</sup>) functionalities could be observed in the products obtained from the reactions conducted at **NS-chitosan**: vanillin weight ratio of 1:1 and 2:1 (Figure d). IR spectra of products from reactions conducted at 3:1, 4:1 and 5:1weight ratios showed only absorption band of the imine (Figure d). This evidence clearly indicated that the maximum amount of aldehyde that would give product with no left-over aldehyde was 3:1. The ratio of 3:1 corresponded to the mole ratio between amino (from **NS-chitosan**) and aldehyde of 1.7:1.0.

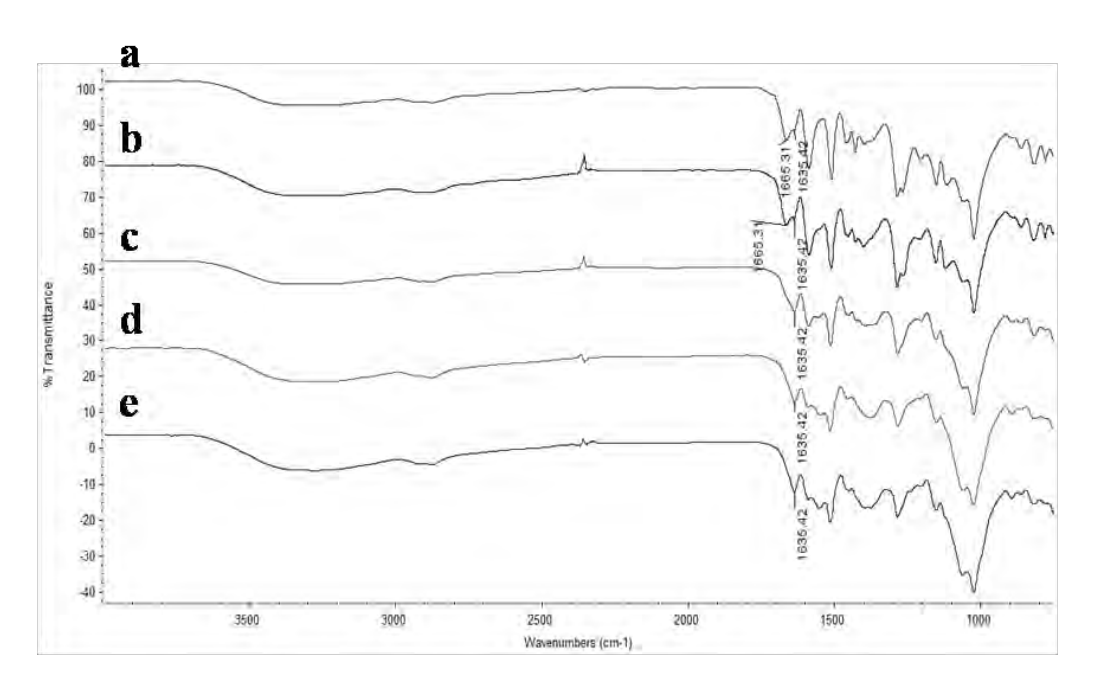


Figure a. ATR-FTIR spectra of N,N'-vanillidene-succinylchitosan studies on imine formation at **NS-chitosan**: vanillin weight ratio of (a) 1:1, (b) 2:1, (c) 3:1, (d) 4:1 and (e) 5:1

#### 2. Structure characterization of the four imine-NS-chitosan.

#### 2.1 Van-NS-chitosan

The IR spectrum of N,N'-vanillidene-succinylchitosan or van-NS-chitosan showed absorption peaks at 1635 cm<sup>-1</sup> and 1592 cm<sup>-1</sup>, and 1512 cm<sup>-1</sup> assignable to C=N stretching vibration and C=C stretching vibration of aromatic, respectively (Figure e). A degree of vanillin substitution (DS) was quantitatively estimated by hydrolyzing the imine from the product, extracting the hydrolysed aldehyde, and quantitating the amount of extracted aldehyde using UV/Vis spectroscopic analysis with the aid of calibration curve. The DS was 0.34.

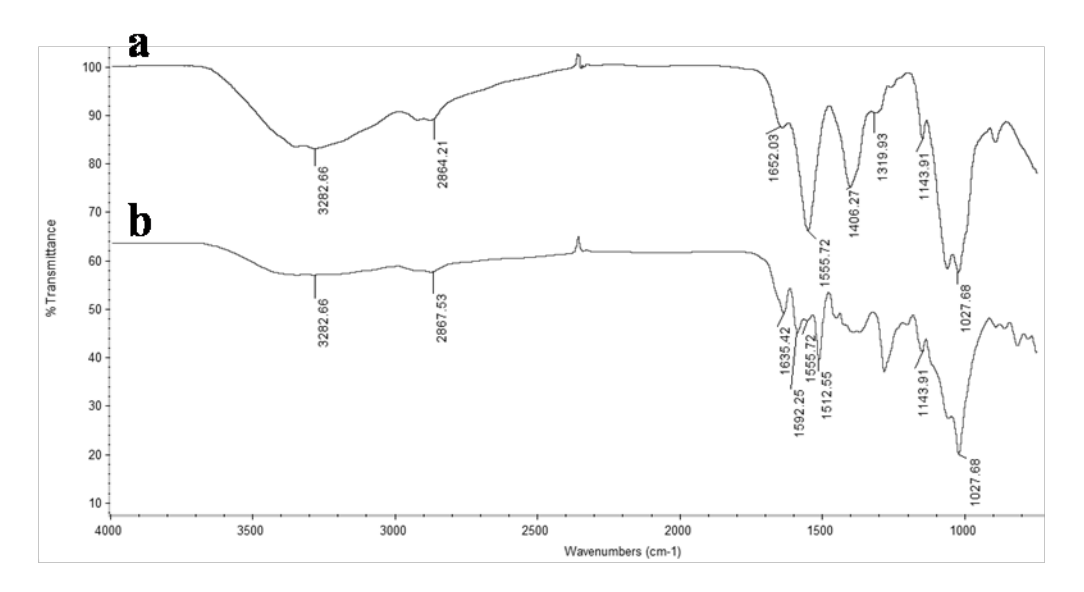


Figure b. ATR-FTIR spectra of (a) NS-chitosan and (b) van-NS-chitosan.

#### 2.2 Cin-NS-chitosan

The IR spectrum of N,N'-cinnamylidene-succinylchitosan or cin-NS-chitosan showed absorption peaks at 1632 cm<sup>-1</sup> and 1592 cm<sup>-1</sup> assignable to C=N stretching vibration, and C=C stretching vibration of aromatic, respectively (Figure f). A degree of cinnamaldehyde substitution (DS) was 0.29 (determined by the same procedure to that of N,N'-vanillidene-succinylchitosan).

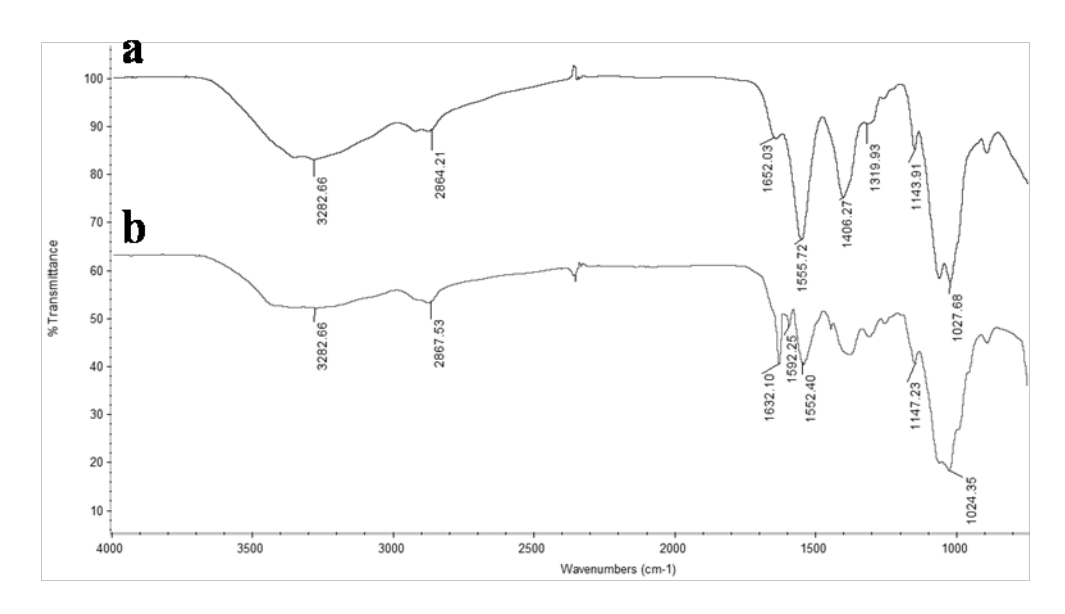


Figure c. ATR-FTIR spectra of (a) NS-chitosan and (b) cin-NS-chitosan.

#### 2.3 Citro-NS-chitosan

The IR spectrum of N,N'-citronellalidene-succinylchitosan or citro-NS-chitosan showed absorption peaks at 1638 cm<sup>-1</sup> and 1612 cm<sup>-1</sup> assignable to C=N stretching vibration, and C=C stretching vibration, respectively (Figure g). A degree of citronellal substitution (DS) was estimated as described above to be 0.38.

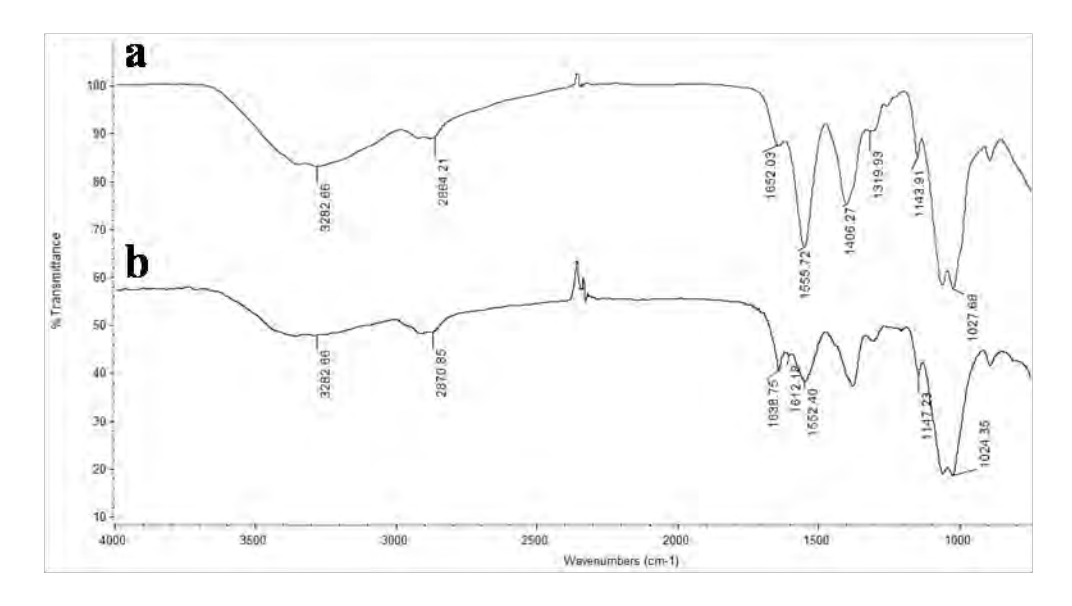


Figure d. ATR-FTIR spectra of (a) NS-chitosan and (b) citro-NS-chitosan.

#### 2.4 Citral-NS-chitosan.

The IR spectrum of N,N'-citralidene-succinylchitosan or citral-NS-chitosan showed absorption peaks at 1638 cm<sup>-1</sup> and 1612 cm<sup>-1</sup> assignable to C=N stretching vibration and C=C stretching vibration, respectively (Figure h). A degree of citral substitution (DS) was 0.38.

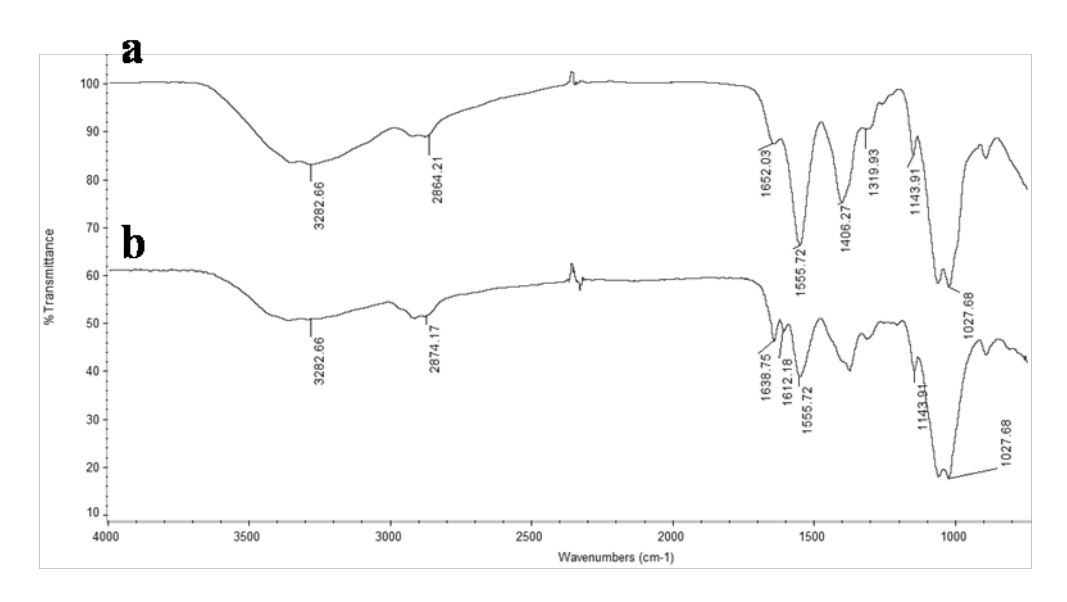


Figure e. ATR-FTIR spectra of (a) NS-chitosan and (b) citral-NS-chitosan.

#### 3. Morphology characterization of imine-NS-chitosan.

The aqueous suspension of all four imine-NS-chitosan was quickly frozen at -80 °C before subjecting to water removal under vacuum (freez-dried). Then the dry products were analyzed by AFM. (see AFM image of van-NS-chitosan in the main article)

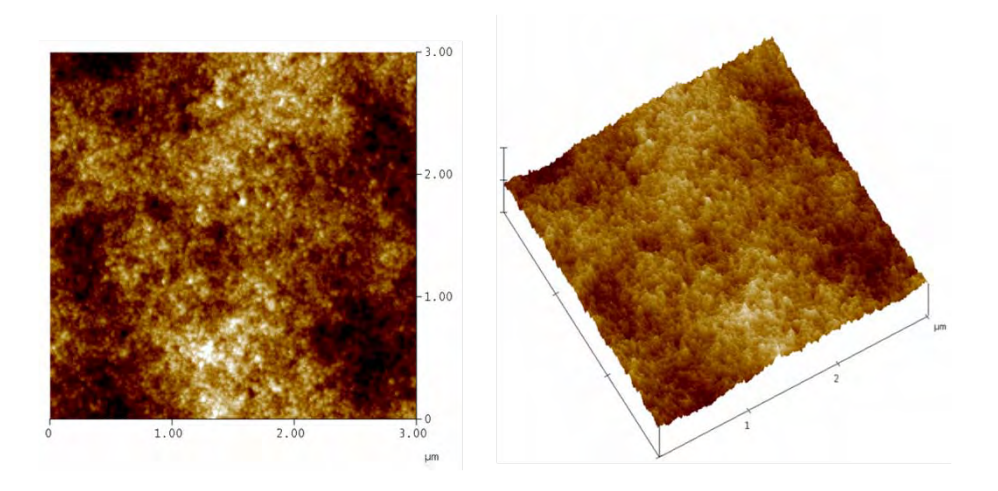


Figure f. AFM images of cin-NS-chitosan.

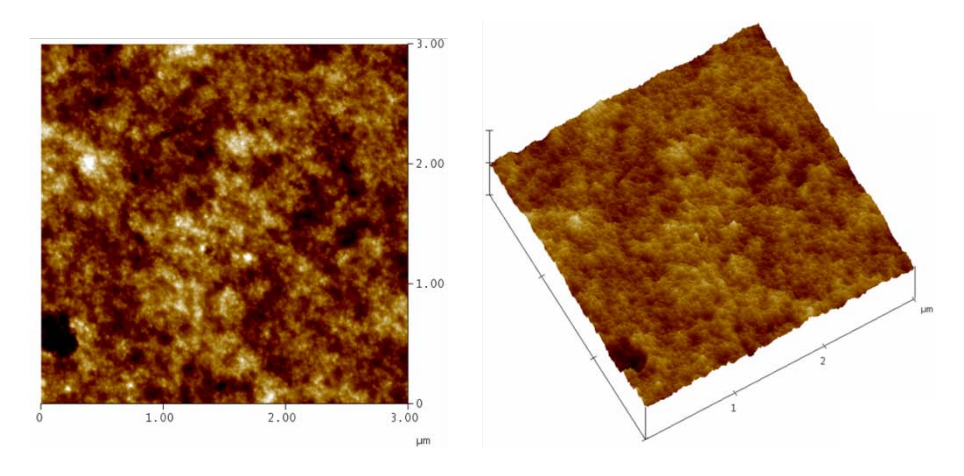


Figure g. AFM images of citro-NS-chitosan.

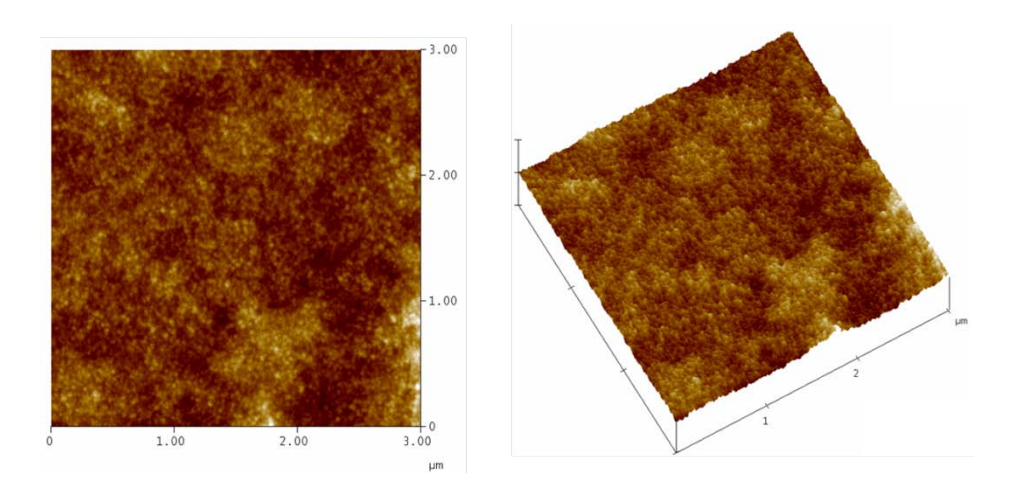


Figure h. AFM images of citral-NS-chitosan.

#### 4. Critical aggregation concentration

Aggregation behavior of the micelles was monitored by fluorescence spectroscopy with pyrene as a fluorescence probe. We compared two aqueous systems, **NS-chitosan** and N,N'-citronellalidene-succinylchitosan. The samples (the test polymer of various concentrations ranging from 0.05 to 0.60 mg/ml in the presence of pyrene) were excited at 334 nm and the emission of pyrene was recorded from 350 to 450 nm. The intensity ratio between the first peak at 372 nm ( $I_{372}$ ) and the third peak at ( $I_{384}$ ) of pyrene emission spectrum was used for monitoring the behavior of polymer aggregation around the pyrene molecules. The  $I_{372}/I_{384}$  value plot versus polymer concentrations was further calculated for prediction of the polymer critical aggregation concentration (cac).

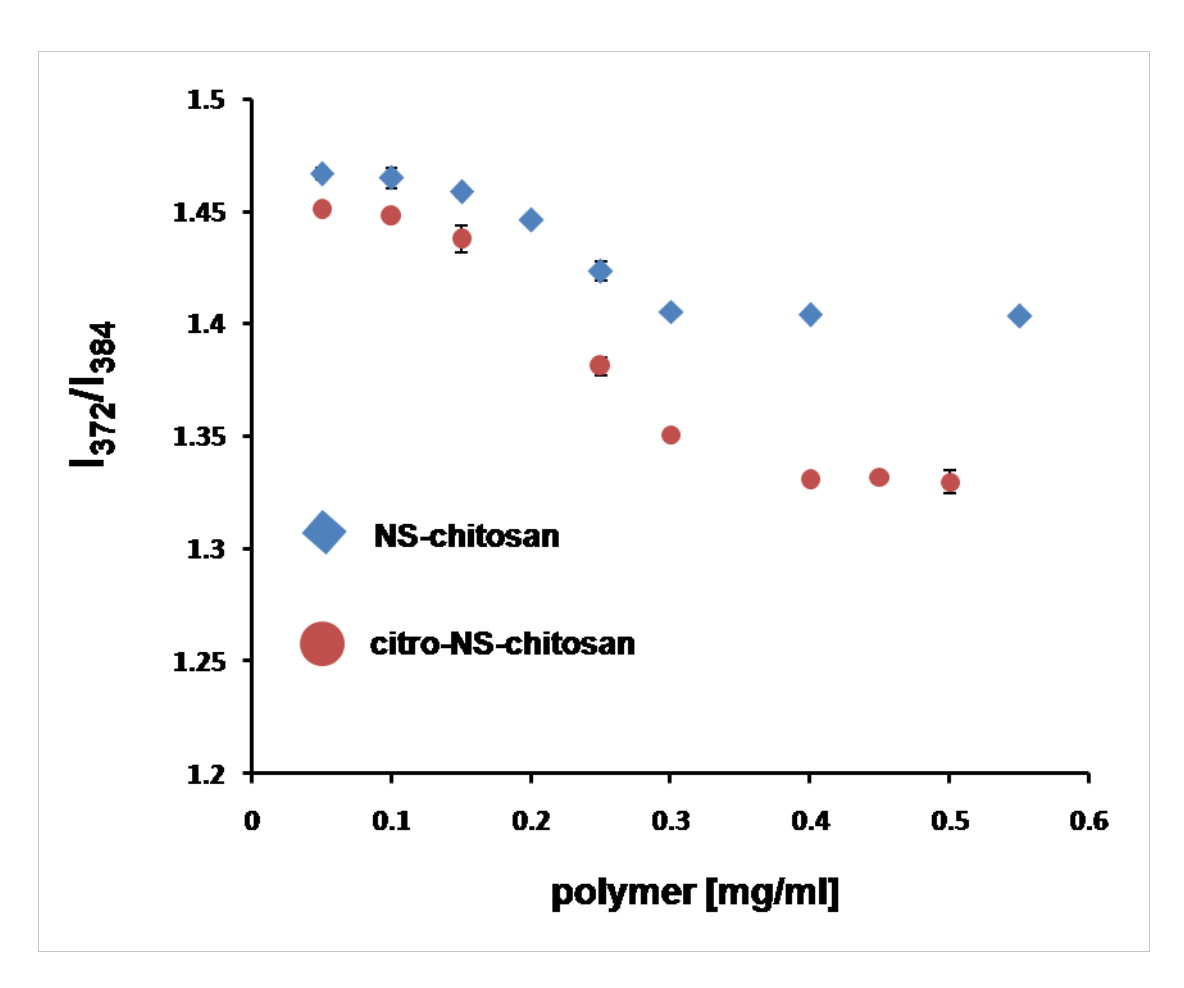


Figure i. Change of intensity ratio ( $I_{372}/I_{384}$ ) versus polymer concentration for NS-chitosan (a) and citro-NS-chitosan (b).

Received: 23 March 2012,

Revised: 14 June 2012,

Accepted: 16 June 2012

Published online in Wiley Online Library

(wileyonlinelibrary.com) DOI 10.1002/ffj.3116

# A refillable fragrance carrier with a tuneable thermal switch

# Jiraporn Seemork, a,b Thapakorn Tree-Udom and Supason Wanichwecharungruang \*\*

ABSTRACT: Release of fragrant molecules from poly(ethylene oxide) (PEO) grafted chitosan particles could be controlled in a switchable manner through the thermo-responsive hydration/dehydration of the PEO corona of the spheres that resulted in the de-aggregation/aggregation among particles and corresponded to an on/off fragrant release switch. In water, mPEO-chitosan self-assembled into spherical particles with the mPEO corona covering the surface and vanillin and citral could be loaded into the particles. The mPEO-water interaction took place at temperatures lower than the lower critical solution temperature (LCST) value and resulted in de-aggregation among spheres which enabled release of the loaded fragrance molecules, whilst mPEO-mPEO interactions occurred at temperatures higher than the LCST value and resulted in aggregation among spheres which also halted the fragrance release. This thermal switch could be tuned to a desired temperature by adjusting the salt concentration. After the release of all fragrances, the thermo-responsive carriers could be refilled again. Copyright © 2012 John Wiley & Sons, Ltd.

Supporting information may be found in the online version of this article.

**Keywords:** chitosan; fragrance; controlled release; thermal switch; aggregation

#### Introduction

Among many daily used chemicals, fragrance is one of the chemical categories that needs controlled release technology to prolong its efficacy. Conventionally, fragrance controlled release strategies can be categorized into those that use a physical barrier, in which the diffusion of the fragrant molecules is controlled by entrapping them into a shell material and those that involve a chemical barrier, in which the fragrances are modulated via chemical derivatization using reversible linkages so that the fragrant molecules can be regenerated.<sup>[1]</sup>

Physical barrier systems used for the controlled release of odorous compounds include double emulsion systems, <sup>[2]</sup> solid lipid nanoparticles, <sup>[3]</sup> carbohydrate coacervation, <sup>[4–6]</sup> cyclodextrin inclusion complexation, <sup>[7]</sup> polymeric microspheres formed by interfacial polymerization or *in situ* polymerization, <sup>[8,9]</sup> and self-assembled particles of amphiphilic polymer. <sup>[10,11]</sup> Recently, a system with both physical and chemical barriers was also demonstrated. <sup>[12]</sup>

Stimuli-responsive fragrance controlled release systems have been introduced in the past decade. Examples of photo-responsive chemical barriers include the use of Norrish type II photo-fragmentation to control the delivery of various fragrant chemicals, such as alkenes and acetophenones,  $^{[13]}$  and aldehydes and ketones,  $^{[14,15]}$  and the photo-assisted release of fragrant aldehydes from their  $\alpha$ -acetoxy ether derivatives.  $^{[16]}$  Another popular stimulus is pH, and examples of pH stimuli systems comprise the use of bicyclo bisoxazolidine functionality to control the release of aldehyde in poly(ethylene glycol)-*grafted*-polymethacrylate (PEG-*g*-PMA),  $^{[17]}$  the use of neighbouring-group-assisted alkaline ester hydrolysis of perfumery alcohols from precursor molecules,  $^{[18]}$  and the use of acid hydrolysis to release fragrant aldehyde from the acetal functional group on the PMA-based polymer with

quaternarized amine groups<sup>[19,20]</sup> or from the imine functional group of p- and m-aminostyrenes.<sup>[21]</sup> Another practical stimulus for controlling the release of fragrant molecules is temperature. Examples of thermo-responsive fragrance controlled release systems include the use of PEG-grafted-PMMA polymer with the fragrant lilial grafted to the polymer via the acetal linkage,<sup>[22]</sup> and the poly(N-isopropylacrylamide) grafted chitosan with the lilial grafted to the polymer via the imine linkage.<sup>[23]</sup>

Here, we fabricated a fragrance controlled release system with a thermal switch and refill-ability characters, using the well-accepted non-toxic, biocompatible polyethylene oxide (PEO)<sup>[24,25]</sup> and chitosan polymers. Chitosan spheres were synthesized to have the outer surface covered with thermoresponsive mPEO polymer while the fragrant molecules were entrapped into the chitosan matrix of the particles. The on/off switch was modulated through the thermally induced phase separation of the fragrant spheres from the aqueous medium, which resulted in limiting the efflux of the fragrant molecules from the particles. In addition, the system was fabricated to be refillable and the on/off switch could be tuned to a desired temperature.



<sup>\*</sup> Correspondence to: Supason Wanichwecharungruang, Department of Chemistry, Faculty of Science, Chulalongkorn University, Bangkok 10330, Thailand. E-mail: psupason@chula.ac.th

<sup>&</sup>lt;sup>a</sup> Program of Petrochemistry and Polymer Science, Faculty of Science, Chulalongkorn University, Bangkok 10330, Thailand

<sup>&</sup>lt;sup>b</sup> National Center of Petroleum, Petrochemicals and Advanced Materials, Chulalongkorn University, Bangkok 10330, Thailand

<sup>&</sup>lt;sup>c</sup> Department of Chemistry, Faculty of Science, Chulalongkorn University, Bangkok 10330, Thailand

#### **Materials and Methods**

<sup>1</sup>H NMR spectra were acquired in D<sub>2</sub>O at 400 MHz (Varian Company, Palo Alto, California, USA). UV-visible spectra were recorded on a CARY 100 Bio UV-visible spectrophotometer equipped with a temperature controller (Varian Company). Attenuated Total Reflectance-Fourier transform infrared (ATR-FTIR) spectra were recorded on a ContinuµmTM infrared microscope with a Nicolet 6700 FT-IR spectrometer (Thermo Electron Corporation, Waltham, Massachusetts, USA). Transmission electron microscopy photographs were obtained by a JEM-2100 transmission electron microscope (JEOL, Tokyo, Japan). Hydrodynamic diameters were acquired on a Zetasizer nanoseries instrument (Malvern Instruments, Malvern, UK). X-ray diffraction spectra were obtained using a Rigaku DMAX 2200/Ultima+ diffractometer (Rigaku International Corporation, Tokyo, Japan) operating with Cu Kα radiation at 40 kV and 30 mA. Fluorescent and differential interference contrast images were acquired using a Nikon Ti-E Inverted Microscope Confocal Nikon C1si confocal microscope (Nikon Corporation, Tokyo, Japan).

#### Synthesis of Carboxy-terminated PEG (Scheme 1)

Polyethyleneglycol methyl ether (mPEG) (10.00 g,  $M_{\rm n}$  5000; Fluka, Seelze, Germany) was reacted with succinic anhydride (4.00 g or 20 mol equivalent to mPEG, analytical grade; Acros Organics, Geel, Belgium) in freshly distilled dimethyl formamide (20 ml) with a catalytic amount of pyridine (Carlo Erba Reagents, Val de Reuil, France) at  $60^{\circ}$ C overnight. The obtained product was purified by dialysis against excess water using benzoylate dialysis tubing (MWCO 2000; Sigma-Aldrich, St Louis, MO, USA) before freeze drying.

Methoxy-terminated polyethylene oxide carboxylic acid (mPEO-COOH)

Yield = 60%.

<sup>1</sup>H NMR (D<sub>2</sub>O, 400 MHz,  $\delta$ , ppm): 2.51 (-COCH<sub>2</sub>CH<sub>2</sub>COOH), 4.11 (-OCH<sub>2</sub>CH<sub>2</sub>OCOCH<sub>2</sub>CH<sub>2</sub>-COOH), 3.35–3.70 (-OCH<sub>2</sub>CH<sub>2</sub>OCH<sub>3</sub>) and 3.20 (-OCH<sub>2</sub>CH<sub>2</sub>OCH<sub>3</sub>).

<sup>13</sup>C NMR (D<sub>2</sub>O, 400 MHz,  $\delta$ , ppm): 59 (-OCH<sub>2</sub>CH<sub>2</sub>OCH<sub>3</sub>), 82 (-OCH<sub>2</sub>CH<sub>2</sub>OCH<sub>3</sub>), 73 (-OCH<sub>2</sub>CH<sub>2</sub>OCH<sub>3</sub>), 70 (-OCH<sub>2</sub>CH<sub>2</sub>OCO+<sub>2</sub>O-), 63 (-OCH<sub>2</sub>CH<sub>2</sub>OCOCH<sub>2</sub>CH<sub>2</sub>-), 60 (-OCH<sub>2</sub>CH<sub>2</sub>OCOCH<sub>2</sub>CH<sub>2</sub>-), 168 (-OCOCH<sub>2</sub>CH<sub>2</sub>COOH), 29 (-OCOCH<sub>2</sub>CH<sub>2</sub>COOH).

Scheme 1. Synthesis and structural details of mPEO-chitosan

ATR-FTIR (cm<sup>-1</sup>): 2943 (O-H stretching of carboxylic acid), 2881 (C-H stretching), 1731 (C-O stretching of ester) and 1092 (C-O-C stretching).

UV-visible (nm):  $\lambda_{\text{max}}$  263.

#### Synthesis of mPEO-grafted Chitosan (mPEO-Chitosan) (Scheme 1)

Chitosan (0.25 g,  $M_v$  = 30 000 Da, 85% deacetylated; Seafresh Chitosan Lab, Chumphon, Thailand) was stirred with 1-hydroxybenzotriazole or HOBt (0.206 g, freshly recrystallized in MeOH) in deionized water (20 ml) until a clear solution was obtained. Aqueous solution of mPEO-COOH (0.765 g) was added to the chitosan solution before the addition of 1-ethyl-3-(3-dimethyllaminopropyl) carbodiimide hydrochloride (EDCI-HCI) aqueous solution (0.293 g; Acros Organics). The reaction was stirred at room temperature for 24 h. The mixture was then poured into excess acetone and a crude gel was obtained. The gel was vacuum filtered, washed with excess acetone and then ethanol several times and dried under vacuum at room temperature.

Methoxypolyethylene oxide grafted chitosan (mPEO-chitosan)

Yield = 64%.

Substitution degree of mPEO = 0.12.

 $^{1}$ H NMR (D<sub>2</sub>O, 400 MHz, δ, ppm): 2.83–2.89 (-COCH<sub>2</sub>CH<sub>2</sub>COOH), 4.23 (-OCH<sub>2</sub>CH<sub>2</sub>OC(O)), 3.34 (-OCH<sub>2</sub>CH<sub>2</sub>OCH<sub>3</sub>), 2.02 (-NHCOCH<sub>3</sub>), 3.56–3.72 (-OCH<sub>2</sub>CH<sub>2</sub>OCH<sub>3</sub>, H2′ of *N*-acetylglucosamine, H3–H6 of glucosamine (GlcN)), 4.78 (H1 of GlcN), 3.07 (H2 of GlcN).

 $^{13}$ C NMR (D<sub>2</sub>O, 400 MHz,  $\delta$ , ppm): 72 (-OCH<sub>2</sub>CH<sub>2</sub>O-), 100 (C1 of glucosamine). ATR-FTIR (cm $^{-1}$ ): 3378 (N-H and O-H stretching), 2877 (C-H stretching), 1645 (C=O stretching of amide I), 1515 (N-H bending of amide II), 1343 (C-N stretching of amide III), 1731 (C=O stretching of ester), 1140 (C-O-C stretching) and 1090 (C-O stretching of glucosamine unit).

UV-visible (nm):  $\lambda_{\text{max}}$  306.

# Preparation of Fragrance-loaded mPEO-Chitosan (Scheme 1)

mPEO-chitosan (90 mg) was dispersed in 30 ml of deionized water. Each perfumery material (30 mg, vanillin and citral, analytical grade from Acros Organics) as an ethanolic solution (2 ml) was added to the mPEO-chitosan suspension drop-wise with ultrasonication (40 kHz, 4 h). Fragrance loading capacity was determined by adding 1 ml of 1 m HCl solution to 5 ml of the obtained polymer suspension to fully swell the chitosan matrix, followed with addition of 15 ml hexane to extract the fragrance, then the mixture was vortexed for 5 min in a closed container and the hexane layer was analysed by UV-visible spectrophotometry with the aid of corresponding calibration curve.

#### **Determination of the Phase Transition Profile**

The phase transition profiles of vanillin-loaded mPEO–chitosan and citral-loaded mPEO–chitosan were separately acquired in aqueous medium at a polymer concentration of 3 g/l in the presence of ZnSO $_4$  (ZnSO $_4$ ·7H $_2$ O purchased from Carlo Erba) at a concentration of 0, 0.8, 0.9 and 1.0  $_{\rm M}$  for vanillin-loaded mPEO–chitosan or 0, 1.0, 1.3 and 1.5  $_{\rm M}$  for citral-loaded mPEO–chitosan. In the UV–visible spectrometer, equipped with a temperature controller, each sample was heated from 25 to 80°C and then cooled back to 25°C at rate of 1.0°C/min, while the absorbance/transmittance at 500 nm was continuously recorded.

#### Thermal Switching of Aldehyde Release

Phosphate buffer solution (0.1 M, pH 1, 40 ml) was mixed with the vanillin-loaded mPEO-chitosan aqueous suspension (180 mg of the polymer, 60 mg of vanillin or citral, 40 ml). ZnSO<sub>4</sub>·7H<sub>2</sub>O (20.7 g for vanillin and 34.5 g for citral) was added, mixed to dissolve, then the mixture was transferred into 12 vials (5 ml each) and kept uncovered at 55°C for 48 h then at 35°C for another 48 h. This storage cycle was repeated five times (total of 10 days), during which time the volume of the suspension in each vial was kept constant by adding water as required. During the storage, two vials were taken out every 48 h (at each temperature change) for quantification of the amount of fragrance left in the vials. Quantification was carried out by adding 1.0 M HCl (1.0 ml) to the vial, stirring for 30 min and then adding 15.0 ml of a 1:1 (v/v) ethanol-water mixture and subjecting the mixture to UV-visible spectroscopic analysis. Standard vanillin solutions used in the preparation of calibration curve were prepared in the same medium (5 ml water, 1 ml 1.0 M HCl, 15 ml of 1:1 (v/v) ethanol-water mixture).

A similar experiment was performed for citral-loaded mPEO-chitosan, except that a temperature of 45°C was used instead of 55°C, the temperature was switched every 24 h instead of 48 h giving a total storage time of 5 days instead of 10 days. Extraction of citral from the particles was performed as in the extraction of vanillin, except that 15.0 ml of hexane was used in place of the 15.0 ml ethanol–water mixture, and the hexane layer was subjected to UV–visible analysis. Citral standard solutions for the construction of calibration curve were prepared in hexane.

# Controlling the Rate of Fragrance Release by Adjusting the Salt Concentration

A suspension of 3.0 g/l citral-loaded mPEO–chitosan in water was divided into two parts. To the first part was added ZnSO<sub>4</sub> to a final concentration of 1.5 M, whilst no ZnSO<sub>4</sub> was added to the second part. Then each part was divided into 5.0-ml portions, and each portion kept in an open vial at  $40^{\circ}$ C. On days 0, 1, 2 and 5, at least two vials from each group were taken out and quantified for the amount of residual citral, as described above.

#### Refilling Citral into the System

To the suspension of citral-loaded mPEO–chitosan obtained after the 5 day-release experiment (no citral left in the system, thus it was 180 mg mPEO–chitosan in 40 ml of aqueous 1.5 m ZnSO $_4$  solution), was added citral (60 mg) and the mixture was either subjected to ultrasonication for 4 h or stirred overnight in the closed container, at 25°C. The obtained suspensions were characterized and evaluated for their fragrance release as described in previous section.

#### **Results and Discussion**

# Synthesis and Characterization of Fragrance-loaded mPEO-Chitosan Particles

mPEO-chitosan was successfully synthesized using the homogeneous coupling reaction in aqueous media. The <sup>1</sup>H NMR spectrum of mPEO-chitosan (Figure 1) showed peaks at 3.7 and 4.2 ppm

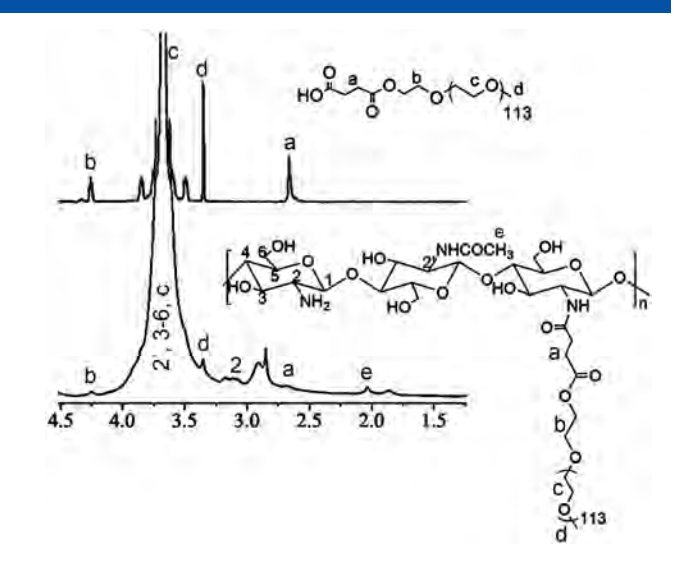


**Figure 1.** Representative <sup>1</sup>H NMR spectra of (top) mPEO-COOH and (bottom) mPEO-chitosan

corresponding to methylene protons of the mPEO moiety. Amide bonds formed from the reaction between the carboxylic groups of mPEO-COOH and the amino groups on chitosan chains could be confirmed through the ATR-FTIR spectrum of mPEO-chitosan, i.e. the presence of peaks at 1645 cm<sup>-1</sup> (C=O stretching of amide I), 1515 (N-H bending of amide II) and 1343 (C-N stretching of amide III) cm<sup>-1</sup>. A small peak representing C=O stretching of ester from the succinyl moiety could also be observed at 1731 cm<sup>-1</sup>. The X-ray diffraction pattern of chitosan (Figure S3 in supporting material) showed broad peaks at  $2\theta$  of 10 and  $20^{\circ}$  while the pattern of mPEO-COOH gave sharp peaks at  $2\theta$  of 19 and  $23^{\circ}$ . The coupling product, mPEO-chitosan, showed broad peaks at  $2\theta$  values of 19 and 23° indicating a lower degree of crystallinity for the grafted mPEO moieties compared to the starting mPEO-COOH, implying some disruption of the crystal packing of the mPEO chains after being grafted onto chitosan.

The mPEO substitution degree on chitosan chains of 0.12 could be deduced from the <sup>1</sup>H NMR spectrum using the ratio of the area of resonance peaks at 4.25 (the ethylene oxide protons next to the succinyl moiety) and 2.05 (the *N*-acetyl protons on the glucosamine unit) ppm. It should be noted here that with the high molecular weight of the mPEO (5000 Da), the substitution degree of 0.12 was enough to inherit thermoresposive property into the copolymer (see results below).

The fragrances (vanillin and citral) were successfully loaded into the mPEO-chitosan particles via an ultrasonic aided diffusion process. The fragrance loading was carried out at the fragrance to polymer weight ratio of 1:3. This ratio gave fragrance-loaded particle suspension with complete encapsulation, i.e. no unencapsulated fragrance was found in the medium obtained from centrifugally filtering the suspension. The centrifugally filtered (through Millipore, MWCO 10 000 membrane) fragrance-loaded particles were subjected to acid hydrolysis following with hexane extraction and the hexane extract was subjected to UV-visible spectroscopic analysis with aids of calibration curve. The loading of ~30% (weight of fragrance to weight of polymer) could be obtained.

Since imine linkages between aldehydes and amino groups on the chitosan chains have been reported, [12,23] it was speculated that some imine bonds between the fragranced aldehyde

molecules and amino groups on the mPEO-chitosan chains might be formed. However, such formation took place only in a small amount since only weak C=N stretching vibration ( $\sim$ 1635–1639 cm $^{-1}$ ) in the IR spectrum of the products was observed (comparing to the background vibrational peaks from the mPEO-chitosan around the same wavenumbers, Figure 2). The reason for this probably is likely to be the steric effect from the grafted mPEO ( $M_{\rm n}$  of 5000) moieties.

#### Morphology of Fragrance-loaded mPEO-Chitosan Particles

At an aqueous concentration of 3.0 g/l, at room temperature, the two encapsulated fragrance suspensions although appeared as transparent liquids, transmission electron microscopy analysis revealed spherical particles (Figure 3a and b) with dry size of approximately 100-300 nm. Hydrodynamic size, estimated from dynamic light scattering, were 410.67  $\pm$  11.68 nm with a polydispersity index of  $0.453 \pm 0.02$  for citral-loaded mPEO-chitosan. Optical microscopy images of the citral- and vanillin-loaded mPEO-chitosan suspensions also showed spherical morphology with the size of approximately  $332 \pm 80$  and  $565 \pm 51$  nm, respectively (Figure 3c and e). It should be noted here that the critical aggregation concentration of the mPEO-chitosan in the presence of fragrance (at 30% weight ratio) was only ~0.47 g/l (Figure S2 in supporting material), thus the concentration of 3.0 g/l used in all the encapsulation experiments was well above the critical aggregation concentration.

It was speculated that the water-immisible hydrophobic fragrance molecules were embedded inside the particles, having minimal contact with water medium, while the hydrophilic mPEO moieties of the polymer should position themselves at the outer spherical surfaces, contacting with hydrophilic water medium.

## Thermo-responsive Phase Transition of the Fragrance-loaded mPEO-Chitosan Particles

When the aqueous suspension of the two fragrance-loaded mPEO-chitosan particles were heated from 25 to 80°C, no change in the light absorption at 500 nm could be observed, indicating no phase transition of the materials. The suspensions appeared transparent throughout the temperature change. However, in the presence of ZnSO<sub>4</sub>, a sudden decrease in the light transmittance when the temperature reached a critical point, could be observed (solid line Figure 4a and b), indicating

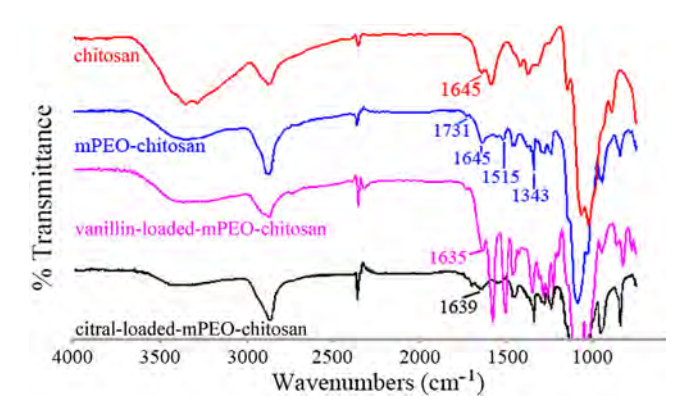


**Figure 2.** ATR-FTIR spectra of chitosan, mPEO–chitosan and the two aldehyde-loaded mPEO–chitosan particles

some phase transition of the materials at that temperature. The decrease in light transmittance was accompanied with a change from a transparent to a cloudy liquid. The critical temperature that induced this change decreased with increasing ZnSO<sub>4</sub> concentrations. When the same samples were then cooled, a sudden increase in the light transmittance was witnessed at the same critical temperature as when heated up, implying the reverse phase transition of the materials (dotted line Figure 4a), and the cloudy samples reverted their appearances back into a transparent liquid.

Therefore, it can be concluded that the two fragrance-loaded mPEO-chitosans possess a reversible phase transition property which is triggered by the change in temperature. When the suspension of the citral-loaded mPEO-chitosan was observed under the optical microscope using the differential interference contrast mode, at a temperature below the critical temperature (25°C) the ~ 300 nm spheres were well distributed in the medium (Figure 3c), but at 50°C (temperature above the critical temperature), aggregates with a size of more than 10 µm were clearly observed (Figure 3d). Similarly, at 25°C, the aqueous suspension of vanillin-loaded mPEO-chitosan (with ZnSO<sub>4</sub>) was comprised of well-dispersed spherical particles with a size of ~600 nm (Figure 3e) which aggregated to form > 10  $\mu$ m size aggregates when the temperature was raised to 50°C (Figure 3f). Therefore, the temperature dependent cloudiness that was accompanied with the sudden change in transmittance was likely to be the result of aggregation among sub-micron size spheres into much larger sized particulates which then scattered the visible light more severely.

It has been reported that the lower critical solution temperature (LCST) of PEO is around 185°C in water.<sup>[21]</sup> Thus, this polymer should be well hydrated at temperatures below 185°C. As discussed earlier, since the surface of the fragrant particles was covered with mPEO, it was expected that at 25-80°C with no salt in the system these PEO coronas would be well hydrated and so binding among PEO chains would be minimal, preventing aggregation among particles. When  $Zn^{2+}$  and  $SO_4^{2-}$ ions were present in the system, the LCST of the polymer was significantly decreased because water hydration of the Zn<sup>2+</sup> and  $SO_4^{2-}$  ions significantly affect the hydration of the PEO chains encouraging the hydrophobic interaction amongst the PEO chains. [26,27] In other words, in the presence of Zn<sup>2+</sup> and SO<sub>4</sub><sup>2-</sup> ions, the entropy contribution becomes the driving force towards minimal free energy at a lower temperature compared to the system with no ions. The salt thus lowers the LCST of the system. As the concentration of the ions increases, this effect kicks in at a lower temperature and so the LCST of the system decreases as the temperature increases. At temperatures lower than the LCST, the mPEO chains at the surface of the spheres interact amongst themselves through hydrophobic van der Waals forces. Both intra- and inter-sphere interactions take place, resulting in aggregation amongst the spheres into particulates of >10 µm size. In support of this notion, in addition to the microscopy images under the differential interference contrast mode is that the fluorescence microscopic images of the two materials at 25 and 50°C also showed clear aggregation among particles at the latter temperature (Figure S3 in supporting material).

#### Thermal Switching of the Aldehyde Release

The aggregation-deaggregation of the fragrance-loaded mPEO-chitosan particles is a result of the switching from the mPEO

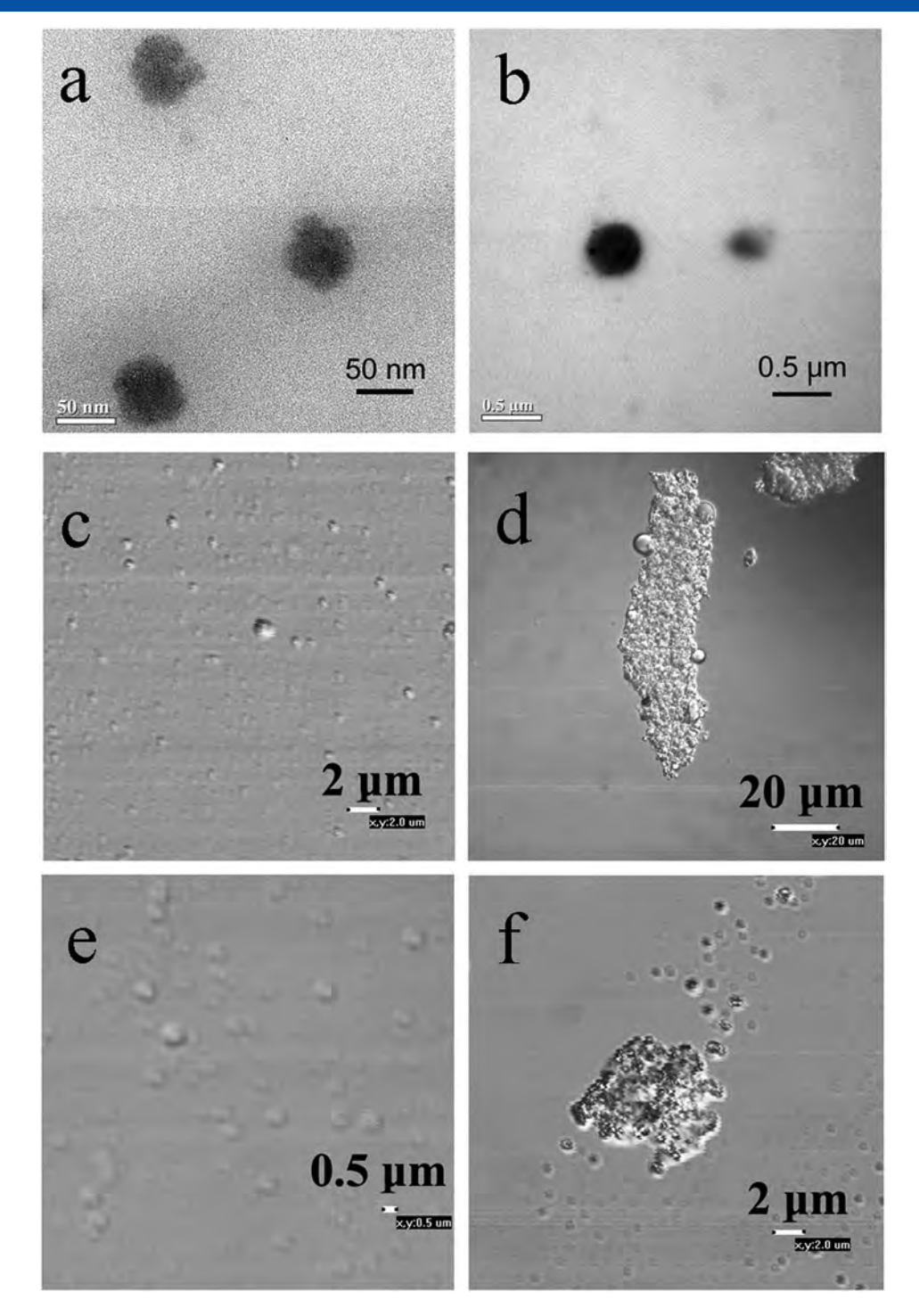


Figure 3. Representative transmission electron microscopy micrographs of (a) citral-loaded mPEO–chitosan and (b) vanillin-loaded mPEO–chitosan particles. Representative differential interference contrast microscopic pictures of (c, d) citral-loaded mPEO–chitosan and (e, f) and vanillin-loaded mPEO–chitosan with 1.5 M ZnSO<sub>4</sub> at (c, e) ambient temperature, (d) 40°C and (f) 55°C

inter-chains interaction to the mPEO-water hydration which then drives toward the minimal free energy of the system. Aggregation and de-aggregation among self-assembled particles significantly affects the efflux of fragrance molecules from the spheres. The efflux is minimized when the aggregation of nanospheres takes place (temperatures above the LCST value) since the packing of mPEO chains acts as another barrier layer. Thus, it is expected that the switching from fast to slow releases

of fragrant aldehydes will actually be the LCST and, as mentioned earlier, that the LCST is directly affected by the presence of salt in the system. Therefore, the thermo-switch should be tuneable by adjusting the salt concentration of the system.

Indeed, the thermo-responsive controlled release of aldehyde fragrance was demonstrated for vanillin and citral from vanillin-loaded mPEO-chitosan at a ZnSO $_4$  concentration of 0.9 M (LCST = 55°C), and from citral-loaded mPEO-chitosan at a ZnSO $_4$ 

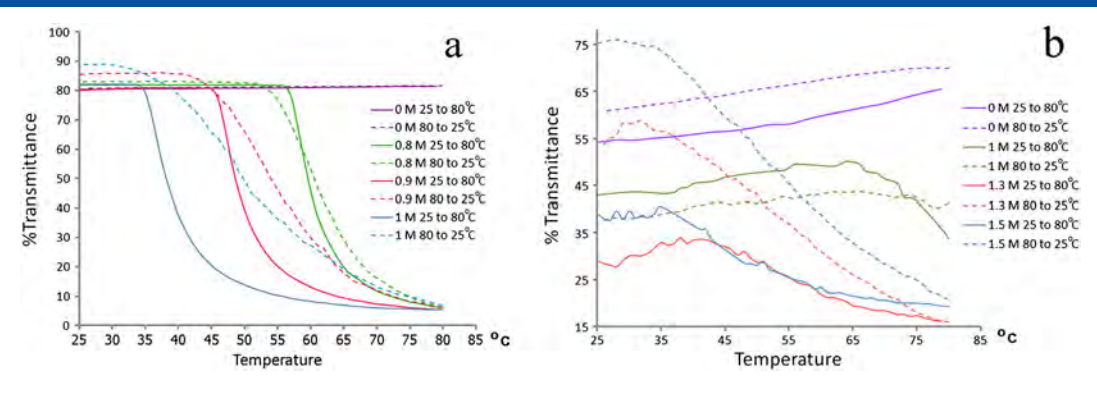
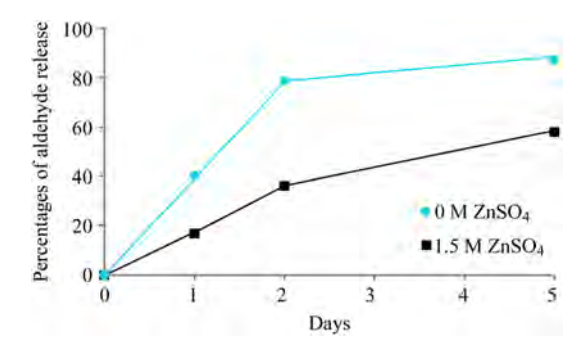
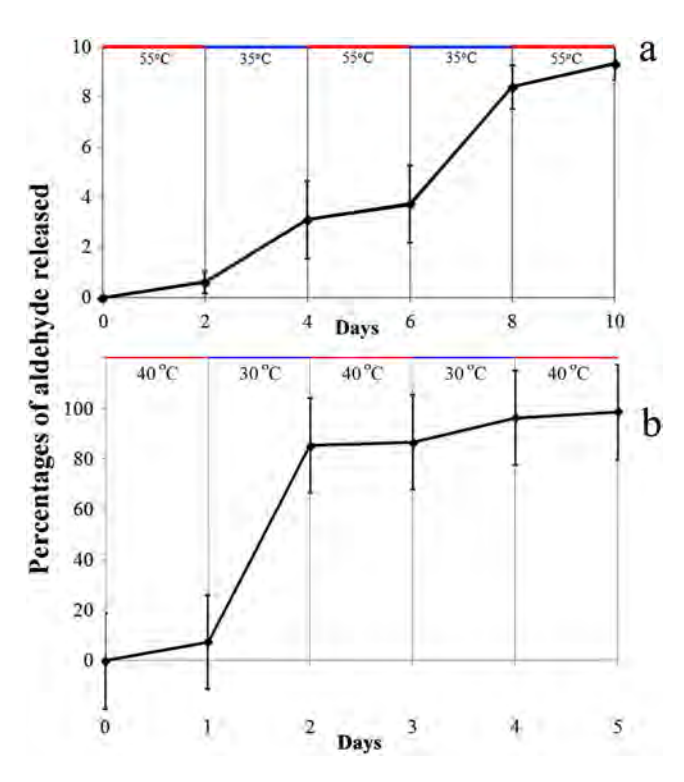


Figure 4. Light transmittance profiles of vanillin-loaded mPEO–chitosan (a) and citral-loaded mPEO–chitosan (b) aqueous suspensions, at various ZnSO<sub>4</sub> concentrations

concentration of 1.5  $\,\mathrm{m}$  (LCST = 45°C), respectively, both at a polymer concentration of 3 g/l. At 55°C, the release of vanillin was minimized (release rate of 0.6–0.9%/day), while at 35°C a faster release of vanillin (release rate of 2.5–4.7%/day) could be observed (Figure 5a). Similarly, the release of citral was very fast (release rate of 74.9%/day) at 35°C while at 45°C the release was much slower (release rate of 2.4–7.3%/day) (Figure 5b). It was obvious that citral could be released from the mPEO–chitosan particles at a faster rate than vanillin did. This result agrees well with the fact that citral is more volatile than vanillin, the vapour pressure of citral is ~12 Pa while that of vanillin is ~0.3 Pa at 25°C.



**Figure 6.** Release of citral from 3 g/l citral-loaded mPEO–chitosan at  $40^{\circ}\text{C}$ 



**Figure 5.** On/off fragrance release at two different temperatures from (a) vanillin-loaded mPEO–chitosan particle suspension in 0.9~M aqueous ZnSO<sub>4</sub> solution, and (b) citral-loaded mPEO–chitosan particle suspension in 1.5~M aqueous ZnSO<sub>4</sub> solution, both at a polymer concentration of 3 g/l and a pH of 1

# **Controlling the Rate of Fragrance Release by Adjusting Salt Concentration**

The citral-loaded mPEO-chitosan system was also tested for the release at 40°C under two different conditions: in water with no  $ZnSO_4$  (LCST > 185°C) and in 1.5 M aqueous  $ZnSO_4$  solution (LCST~35-55°C). A faster release of citral was seen in the absence of the salt than with it (Figure 6), which agrees well with the fact that the LCST of PEO is higher than 185°C, and so no dehydration at the PEO corona will take place at 40°C, allowing the release of fragrance molecules. In contrast, in the presence of 1.5  $\rm M$  ZnSO4, the LCST of the polymer decreased to around 35-55°C (Figure 4b), and so at 40°C some dehydration of the mPEO corona took place and association among spheres occurred, causing a much more limited fragrance release. This example demonstrates that in addition to the thermo-switch character demonstrated above, the fragrance reservoir fabricated here is also tuneable in terms of the fragrance release rate at a fixed temperature by varying the salt concentration.

#### **Refilling the System**

When most of the fragrance molecules had been released, it was observed that in the addition of fresh fragrant aldehyde molecules followed by either ultra-sonication for 4 h or stirring, at 25°C, led to the encapsulation of the fragrance into the spheres. The newly obtained spheres showed the same thermo-responsive fragrance release characteristics as the previous fragrance spheres (data not shown). Thus, this fragrance controlled release system is refillable.

#### **Conclusion**

Here a thermo-switchable fragrance controlled release system was fabricated using the non-toxic biocompatible PEO and chitosan polymers. The mPEO-chitosan grafted polymer was synthesized and in the presence of hydrophobic water immisible fragrance molecules, the obtained material self-assembled into fragrance-loaded spherical particles with the mPEO corona covering the surface. Modulation of the switching between the mPEO-water and the mPEO-mPEO interactions was used to control the efflux of the fragrance molecules. The mPEO-water interaction took place at temperatures lower than the LCST value, resulting in water dispersion of each sphere. In contrast, mPEO-mPEO interactions occurred at temperatures higher than the LCST value, resulting in aggregation among particles and limiting the efflux of fragrance molecules from the spheres. The LCST value could be tuned by adjusting the concentration of the ZnSO<sub>4</sub> in the system. For example, the vanillin-loaded mPEO-chitosan aqueous system with 0.8, 0.9 and 1 M ZnSO<sub>4</sub> showed LCST values of 55, 45 and 35°C, respectively, while the citral-loaded mPEO-chitosan aqueous system with 1, 1.3 and 1.5 M ZnSO<sub>4</sub> showed LCST values of 65, 43 and 35°C, respectively. Release of vanillin at 0.9 M ZnSO<sub>4</sub> was steady at temperatures lower than 45°C, but was halted at the temperatures above that value. When all the fragrance molecules were released, new fragrance could be loaded into the spheres by just stirring into the system the fragrant molecules at the temperature below the LCST.

#### **Acknowledgements**

The authors thank the Commission of Higher Education–Thailand Research Fund (BRG5280004), the Special Task Force for Activating Research (STAR) and the Center of Innovative Nanotechnology from the Centenary Academic Development Project, Chulalongkorn University. The work is part of the project for the Establishment of Comprehensive Center for Innovative Food, Health Products and Agriculture supported by the Thai Government SP 2 (TKK2555) and the National Research University Project of CHE (AM1006A).

#### Supporting Information

Supporting information may be found in the online version of this article.

#### References

- 1. A. Herrmann. Angew. Chem. Int. Ed. 2007, 46, 5836.
- 2. A. Edris, B. Bergnståhl. Die Nahrung 2001, 45,133.
- 3. F. Lai, S. A. Wissing, R. H. Müller, A. M. Fadda. AAPS PharmSciTechnol 2006, 7, 1.
- J. Karlsen. In Handbook of Essential Oils, K. Hüsnü Can Baser and G. Buchbauer (eds). CRC Press: New York, 2010; 855–861.
- I. Goubet, J. L. Le Quere, A. J. Voilley. J. Agric. Food Chem. 1998, 46, 1981.
- V. Normand, P. E. Bouquerand, R. Mciver, A. Subramaniam. Agro. Food Ind. Hi-Technol. 2009, 20, 21.
- 7. S. Choi, S. Amajjahe, H. Ritter. Adv. Polym. Sci. **2009**, 222, 175.
- P. Scarfato, E. Avallone, P. lannelli, V. De Feo, D. Aderno. J. Appl. Polym. Sci. 2007, 105, 3568.
- 9. J. S. Hwang, J. N. Kim, Y. J. Wee, J. S. Yun, H. G. Jang, S. H. Kim, H. W. Ryu. *Biotechnol. Bioprocess Eng.* **2006**, *11*, 332.
- A. Sansukcharearnpon, S. Wanichwecharungruang, N. Leepipatpaiboon, T. Kerdcharoen, S. Arayachukeat. *Int. J. Pharm.* 2010, 391, 267.
- 11. D. L. Berthier, A. Herrmann, L. Ouali, Polym. Chem. 2011, 2, 2093.
- T. Tree-Udom, S. P. Wanichwecharungruang, J. Seemork, S. Arayachukeat. Carbohydr. Polym. 2011, 86, 1602.
- 13. B. Levrand, A. Herrmann. Photochem. Photobiol. Sci. 2002, 1, 907.
- 14. B. Levrand, A. Herrmann. Chimia 2007, 61, 661.
- S. Rochat, C. Minardi, J. Y. De Saint Laumer, A. Herrmann. Helv. Chim. Acta 2000, 83, 1645.
- 16. J. L. Robles, C. G. Bochet. Org. Lett. 2005, 7, 3545.
- Y. Wang, H. Morinaga, A. Sudo, T. Endo. J. Polym. Sci., Part A: Polym. Chem. 2011, 49, 1881.
- J. Y. De Saint Laumer, E. Frérot, A. Herrmann. Helv. Chim. Acta 2003, 86, 2871.
- H. Morinaga, H. Morikawa, A. Sudo, T. Endo. J. Polym. Sci., Part A: Polym. Chem. 2009, 47, 3241.
- A. Trachsel, J. Y. de Saint Laumer, O. P. Haefliger, A. Herrmann. *Chem. Eur. J.* 2009, *15*, 2846.
- H. Kamogawa, H. Mukai, Y. Nakajima, M. Nanasawa. J. Polym. Sci., Polym. Chem. Ed. 1982, 20, 3121.
- H. Morinaga, H. Morikawa, Y. Wang, A. Sudo, T. Endo. *Macromolecules* 2009, 42, 2229.
- D. Hua, J. Jiang, L. Kuang, W. Zheng, H. Liang. *Macromolecules* 2011, 44, 1298.
- M. J. Joralemon, S. McRae, T. Emrick. Chem. Commun. 2010, 46, 1377.
- K. Knop, R. Hoogenboom, D. Fischer, U. S. Schubert. *Angew. Chem. Int. Ed.* 2010, 49, 6288.
- J. F. Lutz, Ö. Akdemir, A. Hoth. J. Am. Chem. Soc. 2006, 128, 13046.
- J. P. Magnusson, A. Khan, G. Pasparakis, A. O. Saeed, W. Wang, C. Alexander. J. Am. Chem. Soc. 2008, 130, 10852.

#### Self-Assembly of Negatively Charged Poly(vinyl alcohol) Derivatives

#### Paramee Jitjumnong<sup>1,2</sup>, Supason P. Wanichwecharungruang<sup>1,\*</sup>, and Sunatda Arayachukeat<sup>2</sup>

<sup>1</sup>Department of Chemistry, Faculty of Science, Chulalongkorn University, Bangkok 10330, Thailand <sup>2</sup>National Center of Petroleum, Petrochemicals and Advanced Materials, Chulalongkorn University, Bangkok 10330, Thailand

Received December 21, 2009; Revised April 29, 2010; Accepted April 29, 2010

**Abstract:** This paper reports the relationship between the degree of negatively charged groups on the poly(4-vinyloxybutane sulfonate-*co*-vinyl alcohol) or PVA-BS and poly(4-vinyloxybutane sulfonate-*co*-vinyloxydodecane-*co*-vinyl alcohol) or PVA-12C-BS polymers and their self-assembled particles' morphologies. With grafted hydrophobic moieties (PVA-12C-BS polymers), the size of the self-assembled particles decreased with increasing levels of butane sulfonate substitution. However, with no hydrophobic moiety grafted (PVA-BS), the size of the self-assembled particles increased with increasing levels of butane sulfonate substitution. The response of the PVA-BS and PVA-12C-BS polymeric particles to the loading of a model hydrophobic compound, 2-ethylhexyl-4-methoxycinnamate (EHMC), was markedly different. With the drug as a hydrophobic core, EHMC-loaded PVA-BS particles were smaller in size and more stable than the unloaded particles. In contrast, the EHMC-loaded PVA-12C-BS particles were larger than the corresponding unloaded particles.

Keywords: poly(vinyl alcohol), negatively charged particle, butane sulfonate, self-assembly.

#### Introduction

Poly(vinyl alcohol) (PVA or PVOH) is a hydrophilic polymer that is biodegradable, biocompatible, nontoxic, noncarcinogenic and can be eliminated from the human body by renal excretion. Thus, it is a well accepted 'pharmaceutically safe' polymer for both humans and the environment, and as such has been used in various pharmaceutical, medical, cosmetic, food and agricultural products. In the area of drug delivery, PVA is commonly used as an emulsion stabilizer in the preparation of nanoparticles, and as a starting material to prepare hydrogels, micelles and polymeric micro/nanoparticles. In addition, the preparation of cationic spheres based on either a blend of PVA and polyethylenimine with poly(D,L-lactide-*co*-glycolide), or melamine formaldehyde particles coated with chitosan-PVA-borate gel, have also been reported.

Reports on the use of PVA as the main polymeric carrier include the use of PVA hydrogel nanoparticles, prepared by water-in-oil emulsification plus repeating freezing-thawing process for protein/peptide drug delivery, PVA-DNA nanoparticles, prepared by ultra high pressure technology for gene delivery, PVA-poly(vinyl pyrrolidone) nanoparticles, and crosslinked PVA hydrogels. Indeed, the Orienti team and some other research groups have prepared various PVA derivatives for use as drug carriers. Most of the

reported PVA derivatives have been prepared by grafting the appropriate functional chemical moieties, such as various acyl chains, <sup>15,16</sup> functional 2-hydroxypropyltrimethylammonium derivatives, <sup>7</sup> triethylene glycol monoethyl ether, <sup>17</sup> tetraethylene glycol monoethyl ether, <sup>18</sup> functional amine derivatives, <sup>19</sup> amino/poly(D,L-lactide-*co*-glycolide), <sup>20</sup> oleyl amine, <sup>21</sup> various cinnamoyl derivatives, <sup>22</sup> and sulfobutyl/poly(lactide-*co*-glycolide), <sup>23</sup> onto the PVA backbone. Amongst these, PVA grafted with functional 2-hydroxypropyltrimethylammonium or amino groups possess positive charge characteristics, while those grafted with sulfobutylated poly(vinyl alcohol)-*graft*-poly(lactide-*co*-glycolide)s provides negative charges.

Within the limited number of available reports on the negatively charged polymers, a relationship between a number of negative charges on the polymer and its self-assembled morphology has never been reported. In this work, thus, several derivatives of the negatively charged poly(4-vinyloxybutane sulfonate-co-vinyl alcohol), or PVA-BS, and poly (4-vinyloxybutane sulfonate-co-vinyloxydodecane-co-vinyl alcohol), or PVA-12C-BS, with various degrees of substitution of either the dodecane or the butane sulfonate moieties on the PVA backbone, were prepared and allowed to self-assemble into nanospheres. The correlation between the morphology of the particles and the polymer structure is discussed. In addition, loading of the model hydrophobic compound, 2-ethylhexyl-4-methoxycinnamate, into the nanospheres was also evaluated and is discussed.

<sup>\*</sup>Corresponding Author. E-mail: psupason@chula.ac.th





#### **Experimental**

Materials. Poly(vinyl alcohol) or PVA (Mw 124,000-186,000, 87-89% deacetylated, Aldrich), 1,4-butane sultone (Acros), 1-bromododecane (Fluka) and all other chemicals were reagent grade and were used without additional purification.

**Analytical Measurements.** The <sup>1</sup>H and <sup>13</sup>C NMR analyses were performed using a Varian Mercury spectrometer, operated at 400.00 MHz for <sup>1</sup>H and 100.00 MHz for <sup>13</sup>C nuclei in CDCl<sub>3</sub> or DMSO-d<sub>6</sub> or D<sub>2</sub>O. UV absorption spectra were acquired with a UV 2500 UV-vis spectrophotometer (Shimadzu) using a quartz cell with a 1 cm path length. FTIR spectra were obtained using a Nicolet Fourier transform infrared spectrophotometer, model Impact 410. The thermogram of each sample was acquired at 20-220 °C under nitrogen with a scanning rate of 10 °C/min using differential scanning calorimetry: DSC 204 (Netzsch). The hydrodynamic size and  $\zeta$  potential of the particles were acquired using a Mastersizer S and Zetasizer nanoseries (Mulvern Instruments), respectively, equipped with a He-Ne laser beam at 632.8 nm (scattering angle of 173°). Measurements were carried out on an 800 ppm aqueous suspension of the particles. Transmission electron micrographs (TEM) were obtained using a JEM-2100 electron microscope (Jeol) with an accelerating voltage of 100-120 kV in con-

Scheme I. Synthesis of PVA-BS and PVA-12C-BS polymers.

junction with selected area electron diffraction (SAED).

**Synthesis of PVA-BS (Scheme I).** PVA-BS was synthesized by reacting PVA with 1,4-butane sultone under anhydrous conditions using NaH as a catalyst. PVA (0.44 g, 10 mmol monomeric units) was dissolved in 45 mL of heated anhydrous DMF. Then, NaH (0.24 g, 10 mmol) and 1,4-butane sultone (see Table I for amounts) were added. The mixture was stirred overnight at room temperature and then

Table I. The Amounts of Reactants Used During the Synthesis, Structures, and Physicochemical Properties of PVA-BS and PVA-12C-BS Derivatives Together with the Zeta Potential Values of the Nanoparticles Obtained from Self-assembly of Each Polymer

Polymers	Amounts of 1-Bro- mododecane Used Butane Sultone Used in the Reaction in the Reaction	Structural Characterization					Zetapotential		
			l	n	m	p	$T_g^a(^{ m o}{ m C})$	$T_m^b$ (°C)	of the Particles (mV)
PVA <sup>c</sup>	-	-	0.11	-	0.89	-	-	191.5	-
PVA-BS1	-	10 mmol	-	-	0.806	0.194	104.4	-	-
PVA-BS2	-	5 mmol	-	-	0.934	0.066	83.7	-	-11.6±1.6
PVA-BS3	-	2 mmol	-	-	0.964	0.036	81.7	-	-20.6±0.3
PVA-BS4	-	1 mmol	-	-	0.987	0.013	76.9	-	-28.7±0.2
PVA-12C2-BS1	0.5 mmol	10 mmol	-	0.021	0.943	0.036	80.3	-	-24.5±0.07
PVA-12C2-BS2	0.5 mmol	5 mmol	-	0.021	0.952	0.027	76.9	-	-29.9±0.04
PVA-12C2-BS3	0.5 mmol	2 mmol	-	0.021	0.954	0.025	78.3	-	-30.8±0.4
PVA-12C1-BS1	2 mmol	20 mmol	-	0.033	0.832	0.135	81.3	-	-35.6±0.8
PVA-12C1-BS2	2 mmol	10 mmol	-	0.033	0.930	0.037	71.6	-	-31.6±0.3
PVA-12C1-BS3	2 mmol	5 mmol	-	0.033	0.939	0.026	70.6	-	-31.6±0.08
PVA-12C1-BS4	2 mmol	2 mmol	-	0.033	0.945	0.024	69.0	-	-32.6±0.4

<sup>&</sup>lt;sup>a</sup>Glass transition temperature as obtained from DSC analysis. <sup>b</sup>Melting temperature as obtained from DSC analysis. <sup>c</sup>M<sub>w</sub> 124,000-186,000.

subjected to dialysis against water (7×1,000 mL), for 4 h each time, using a regenerated cellulose tubular membrane (MWCO 12,000-14,000). Dry products were obtained by freeze-drying. Four PVA-BS polymers, each with a different degree of butane sulfonate substitution, were synthesized and their characterization is given below.

**PVA-BS1:** Light orange solid. DS: 0.194. Yield: 76%.  $T_g$ : 104.4 °C. FTIR (KBr, cm<sup>-1</sup>): 3426 (s, br, OH stretching), 2945, 2867 (s, -C-H stretching), 1330 (s, SO<sub>3</sub> stretching), 1442 (m, -CH<sub>2</sub>- bending), 1378 (m, C-O-H bending), 1048 (s, C-O-H stretching) and 1200, 1100 (s, C-O-C stretching). <sup>1</sup>H NMR (400 MHz, D<sub>2</sub>O-d<sub>2</sub>, δ, ppm): 4.0-3.2 (br, 4H, -CH-OH and 3H, -CH-O-CH<sub>2</sub>-), 2.7 (t, J=7.6, 14.4 Hz, 2H, -CH<sub>2</sub>-SO<sub>3</sub>) and 1.0-1.8 (br, 10H, -CH-CH<sub>2</sub>-CH- of the PVA backbone and 4H, O-CH<sub>2</sub>-CH<sub>2</sub>-CH<sub>2</sub>-CH<sub>2</sub>-SO<sub>3</sub>).

**PVA-BS2:** Light orange solid. DS: 0.066. Yield: 85%.  $T_g$ : 83.7 °C. FTIR (KBr, cm<sup>-1</sup>): 3394 (s, br, OH stretching), 2933, 2863 (s, -C-H stretching), 1330, 1144 (s, SO $_3$  stretching), 1430 (m, -CH $_2$ -bending), 1375 (m, C-O-H bending) 1046 (s, C-O-H stretching) and 1196, 1096 (s, C-O-C stretching). H NMR (400 MHz, D $_2$ O-d $_2$ ,  $\delta$ , ppm): 4.0-3.2 (br, 14H, -CH-OH and 3H, -CH-O-CH $_2$ -), 2.7 (t, J=7.6, 15.2 Hz, 2H, -CH $_2$ -SO $_3$ ) and 1.0-1.8 (br, 28H, -CH-CH $_2$ -CH- of the PVA backbone and 4H, O-CH $_2$ -CH $_2$ -CH $_2$ -CH $_2$ -CO $_3$ ).

**PVA-BS3:** Light orange solid. DS: 0.036. Yield: 94%.  $T_g$ : 81.7 °C. FTIR (KBr, cm<sup>-1</sup>): 3381 (s, br, OH stretching), 2936, 2854 (s, -C-H stretching), 1330, 1147 (s, SO $_3$  stretching), 1433 (m, -CH $_2$ - bending), 1375 (m, C-O-H bending) 1040 (s, C-O-H, stretching) and 1199, 1099 (s, C-O-C stretching). <sup>1</sup>H NMR (400 MHz, D $_2$ O-d $_2$ , δ, ppm): 4.0-3.2 (br, 27H, -CH-OH and 3H, -CH-O-CH $_2$ -), 2.7 (t, J=7.4, 14.8 Hz, 2H, -CH $_2$ -SO $_3$ ) and 1.0-1.8 (br, 54H, -CH-CH $_2$ -CH- of the PVA backbone and 4H, O-CH $_2$ -CH $_2$ -CH $_2$ -CH $_2$ -CO $_3$ ).

**PVA-BS4:** Light orange solid. DS: 0.013. Yield: 81%.  $T_g$ : 76.9 °C. FTIR (KBr, cm<sup>-1</sup>): 3372 (s, br, OH stretching), 2927, 2850 (s, -C-H stretching), 1330, 1144 (s, SO $_3$  stretching), 1436 (m, -CH $_2$ - bending), 1375 (m, C-O-H bending) 1037 (s, C-O-H stretching) and 1196, 1095 (s, C-O-C stretching). <sup>1</sup>H NMR (400 MHz, D $_2$ O-d $_2$ , δ, ppm): 4.0-3.2 (br, 76H, -CH-OH and 3H, -CH-O-CH $_2$ -), 2.7 (t, J=7.8, 16 Hz, 2H, -CH $_2$ -SO $_3$ ) and 1.0-1.8 (br, 152H, -CH-CH $_2$ -CH- of the PVA backbone and 4H, O-CH $_2$ -CH $_2$ -CH $_2$ -CH $_2$ -SO $_3$ ).

Synthesis of PVA-12C-BS (Scheme I). PVA-12C-BS was prepared by reacting PVA with 1-bromododecane under anhydrous conditions using NaH as the catalyst. PVA (0.44 g, 10 mmol monomeric units) was dissolved in 45 mL of heated anhydrous DMF. Then, NaH (0.24 g, 10 mmol) and 1-bromododecane (see Table I for amounts) were added. The mixture was stirred overnight at room temperature before being dialyzed (as detailed above) and then dried by reduced pressure evaporation. The obtained polymer was dissolved in 45 mL of heated anhydrous DMF and NaH (0.24 g, 10 mmol) and 1,4-butane sultone (see Table I) were added. The mixture was then stirred overnight at room temperature and the

obtained product was subjected to dialysis and freeze-dried as detailed above. Seven PVA-12C-BS polymers, which vary in the degree of butane sulfonate and dodecyl substitutions, were synthesized and their characterization is detailed below.

**PVA-12C1-BS1:** Light orange solid. DS of dodecyl group: 0.033. DS of butane sulfonate: 0.135. Yield: 101%.  $T_g$ : 81.3 °C. FTIR (KBr, cm<sup>-1</sup>): 3393 (s, br, OH stretching), 2930, 2854 (s, -C-H stretching), 1333 (s, SO $_3$  stretching), 1455 (m, -CH $_2$ -bending), 1375 (m, C-O-H bending) 1043 (s, C-O-H stretching) and 1193, 1095 (s, C-O-C stretching). <sup>1</sup>H NMR (400 MHz, D $_2$ O-d $_2$ , δ, ppm): 4.2-4.9 (br, 9H, -OH), 4.0-3.2 (br, 9H, -CH-OH and 1H, -CH-O-CH $_2$ -), 2.7 (t, J=7.2, 14.4 Hz, 3H, -CH $_2$ -SO $_3$  ), 0.8-1.8 (br, 7H, -CH $_2$ - of the dodecyl moiety, 6H, -CH $_2$ -CH $_2$ - and 22H, -CH-CH $_2$ -CH- of the PVA backbone) and 0.7 (t, J=8, 16 Hz, 1H, -CH $_2$ -CH $_3$ ).

**PVA-12C1-BS2:** Light orange solid. DS of dodecyl group: 0.033. DS of butane sulfonate: 0.037. Yield: 96%.  $T_g$ : 71.6 °C. FTIR (KBr, cm<sup>-1</sup>): 3384 (s, br, OH stretching), 2924, 2854 (s, -C-H stretching), 1330, 1141 (s, SO<sub>3</sub> stretching), 1455 (m, -CH<sub>2</sub>- bending), 1375 (m, C-O-H bending) 1043 (s, C-O-H stretching) and 1196, 1095 (s, C-O-C stretching). <sup>1</sup>H NMR (400 MHz, D<sub>2</sub>O-d<sub>2</sub>,  $\delta$ , ppm): 4.5 (br, 13H, -OH), 4.0-3.2 (br, 13H, -CH-OH and 1H, -CH-O-CH<sub>2</sub>-), 2.7 (t, J=6.8, 13.6 Hz, 1H, -CH<sub>2</sub>-SO<sub>3</sub> ), 0.8-1.7 (br, 10H, -CH<sub>2</sub>- of the dodecyl moiety, 2H, -CH<sub>2</sub>-CH<sub>2</sub>- and 27H, -CH-CH<sub>2</sub>-CH- of the PVA backbone) and 0.694 0.711 0.728 (t, J=6.8, 13.6 Hz, 1H, -CH<sub>2</sub>-CH<sub>3</sub>).

**PVA-12C1-BS3:** Light orange solid. DS of dodecyl group: 0.033. DS of butane sulfonate: 0.028. Yield: 94%.  $T_g$ : 70.6 °C. FTIR (KBr, cm<sup>-1</sup>): 3378 (s, br, OH stretching), 2924, 2854 (s, -C-H stretching), 1330, 1144 (s, SO $_3$  stretching), 1446 (m, -CH $_2$ - bending), 1375 (m, C-O-H bending) 1040 (s, C-O-H stretching) and 1199, 1098 (s, C-O-C stretching).  $^1$ H NMR (400 MHz, D $_2$ O-d $_2$ , δ, ppm): 4.5 (br, 17H, -OH), 4.0-3.2 (br, 17H, -CH-OH and 2H, -CH-O-CH $_2$ -), 2.7 (t, J=7.4, 14.8 Hz, 1H, -CH $_2$ -SO $_3$ -), 0.8-1.7 (br, 13H, -CH $_2$ - of the dodecyl moiety, 2H, -CH $_2$ -CH $_2$ - and 36H, -CH-CH $_2$ -CH- of the PVA backbone) and 0.7 (t, J=6.8, 13.6 Hz, 2H, -CH $_2$ -CH $_3$ ).

**PVA-12C1-BS4:** Light orange solid. DS of dodecyl group: 0.033. DS of butane sulfonate: 0.022. Yield: 100%.  $T_g$ : 69.0 °C. FTIR (KBr, cm<sup>-1</sup>): 3378 (s, br, OH stretching), 2921, 2848 (s, -C-H stretching), 1333, 1141 (s, SO<sub>3</sub><sup>-</sup> stretching), 1449 (m, -CH<sub>2</sub>- bending), 1375 (m, C-O-H bending) 1040 (s, C-O-H stretching) and 1193, 1095 (s, C-O-C stretching). <sup>1</sup>H NMR (400 MHz, D<sub>2</sub>O-d<sub>2</sub>, δ, ppm): 4.5 (br, 21H, -OH), 4.2-3.2 (br, 21H, -CH-OH and 2H, -CH-O-CH<sub>2</sub>-), 2.7 (t, J=7.2, 14.4 Hz, 1H, -CH<sub>2</sub>-SO<sub>3</sub><sup>-</sup>), 0.8-1.9 (br, 16H, -CH<sub>2</sub>- of the dodecyl moiety, 2H, -CH<sub>2</sub>-CH<sub>2</sub>- and 45H, -CH-CH<sub>2</sub>-CH- of the PVA backbone) and 0.7 (t, J=7.2, 14.4 Hz, H, 2H, -CH<sub>2</sub>-CH<sub>3</sub>).

**PVA-12C2-BS1:** Light orange solid. DS of dodecyl group: 0.021. DS of butane sulfonate: 0.036. Yield: 107%.  $T_g$ : 80.3 °C. FTIR (KBr, cm<sup>-1</sup>): 3369 (s, br, OH stretching), 2918, 2851 (s, -C-H stretching), 1330, 1144 (s,  $SO_3^-$  stretching), 1439 (m, -CH<sub>2</sub>- bending), 1375 (m, C-O-H bending) 1040 (s, C-

O-H stretching) and 1199, 1092 (s, C-O-C stretching).  $^{1}$ H NMR (400 MHz, D<sub>2</sub>O-d<sub>2</sub>,  $\delta$ , ppm): 4.5 (br, 15H, -OH), 4.0-3.2 (br, 15H, -CH-OH and 1H, -CH-O-CH<sub>2</sub>-), 2.7 (t, J=8, 16.4 Hz, 1H, -CH<sub>2</sub>-SO<sub>3</sub><sup>-</sup>), 0.8-1.8 (br, 7H, -CH<sub>2</sub>- of the dodecyl moiety, 2H, -CH<sub>2</sub>-CH<sub>2</sub>- and 32H, -CH-CH<sub>2</sub>-CH- of the PVA backbone) and 0.7 (t, J=8.2, 20.4 Hz, 1H, -CH<sub>2</sub>-CH<sub>3</sub>).

**PVA-12C2-BS2:** Light orange solid. DS of dodecyl group: 0.021. DS of butane sulfonate: 0.027. Yield: 110%.  $T_g$ : 76.9 °C. FTIR (KBr, cm<sup>-1</sup>): 3381 (s, br, OH stretching), 2924, 2854 (s, -C-H stretching), 1330, 1144 (s, SO<sub>3</sub> stretching), 1443 (m, -CH<sub>2</sub>- bending), 1375 (m, C-O-H bending) 1043 (s, C-O-H stretching) and 1196, 1095 (s, C-O-C stretching). <sup>1</sup>H NMR (400 MHz, D<sub>2</sub>O-d<sub>2</sub>, δ, ppm): 4.5 (br, 18H, -OH), 4.0-3.2 (br, 18H, -CH-OH and 1H, -CH-O-CH<sub>2</sub>-), 2.7 (t, J=7.8, 15.6 Hz, 1H, -CH<sub>2</sub>-SO<sub>3</sub> ), 0.8-1.8 (br, 8H, -CH<sub>2</sub>- of the dodecyl moiety, 2H, -CH<sub>2</sub>-CH<sub>2</sub>- and 37H, -CH-CH<sub>2</sub>-CH- of the PVA backbone) and 0.7 (t, J=7.4, 14.8 Hz, 1H, -CH<sub>2</sub>-CH<sub>3</sub>).

**PVA-12C2-BS3:** Light orange solid. DS of dodecyl group: 0.021. DS of butane sulfonate: 0.025. Yield: 106%.  $T_g$ : 78.3 °C. FTIR (KBr, cm<sup>-1</sup>): 3369 (s, br, OH stretching), 2918, 2851 (s, -C-H stretching), 1330, 1144 (s, SO $_3$  stretching), 1439 (m, -CH $_2$ - bending), 1375 (m, C-O-H bending) 1040 (s, C-O-H stretching) and 1199, 1092 (s, C-O-C stretching). <sup>1</sup>H NMR (400 MHz, D $_2$ O-d $_2$ , δ, ppm): 4.5 (br, 19H, -OH), 4.0-3.2 (br, 19H, -CH-OH and 1H, -CH-O-CH $_2$ -), 2.7 (t, J=6.6, 13.2 Hz, 1H, -CH $_2$ -SO $_3$ -), 0.8-1.8 (br, 8H, -CH $_2$ - of the dodecyl moiety, 2H, -CH $_2$ -CH $_2$ - and 40H, -CH-CH $_2$ -CH- of the PVA backbone) and 0.7 (t, J=7.8, 15.6 Hz, 1H, -CH $_2$ -CH $_3$ ).

Preparation of the Polymeric Nanoparticles. Each of the 11 obtained polymers (four PVA-BS and seven PVA-12C-BS) was induced into nanosphere formation through the solvent displacement technique. Forty milligrams of the polymer sample was dissolved in 10 mL of DMSO and transferred into a dialysis tube (regenerated cellulose tubular membrane, MWCO 12,000-14,000). The distance between the two clipped ends (~5 cm length of the flat tube) was set so as to account for approximately 20-25 mL volume, leaving approximately 10-15 mL void volume inside the dialysis tube at the beginning of the dialysis process. The dialysis was performed against seven changes (3, 8, 15, 20, 25, 30 and 40 h) of 1,000 mL deionized water (Milli-Q<sup>®</sup>) at room temperature. After dialysis, the volume of the obtained colloidal suspension inside the dialysis tube (normally ~doubled that of the starting volume) was adjusted to exactly 50 mL by adding water.

**2-Ethylhexyl-4-methoxycinnamate (EHMC) Encapsulation.** Twenty milligrams of one of each of the two main categories of the polymer sample (PVA-BS3 or PVA-12C3-BS1) and 20 milligrams of EHMC were dissolved in 5 mL of DMSO, transferred into a dialysis tube and dialyzed against deionized water (7×500 mL). The encapsulation efficiency (EE) was determined by quantitating the amount of EHMC in the dialysate using UV/VIS spectrophotometry at 310 nm with the aid of a calibration curve. The % encapsulation

efficiency (%EE) was calculated using eq. (1). The amount of EHMC loaded into nanoparticles was determined as loading capacity and was calculated using eq. (2).

$$\%EE = \frac{EHMC \text{ used - EHMC found in the medium}}{EHMC \text{ used}} \times 100$$

$$\text{Loading Capacity} = \frac{\text{Amount of drug in nanoparticles}}{\text{Amount of nanoparticles}} \times 100$$

$$(2)$$

#### **Results and Discussion**

**Synthesis of PVA-BS and PVA-12C-BS.** Grafting of butane sulfonate, a negatively charged moiety, onto the PVA backbone was successfully carried out and four PVA-BS polymers, each with a different degree of butane sulfonate substitution on the PVA were obtained (Table I). In the same way, grafting of the hydrophobic dodecyl moiety onto the PVA backbone attained seven different PVA-C12-BS polymers, each with a different degree of butane sulfonate and dodecyl substitution on the PVA backbone (Table I).

As shown in Figure 1, the <sup>1</sup>H NMR spectrum of PVA in D<sub>2</sub>O shows the resonances of the backbone methylene pro-

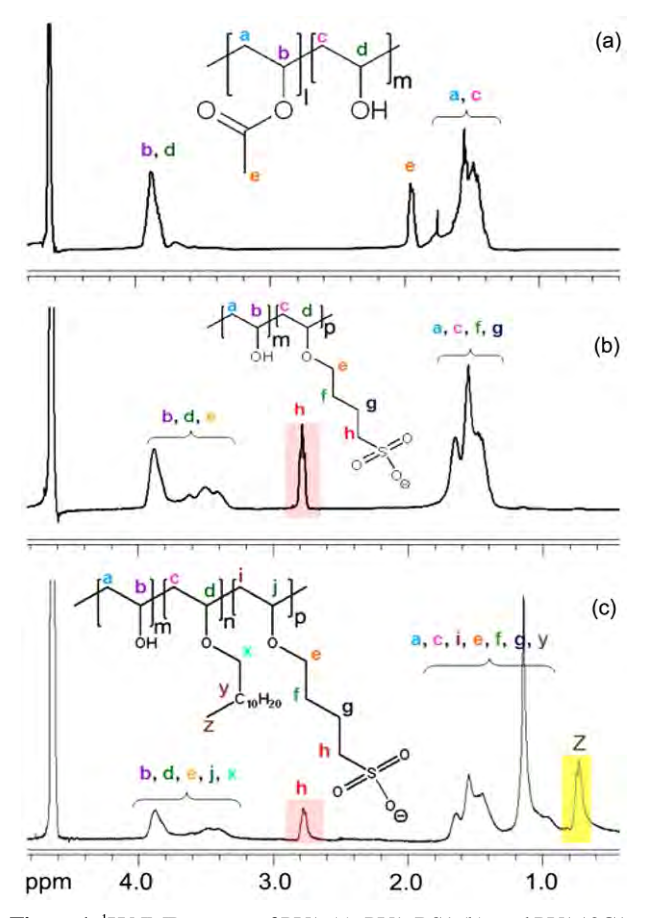
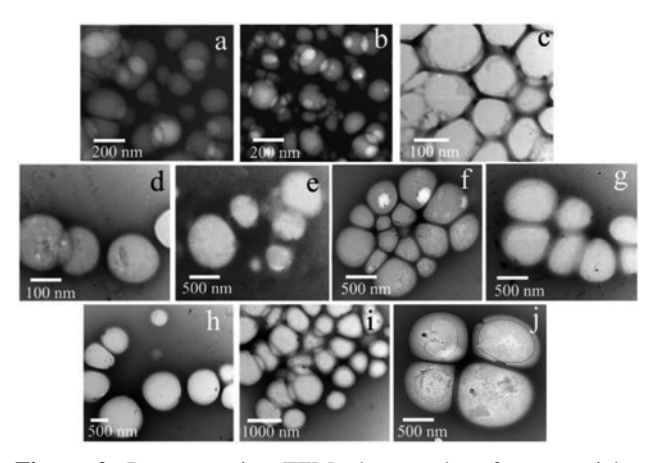


Figure 1. <sup>1</sup>H NMR spectra of PVA (a), PVA-BS1 (b), and PVA12C1-BS1 (c).

tons at 1.32-1.88 ppm and the methylene protons attached to -OH and -OCOCH<sub>3</sub> at 3.88 and 3.83 ppm, respectively. The -CH<sub>3</sub> protons of the acetate group resonate at 1.95 ppm while the resonance of the hydroxyl protons is at the same position as that of D<sub>2</sub>O, i.e., at 4.58-4.69 ppm. The <sup>1</sup>H spectra of the synthesized PVA-BS in D<sub>2</sub>O show the described peaks with a few additional resonances, including that at 3.45 ppm from the methane protons on the PVA backbone that are attached to oxygen and connected to the butane sulfonate group, and that at 2.78 ppm from the methylene protons attached to the sulfonate group. The <sup>1</sup>H spectrum of the synthesized PVA-C12-BS in D<sub>2</sub>O show similar resonances to that of the PVA-BS but with an additional resonance at 0.7 ppm, derived from the terminal methyl protons of the dodecyl group, and a bigger resonance peak at 1.18 ppm, from the contribution of the methylene protons from the dodecyl moieties. The degree of substitution (l, m, n and p)see Figure 1 and Table I) could be calculated from the integration of peaks at 0.8-1.8 ppm (-CH<sub>2</sub>- of the dodecyl group, -CH<sub>2</sub>-CH<sub>2</sub>- of the butane sulfonate group and -CH-CH<sub>2</sub>-CHof the PVA backbone), 0.7 ppm (-CH<sub>2</sub>-CH<sub>3</sub> of the dodecyl group) and 2.7 ppm (-CH<sub>2</sub>-SO<sub>3</sub>). It should be noted here that the <sup>1</sup>H NMR spectra that were obtained using a long delay time between pulses (25 s for 45° pulses) were similar to the spectra obtained using a normal delay time (1 s for 45° pulses).

**Nanoparticle Formation.** The ratio of the hydroxyl group/hydrophobic group (12C) to the negatively charged group (BS) on the obtained polymer should govern the hydrophobic/hydrophilic ratio and the charge characteristics of the obtained polymers. Analyzing the morphology of the self-assembled particles obtained from these polymers should offer information on how such characteristics affect the particle morphology.

Ten of the 11 prepared polymers could be induced into



**Figure 2.** Representative TEM photographs of nanoparticles derived from; (a) PVA-BS2, (b) PVA-BS3, (c) PVA-BS4, (d) PVA-12C1-BS1, (e) PVA-12C1-BS2, (f) PVA-12C1-BS3, (g) PVA-12C1-BS4, (h) PVA-12C2-BS1, (i) PVA-12C2-BS2, and (j) PVA-12C2-BS3.

stable water dispersible spherical particles (Figure 2) through solvent displacement of DMSO with water. The exception was PVA-BS1 which could not be induced to form nanoparticles under these conditions. That aside, interestingly, the particle size of the three other PVA-BS derivatives (PVA-BS2-4) increased with increasing the substitution degree of butane sulfonate on the PVA backbone, while, in contrast, the particle sizes of the seven PVA-12C-BS polymers decreased with increasing butane sulfonate substitution levels (Figure 4 and Table I).

The fact that the least butane sulfonate-substituted PVA (PVA-BS4, DS of the butane sulfonate = 0.013) gave particles with the most negative  $\zeta$  potential value of the three PVA-BS samples (Table I) indicated that most of the sulfonate groups must be around the surface of the PVA-BS4 particles. That the particles from the polymer with highest butane sulfonate substitution (PVA-BS2, DS of the butane sulfonate = 0.066) gave particles with the least negative  $\zeta$ potential, at some 0.6-fold lower implied that some of the charged sulfonate moieties were likely to assemble themselves inside the particles, so as to reduce the charge repulsion on the surface of the particles. The hydration of water molecules around these buried charged moieties would then swell the particles causing their larger size, increasing their surface area and so reducing the  $\zeta$  potential on the outer surface of the particles. The internal swelling also likely accounts for the broader size distribution of particles (Figure 3). As a result, it was observed that particles prepared from the PVA-BS polymers with high butane sulfonate substitution (PVA-BS2) possessed a broader size distribution than those with a lower butane sulfonate substitution (Figure 4 and Table I). In other words, in this scenario the hydration around the charges at the surface of the particles did not cause as much swelling as that caused by the hydration of the charges buried inside the particles. Thus, PVA-BS4 gave small particles with a narrow size distribution. It should be noted here that PVA-BS1 (the highest butane sulfonate substituted PVA-BS derivative) did not give any detectable particles.

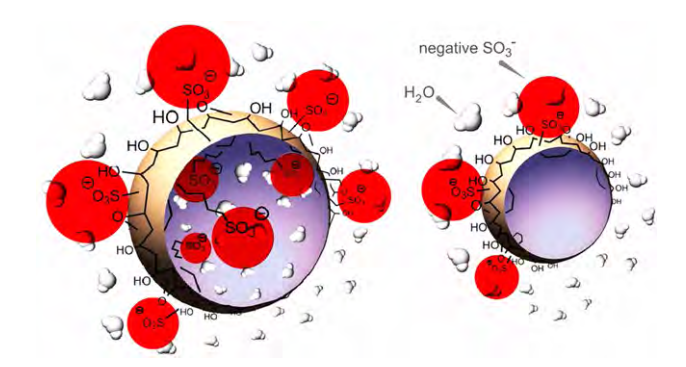


**Figure 3.** Representative model showing the swelling of a particle formed from PVA-BS with high butane sulfonate substitution (left) and the un-swelled particle formed from PVA-BS with less butane sulfonate substitution (right).

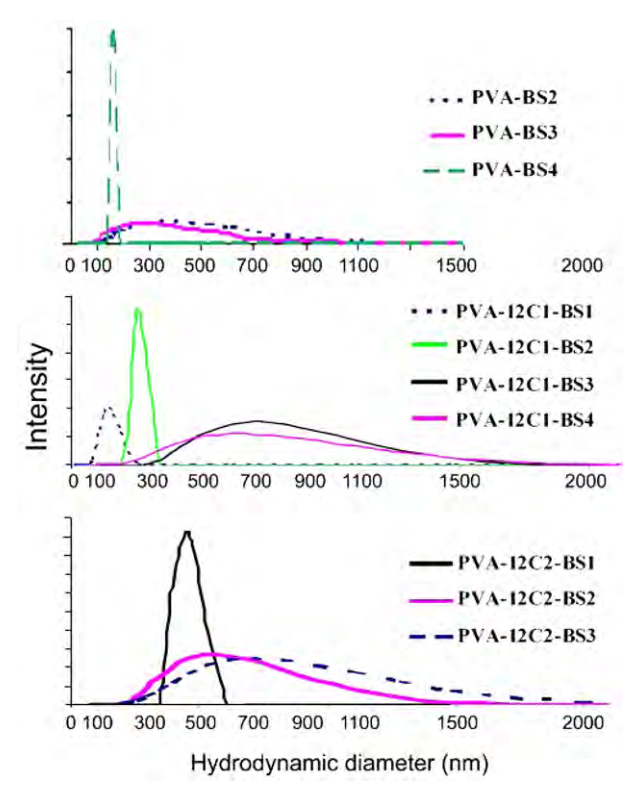


**Figure 4.** Hydrodynamic size distribution of particles prepared from PVA-BS and PVA-12C-BS polymers with various degrees of butane sulfonate and dodecane substitutions. The concentration of the polymeric solutions during particle formation was 0.60 mg/mL.

As mentioned earlier, the size of particles prepared from the seven PVA-12C-BS polymers decreased as the degree of butane sulfonate substitution increased, which is in contrast to the results obtained for the PVA-BS polymeric particles described above. In the case of the PVA-12C-BS particles, the polymer possessed hydrophobic dodecyl moieties which, during self-assembly, likely arranged themselves away from the water into the particles' core and so forcing the charged groups to the rim of the spheres. Since the center of the sphere is hydrophobic, a high surface charge density cannot be reduced by forcing the charge inside the particles. As a result, to reduce the charge density at the surface, particles, therefore, disintegrated into smaller spheres (similar to the Rayleigh effect, Figure 5).

Loading of the model drug, 2-ethylhexyl-4-methoxycinnamate (EHMC), into PVA-BS3 and PVA-12C2-BS1 derived nanoparticles was performed in order to compare the effect of the grafted dodecyl group on the drug loading efficiency. It should be noted here that both PVA-BS3 and PVA-12C2-BS1 possess the same degree of butane sulfonate substitution. It was observed that upon EHMC loading, PVA-BS3 particles became significantly smaller with a narrower size distribution range while, in contrast, the PVA-12C2-BS1

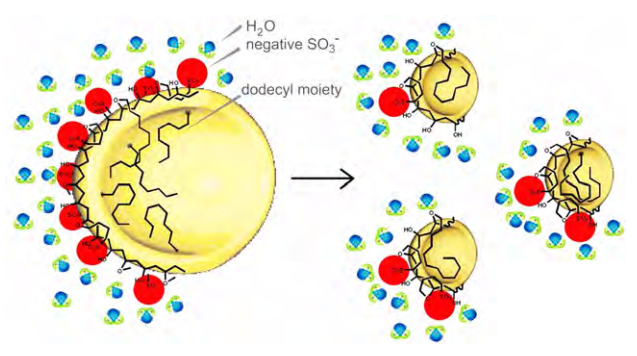


**Figure 5.** Representative model showing the disintegration of a sphere with high negatively charged sulfonate moieties at the surface, into smaller spheres with less charge-density at the surfaces.

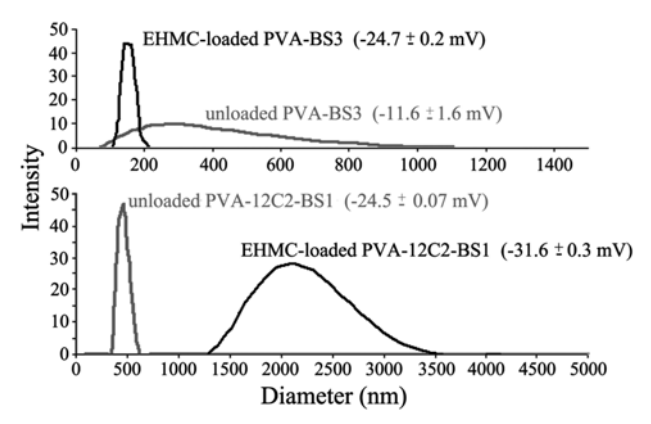


**Figure 6.** Size distributions of unloaded and EHMC-loaded PVA-BS3 and PVA-12C2-BS1 nanoparticles.

particles became larger with a broader size distribution range (Figure 6). The  $\zeta$  potential values of the EHMC-loaded spheres were more negative than those of the corresponding unloaded particles (Figure 6), indicating a better stability, especially for the PVA-BS3 in which the  $\zeta$  potential value increased 2.1-fold from -11.6±1.6 to -24.7±0.2 mV upon EHMC loading. The explanation for this is that with the presence of the hydrophobic EHMC at the center of the spheres, most butane sulfonate functionalities (negative charges) would be forced to move towards the surface of the spheres, and so increase their surface charge density and decrease the number of water molecules inside the spheres (de-swelling the spheres). This will result in spheres with both a smaller hydrodynamic size and a more negative  $\zeta$  potential value compared to the unloaded spheres.

However, when the polymer already contains hydrophobic moieties, as in the case of PVA-12C2-BS1, most of the charged groups are likely to have already been forced towards the rims of the spheres upon self-assembly, and so loading the hydrophobic EHMC into the spheres results in a larger hydrophobic center, composed of both the dodecyl moieties and the encapsulated EHMC, which in turn results in larger spheres, but only with a small increase of the number of

charged groups at the surfaces. This inhibited the Rayleigh effect from taking place and, as a result, the self-assembled PVA-12C2-BS1 particles formed with encapsulated EHMC inside were larger (2146±8 nm microspheres) than the particles without EHMC loading (455±2 nm), but the \$\zeta\$ potential values of the loaded and the unloaded particles did not differ much. Although the two polymer nanoparticles gave a different response in terms of the changes in particle sizes upon EHMC incorporation, the EE was > 99% for both nanoparticle types, at an EHMC loading capacity of 50%. This result is encouraging and suggests further investigation into the potential suitability of poly(2-sulfobutylvinyl-co-vinyl alcohol) and poly(dodecylvinyl-co-2-sulfobutylvinyl-co-vinly alcohol) particles as nano- or micro-carriers for hydrophobic drugs is merited.

#### **Conclusions**

In this work, four negatively charged PVA-BS polymers and seven PVA-12C-BS polymers with different substitution degrees of the dodecane or the butane sulfonate moieties on the PVA backbone, were successfully prepared and self-assembled into nanospheres. The location of the charged groups (at the surface or buried inside of the spheres) appears to directly affect the size and stability of the particles. The response of PVA-BS and PVA-12C-BS polymer particles to the loading of EHMC (a model hydrophobic drug) was markedly different. With the drug as a hydrophobic core, EHMC-loaded PVA-BS particles were smaller in size and more stable than the unloaded particles. In contrast, EHMC-loaded PVA-12C-BS particles were larger than the corresponding unloaded particles.

**Acknowledgements.** The authors thank the Commission of Higher Education-Thailand Research Fund (BRG5280004) and the Ratchadaphiseksomphot endowment fund from Chulalongkorn University for financial support.

#### References

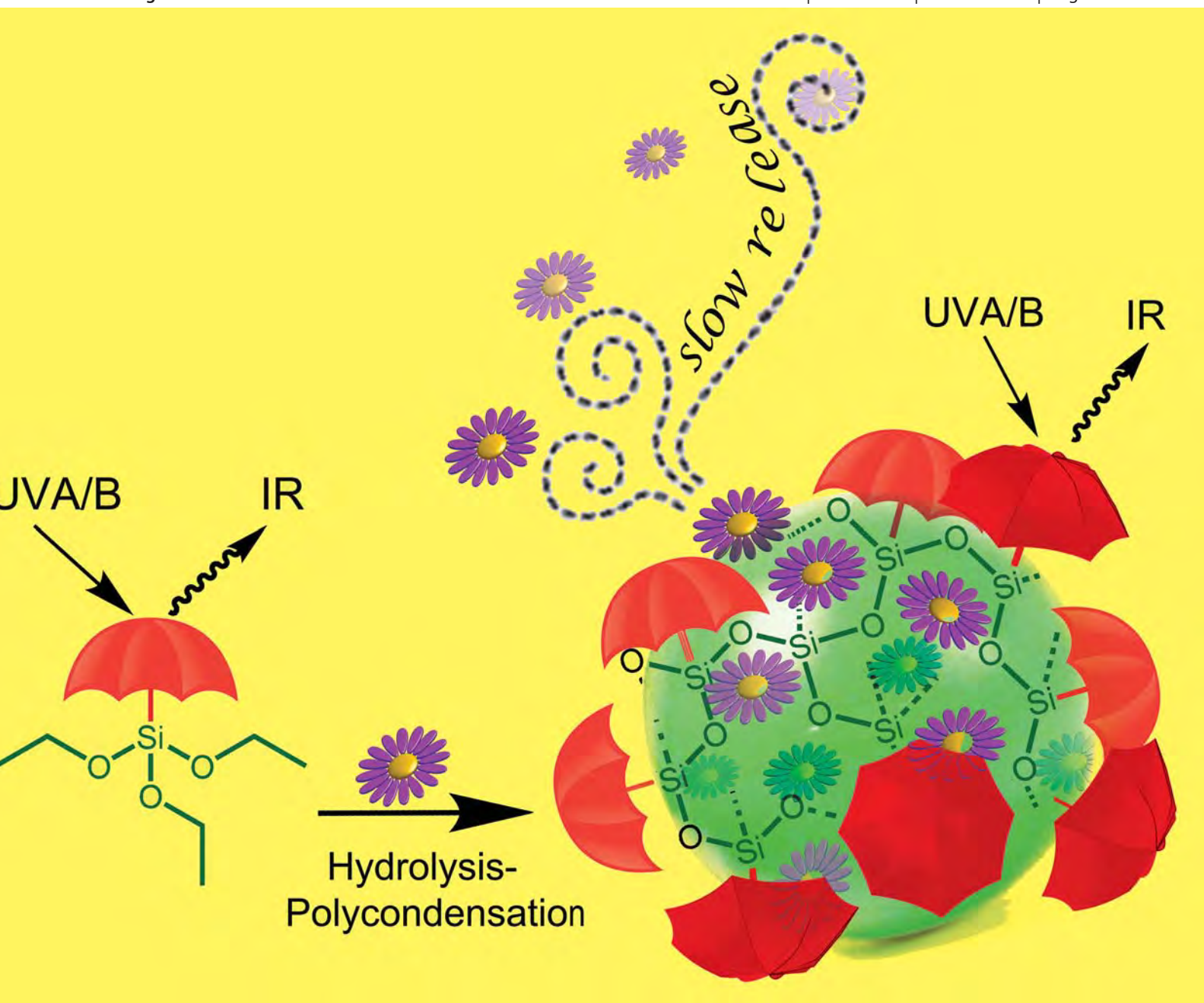
- (1) C. C. DeMerlis and D. R. Schoneker, *Food Chem. Toxicol.*, **41**, 319 (2003).
- (2) C. Wang, W. Ye, Y. Zheng, X. Liu, and Z. Tong, Int. J. Pharm.,

- 338, 165 (2007).
- (3) S.-S. Feng, W. Zeng, Y. Teng Lim, L. Zhao, K. Yin Win, R. Oakley, S. H. Teoh, R. C. Hang Lee, and S. Pan, *Nanomedicine-UK*, 2, 333 (2007).
- (4) K. Y. Win and S.-S. Feng, *Biomaterials*, **26**, 2713 (2005).
- (5) H. Takeuchi, H. Kojima, H. Yamamoto, and Y. Kawashima, J. Control. Release, **68**, 195 (2000).
- (6) S.-S. Feng and G. Huang, J. Control. Release, 71, 53 (2001).
- (7) I. Orienti, F. Bigucci, G. Gentilomi, and V. Zecchi, *J. Pharm. Sci.-US*, **90**, 1435 (2001).
- (8) O. R. Davies, L. Head, D. Armitage, E. A. Pearson, M. C. Davies, M. Marlow, and S. Stolnik, *Langmuir*, 24, 7138 (2008).
- (9) U. Manna and S. Patil, J. Phys. Chem. B, 113, 9137 (2009).
- (10) J. K. Li, N. Wang, and X. S. Wu, *J. Control. Release*, **56**, 117 (1998).
- (11) T. Kimura, A. Okuno, K. Miyazaki, T. Furuzono, Y. Ohya, T. Ouchi, S. Mutsuo, H. Yoshizawa, Y. F. Kitamura, and A. Kishida, *Mat. Sci. Eng.*, **24**, 797 (2004).
- (12) M. Madlova, S. A. Jones, I. Zwerschke, Y. Ma, R. C. Hider, and B. Forbes, Eur. J. Pharm. Biopharm., 72, 438 (2009).
- (13) I. Orienti, R. Trere, and V. Zecchi, *Drug Dev. Ind. Pharm.*, 27, 877 (2001).
- (14) I. Orienti, A. Di Pietra, B. Luppi, and V. Zecchi, Arch. Pharm., 333, 421 (2000).
- (15) T. Cerchiara, B. Luppi, F. Bigucci, I. Orienti, and V. Zecchi, Eur. J. Pharm. Biopharm., **56**, 401 (2003).
- (16) B. Luppi, I. Orienti, F. Bigucci, T. Cerchiara, G. Zuccari, S. Fazzi, and V. Zecchi, *Drug Deliv.*, **9**, 147 (2002).
- (17) I. Orienti, F. Bigucci, B. Luppi, T. Cerchiara, G. Zuccari, P. Giunchedi, and V. Zecchi, Eur. J. Pharm. Biopharm., 54, 229 (2002).
- (18) I. Orienti, G. Zuccari, V. Bergamante, E. Mileo, M. Lucarini, R. Carosio, and P. G. Montaldo, *Biomacromolecules*, 7, 3157 (2006).
- (19) M. Wittmar, J. S. Ellis, F. Morell, F. Unger, J. C. Schumacher, C. J. Roberts, S. J. B. Tendler, M. C. Davies, and T. Kissel, *Bioconjugate Chem.*, 16, 1390 (2005).
- (20) M. Wittmar, F. Unger, and T. Kissel, *Macromolecules*, 39, 1417 (2006).
- (21) G. Zuccari, R. Carosio, A. Fini, P. G. Montaldo, and I. Orienti, J. Control. Release, 103, 369 (2005).
- (22) C. Luadthong, A. Tachaprutinun, and S. P. Wanichwecharungruang, Eur. Polym. J., 44, 1285 (2008).
- (23) T. Jung, A. Breitenbach, and T. Kissel, J. Control. Release, 67, 157 (2000).

# Journal of Materials Chemistry

www.rsc.org/materials

Volume 21 | Number 22 | 14 June 2011 | Pages 7829-8216



ISSN 0959-9428

**RSC**Publishing

# Journal of Materials Chemistry



Cite this: J. Mater. Chem., 2011, 21, 7922

www.rsc.org/materials PAPER

# Organic-inorganic hybrid polysilsesquioxane nanospheres as UVA/UVB absorber and fragrance carrier†

Punnipa Kidsaneepoiboon,  $^{ab}$  Supason Pattanaargson Wanichwecharungruang,  $^{*a}$  Tianchai Chooppawa,  $^a$  Ratthakan Deephum  $^a$  and Thammarat Panyathanmaporn  $^c$ 

Received 7th December 2010, Accepted 24th February 2011 DOI: 10.1039/c0jm04271d

To avoid the photocatalysis property of inorganic UV absorbers, such as TiO<sub>2</sub> and ZnO nanoparticles, and to utilize the minimal transdermal penetration and non-sticky nature of particulate silica particles, whilst at the same time fully harnessing the UV absorption characteristics of organic chromophores, hybrid organic–silica particles with UVA/UVB absorptive chromophores as part of their network structures were synthesized. Two UV absorptive hybrid nanospheres, poly[propyl-4-methoxycinnamamide silsesquioxane] (PTES4C) and poly[propyl-2,4-dimethoxycinnamamide silsesquioxane] (PTES24C), were synthesized through the hydrolysis-polycondensation of triethoxysilylpropyl-4-methoxycinnamamide (TES4C) and triethoxysilylpropyl-2,4-dimethoxycinnamamide (TES24C), respectively. Optimization of the catalyst type (acid, base or self-catalysis) and solvent (ethanol) and monomer concentrations, led to a high yield (71–73%) preparation of the two nanospheres. The two spheres displayed good sun protection factor (SPF) and UVA protection factor (UVA-PF) when used in a gel based formulation. The labile and volatile fragrant citronellal could be effectively loaded into the PTES4C spheres at 35–48% (w/w) via the in situ hydrolysis–polycondensation reaction under self-catalysis conditions, and the obtained citronellal-loaded nanospheres demonstrated clear sustained controlled release of the citronella characteristics.

#### Introduction

It is well accepted that both UVB (280–315 nm) and UVA (315–400 nm) are harmful to human skin, <sup>1,2</sup> and so the use of sunscreen is seriously recommended. <sup>3,4</sup> Sunscreen, both organic types, such as 2-ethylhexyl-*p*-methoxycinnamate (EHMC), benzophenone, dibenzoylmethane and 2,4-bis{[4-(2-ethyl-hexyloxy)-2-hydroxyl]-phenyl}-6-(4-methoxyphenyl)-(1,3,5)-triazin, and inorganic types, such as titanium dioxide (TiO<sub>2</sub>) and zinc oxide (ZnO), are used at high percentages in sunscreen formulations. Advancements in organic synthesis and photochemistry have made available organic UV filters with adequate photostability. <sup>5-8</sup>

However, the systemic absorption of small organic UV filtering molecules across the skin is still a problem that needs more attention, since the materials are used daily over a large skin surface area<sup>9-11</sup> and the xenoestrogen-like activity of many

organic filters has been reported.<sup>12-14</sup> The idea of using organic polymers with a UV absorptive property to minimize systemic absorption has been demonstrated earlier. Examples of proposed polymeric UV filters include UV absorptive silicone,<sup>15</sup> oligoesters based on poly(*p*-alkoxycinnamate) and poly(pentaethylene glycol cinnamate)<sup>16</sup> and UV absorptive chitosan nanospheres.<sup>17</sup> Encapsulation of organic filters into either polymeric carriers<sup>18,19</sup> or inorganic silica particles<sup>20</sup> is another strategy used to lessen the transdermal absorption problem.

Inorganic filters, such as TiO<sub>2</sub> and ZnO, on the other hand, promise minimal systemic absorption due to their insoluble particulate nature, but raise concern over their potential safety due to their photocatalytic properties. Organic—TiO<sub>2</sub> composite particles were recently fabricated using poly(methyl methacrylate-co-sodium sulfopropyl lauryl maleate-co-2-hydroxy-4-(3-methacryloxy-2-hydroxylpropoxy) benzophenone). 28

In order to appreciate the non-sticky nature and minimal transdermal penetration of silica particles, and at the same time fully harness the UV absorption characteristics of organic chromophores without concern over their systemic absorption and stickiness nature, covalent linkage between the two was proposed. To this end the UV absorptive chromophore, benzophenone 3, was linked to triethoxysilyl monomer, producing 2-(hydroxyl-4-(3-triethoxysilylpropoxy))diphenylketone and then this monomer was polymerized together with tetraethyl

<sup>&</sup>quot;Department of Chemistry, Faculty of Science, Chulalongkorn University, Bangkok, 10330, Thailand. E-mail: psupason@chula.ac.th; Fax: (+662) 2541309; Tel: (+662) 2187634

<sup>&</sup>lt;sup>b</sup>National Center of Petroleum, Petrochemicals and Advanced Materials, Chulalongkorn University, Bangkok, 10330, Thailand

<sup>&</sup>lt;sup>c</sup>National Metal and Materials Technology Center, National Science and Technology Development Agency, Ministry of Science and Technology, Thailand Science Park, Pathumthani, 12120, Thailand

<sup>†</sup> Electronic supplementary information (ESI) available: ¹H NMR, FT-IR, and UV absorption spectra. See DOI: 10.1039/c0jm04271d

orthosilicate into hybrid organic–silica particles.<sup>29</sup> Subsequently, UVB absorptive trimethoxysilylpropyl-*p*-methoxycinnamamide and triethoxysilylpropyl-*p*-methoxycinnamamide were synthesized and then polymerized into UV absorptive spherical particles.<sup>30</sup> These two organic–silica hybrid UV filters were prepared using the ammonia catalyst process.<sup>31</sup>

We propose that UV filters in the form of nanoparticles can be made to function not only as UV filtering agents but also as carriers for volatile, labile or photo-unstable active molecules. The use of UV absorptive carriers for topical drugs or cosmetics should i) help protect the unstable active molecules from environmental threats (e.g. reactive oxygen species and light) and ii) reduce the use of unnecessary carriers for other active molecules in the formulation. With no unnecessary carrier, the skin will be in less contact with unnecessary chemicals. In addition, the UV absorptive spheres will serve not only as good reservoirs for delivering the loaded active molecules to the skin, but will also provide UV protection to both the skin and the encapsulated molecules.

Therefore, here we show the synthesis of organic–silica hybrid particles which possess UVA/UVB absorption characteristics and at the same time can be used as labile fragrance reservoirs. The work involves the synthesis of poly[propyl-2.4-dimethoxycinnamamide silsesquioxane] (PTES24C) and poly[propyl-4methoxycinnamamide silsesquioxanel (PTES4C) particles from triethoxysilane monomers containing the chromophoric 2,4dimethoxycinnamoyl and 4-methoxycinnamoyl moieties, using the sol-gel process. Evaluation of the catalysis conditions (base, acid and self-catalysis) was performed and optimized to obtain a process that gave a high yield but under mild enough conditions to be able to perform in situ polycondensation in the presence of labile fragrant molecules. The obtained spheres were evaluated for their UVA/UVB filtering efficiency in a gel based formulation. The encapsulation of the volatile and labile fragrant citronellal into the PTES4C nanospheres was carried out, and its controlled release was investigated and is reported.

#### Result and discussion

#### Synthesis of hybrid monomers

Two chromosphores, 4-methoxycinnamoyl moiety (UVB absorptive chromosphore,  $\lambda_{\text{max}} = 290-300 \text{ nm}$ ) and 2,4-dimethoxycinnamoyl moiety (UVA/B absorptive chromosphore,  $\lambda_{\text{max}} = 320-330 \text{ nm}$ ) were successfully condensed with 3-aminopropyltriethoxysilane (APTES) to produce two UV absorptive hybrid monomers, triethoxysilylpropyl-4-methoxycinnamamide (TES4C) and triethoxysilylpropyl-2,4-dimethoxycinnamamide (TES24C), using a conventional amide bond formation reaction via acid chloride (Scheme 1). The purity of the synthesized TES4C, in terms of the amount of residual APTES was deduced from the <sup>1</sup>H-NMR spectrum of the product using the integration of peaks at 7.56 ppm (Ar-CH=) and 0.67 ppm (-CH<sub>2</sub>-Si=), and revealed a 2% (by mole) APTES residue (Fig. 1). Similarly, the amount of residual APTES in the TES24C was deduced from the <sup>1</sup>H-NMR spectral information (integration of peaks at 7.74 ppm (Ar-CH=) and 0.67 ppm  $(-CH_2-Si-)$ , Fig. 1) and found to be 8% (by mole) (see full NMR spectral interpretation in ESI†).

#### Polycondensation and sphere formation

The polysilsesquioxane products, PTES4C or PTES24C, in the form of spheres, as obtained from the hydrolysis–polycondensation of TES4C or TES24C in the presence of external catalysts (0.1% (v/v) HCl, 3% or 5% (v/v) NH<sub>4</sub>OH) and under self-catalysis conditions, were compared (Table 1). In addition, the amount of ethanol used in the reaction was also optimized.  $^{32,33}$ 

For both PTES4C and PTES24C, the acid-catalysis process gave the highest synthesis yields at 87.4% and 77.9%, respectively, but required by far the longest reaction time at 14 and 3 days, respectively. Self-catalysis gave the second highest synthesis yield at 74.2% and 73%, respectively, and only required 24 h to obtain stable and more uniform spheres compared with the other catalysts. Polymerization under the two basic conditions (3% and 5% (v/v) NH<sub>4</sub>OH) proceeded much faster, being complete within 1 h, but gave significantly lower yields (Table 1).

As the volume of ethanol used (as the monomer solvent) was increased, the particle size (anhydrous and hydrated) of the product increased and the product yield decreased (Table 1). The decrease in the product yield was usually accompanied by a more sticky mass being observed in the reaction. It should be noted here that the process with less than 20% (v/v) ethanol could not be carried out for TES4C in PTES4C synthesis, because the monomer solution was too viscous.

Considering the product yield, reaction time, morphology and uniformity of the spheres, the self-catalysis process was considered the most convenient process for the synthesis of both PTES4C (at 20% (v/v) ethanol) and PTES24C (at 10% (v/v) ethanol) nanospheres. Unlike with the acid catalysis, which gave a little higher yield for PTES4C synthesis (87.4% vs. 74.2%), but not for PTES24C (72.9% vs. 73%), the self-catalysis process required no neutralization nor washing of the product. The mild conditions of the self-catalysis process also provided a good possibility to perform encapsulation of labile compounds through *in situ* polymerization without harming the labile material.

The monomer concentration was then optimized for the self-catalysis process where it was found that the higher the monomer concentration was, in general, the lower the obtained yield was, except for the 0.01 g ml<sup>-1</sup> and the 0.02 g ml<sup>-1</sup> TES4C that gave comparable yields and particle morphologies. Thus, a concentration of 0.02 g ml<sup>-1</sup> and 0.01 g ml<sup>-1</sup> of the respective monomer was chosen as the most appropriate condition for the synthesis of PTES4C and PTES24C nanoparticles under self-catalysis, respectively. It should be noted here that all the PTES24C spheres prepared did not disperse well in water, except those prepared at a monomer concentration of 0.01 g ml<sup>-1</sup>. In fact, those spheres settled down very quickly in water, thus preventing the measurement of their hydrodynamic diameter by dynamic light scattering (DLS).

Instead of using ethanol to dissolve the monomer and then slowly dispersing the monomer solution in water, Triton X-100, a non-ionic surfactant, was used in place of ethanol, at a 5% (w/v) final concentration. Polymerization was carried out by self-catalysis at a final monomer concentration of 0.02 g ml<sup>-1</sup> and 0.01 g ml<sup>-1</sup> for PTES4C and PTES24C synthesis, respectively. Compared to the process with ethanol, the process with Triton

Scheme 1 Synthesis of triethoxysilylpropyl-4-methoxycinnamamide (TES4C) and triethoxysilylpropyl-2,4-dimethoxycinnamamide (TES4C), and the hydrolysis-polycondensation of TES4C and TES24C into poly[propyl-4-methoxycinnamamide silsesquioxane] (PTES4C) and poly[propyl-2,4-dimethoxycinnamamide silsesquioxane] (PTES24C).

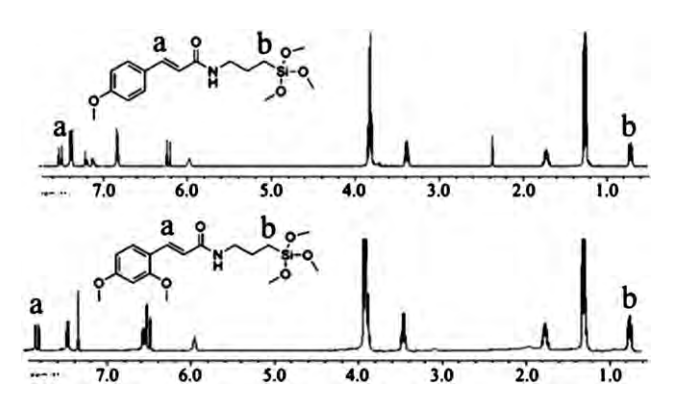


Fig. 1 <sup>1</sup>H NMR of TES4C (top) and TES24C (bottom). The percentage of residual APTES could be deduced from the ratio of integration of peaks a and b.

X-100 gave much larger PTES4C spheres (anhydrous, as DLS could not be performed) and at a much lower yield (Table 1, Fig. 2). In addition, it was accompanied with a more sticky solid mass formation. In contrast, the preparation of PTES24C spheres in the presence of 5% (v/v) Triton X-100 gave more uniform spheres at a comparable spherical size and yield to the process using ethanol (Table 1, Fig. 2).

Thus, it was concluded that PTES4C was best prepared under self-catalysis using 20% (v/v) aqueous ethanol with a final monomer concentration of 0.02 g ml<sup>-1</sup>, whilst PTES24C was best prepared under self-catalysis condition at a final monomer concentration of 0.01 g ml<sup>-1</sup> with either 5% (v/v) Triton X-100 or 10% (v/v) ethanol. Under these optimized conditions, the synthesis yield was 71% and 73% for PTES4C and PTES24C, with average sphere sizes of  $\sim$ 420 nm and  $\sim$ 210 nm, respectively.

The PTES4C and PTES24C spheres obtained under such conditions were subjected to solar protection factor (SPF) and UVA-protection factor (UVA-PF) measurements, and were also

used to encapsulate citronellal. An aqueous suspension of PTES4C spheres showed obvious absorption of UVB radiation  $(\lambda_{max} \sim 290 \text{ nm})$ , while those of the PTES24C possessed both UVB and far UVA absorption characteristics ( $\lambda_{max} \sim 292$  and 322 nm) (Fig. 3a). The dry spherical products (solid) also showed expected UV absorption characteristics (Fig. 3b). It should be noted here that the UV absorption spectra of TES4C and TES24C shown in Fig. 3a, were acquired from the solution samples and, therefore, their absorbances corresponded well with their molar absorption coefficients. However, since the spectra of PTES4C and PTES24C were obtained from the spherical suspension, their absorption spectra did not follow Beer's law and should not be compared to the spectra of the diluted monomer solutions. Nevertheless, the absorption spectra of the suspensions gave good qualitative information and agreed well with the absorption profiles of the dry particles.

#### Solar protection factor (SPF)

The SPF and UVA-PF of PTES4C and PTES24C nanospheres were evaluated and compared with those of EHMC, a widely used UV filter that is accordingly used as a reference standard here. All samples were prepared at 34.5 mM chromophores in aqueous polyacrylic acid gel (Table 2). The molar concentrations of the chromophore for PTES4C and PTES24C were estimated from the polysilsesquioxane network structures assuming similar percentage loss of APTES and TES4C or TES24C at the 71 and 73% yield. No SPF booster was used in the gel formulation, and so the SPF and UVA-PF values obtained should directly correspond to the amount of UVB and UVA light filtered by the tested gel. The SPF and UVA-PF values are usually affected by various factors, including the light absorption property (molar extinction coefficient) of the UV filter chemical used, the homogeneity of the UV filter chemical in the formulation, the concentration of

Table 1 Morphology and yield of PTES4C and PTES24C nanospheres obtained under various synthesis conditions

Monomer	Catalysis	[Monomer] (g ml <sup>-1</sup> )	Reaction time	%EtOH (v/v)	Synthesis yield (%)	Average diameter by SEM <sup>a</sup>	Hydrodynamic diameters <sup>b</sup>	$\mathrm{PDI}^c$
TES4C	HCl	0.02	14 days	20	87.38	$449 \pm 40$	$610 \pm 10$	0.23
		0.02	14 days	30	74.45	$625 \pm 52$	$798 \pm 10$	0.23
		0.02	14 days	40	69.27	$837 \pm 81$	$907 \pm 13$	0.22
	3% NH <sub>4</sub> OH	0.02	1 h	20	47.89	$868 \pm 82$	$910 \pm 44$	0.19
	•	0.02	1 h	30	41.99	$1252 \pm 164$	$1987 \pm 203$	0.16
		0.02	1 h	40	30.56	$2361 \pm 202$	$3028 \pm 299$	0.95
	5% NH₄OH	0.02	1 h	20	37.30	$513 \pm 87$	$687 \pm 54$	0.34
	•	0.02	1 h	30	17.20	$826 \pm 184$	$1456 \pm 81$	0.25
		0.02	1 h	40	11.88	$2254 \pm 212$	$2694 \pm 114$	0.14
TES4C + 20%	Self-catalysis	0.02	1 day	20	71.11	$419 \pm 64$	$559 \pm 9$	0.09
APTES	•	0.02	1 day	30	64.21	$788 \pm 139$	$1354 \pm 44$	0.16
		0.02	1 day	40	X	X	X	X
		0.01	1 day	20	74.15	$423 \pm 65$	$588 \pm 4$	0.20
		0.04	1 day	20	53.76	$437 \pm 57$	$564 \pm 8$	0.15
		0.06	1 day	20	41.34	$465 \pm 49$	$566 \pm 6$	0.14
		0.02	1 day	Triton	<20	$1227\pm198$	nd	nd
				X-100				
TES24C	HCl	0.02	3 days	10	77.91	$576 \pm 78$	$768 \pm 12$	0.13
		0.02	3 days	20	75.11	$615 \pm 58$	$811 \pm 5$	0.09
		0.02	3 days	30	56.70	$755 \pm 84$	$1177 \pm 39$	0.20
	3% NH <sub>4</sub> OH	0.02	1 h	10	24.95	$451 \pm 48$	$482 \pm 17$	0.22
		0.02	1 h	20	38.50	$956 \pm 291$	$929 \pm 22$	0.10
		0.02	1 h	30	31.64	$1792 \pm 377$	$2142 \pm 122$	0.28
	5% NH <sub>4</sub> OH	0.02	1 h	10	22.34	$402 \pm 92$	$471 \pm 16$	0.24
		0.02	1 h	20	40.68	$535 \pm 64$	$706 \pm 9$	0.14
		0.02	1 h	30	20.05	$1557 \pm 132$	$1316 \pm 26$	0.11
TES24C + 20%	Self-catalysis-	0.02	1 day	10	66.36	$448 \pm 66$	nd	nd
APTES		0.02	1 day	20	64.48	$465 \pm 91$	nd	nd
		0.02	1 day	30	X	X	X	X
		0.01	1 day	10	73.04	$210 \pm 67$	$229 \pm 19$	0.18
		0.04	1 day	10	51.70	$409 \pm 99$	nd	nd
		0.06	1 day	10	X	X	X	X
		0.01	1 day	Triton	73.15	$228 \pm 30$	$232 \pm 14$	0.12
			•	X-100				

<sup>&</sup>lt;sup>a</sup> Average anhydrous size (nm)  $\pm$  SD, from SEM photographs. <sup>b</sup> Average hydrated size (nm)  $\pm$  SD, as determined by DLS. <sup>c</sup> The cumulant analysis -polydispersity index (PDI) where a value of 0.08–0.7: means a mid-range polydispersity, the range over which the distribution algorithm based on NNLS best operates. x = no spherical product was formed, and nd not determined.

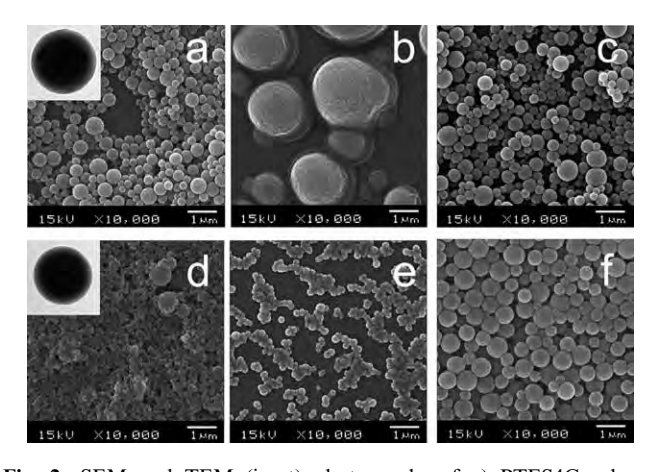


**Fig. 2** SEM and TEM (inset) photographs of a) PTES4C spheres prepared at  $0.02~{\rm g~ml^{-1}}$  monomer and 20% ethanol under self-catalysis, b) PTES4C spheres prepared at  $0.02~{\rm g~ml^{-1}}$  monomer and 5% Triton X-100 under self-catalysis, c) PTES4C spheres prepared at  $0.02~{\rm g~ml^{-1}}$  monomer with 20% ethanol under base catalysis, d) PTES24C spheres prepared at  $0.01~{\rm g~ml^{-1}}$  monomer and 10% ethanol under self-catalysis, e) PTES24C spheres prepared at  $0.01~{\rm g~ml^{-1}}$  monomer and 5% Triton X-100 under self-catalysis, and f) PTES24C spheres prepared at  $0.01~{\rm g~ml^{-1}}$  monomer with 10% ethanol under base catalysis.

the UV filter, and the ability of the tested sample to either absorb or scatter the incoming radiation. Note that the values obtained take into account neither the transdermal penetration of the UV filters nor the stability of the UV filters.

When used at the same molar concentration of chromophore (4-methoxycinnamoyl moiety) in the gel (34.5 mM), PTES4C gave slightly higher (~1.1-fold) SPF and UVA-PF values than the reference standard EHMC (Table 2). As mentioned earlier, the SPF and UVA-PF values are affected by how well the UV filter chemicals are dispersed in the formulation and the ability of the formulation to either scatter or absorb the incoming radiation. In this case, it is likely that the ability of the PTES4C spheres to scatter light compensates well for their lower homogeneity compared to those of the EHMC.

In contrast, the PTES24C gel under the same conditions gave just over ~1.3-fold lower SPF and UVA-PF values than that for the reference standard EHMC. However, the lower SPF and UVA-PF values for PTES24C were expected since PTES24C's chromophore (2,4-dimethoxycinnamoyl moiety) possesses only half the molar extinction coefficient when compared to that of EHMC. In fact, when taking into account the molar extinction coefficients of each UV filter's chromophore, the SPF and UVA-PF values of the PTES24C are higher than the expected values.

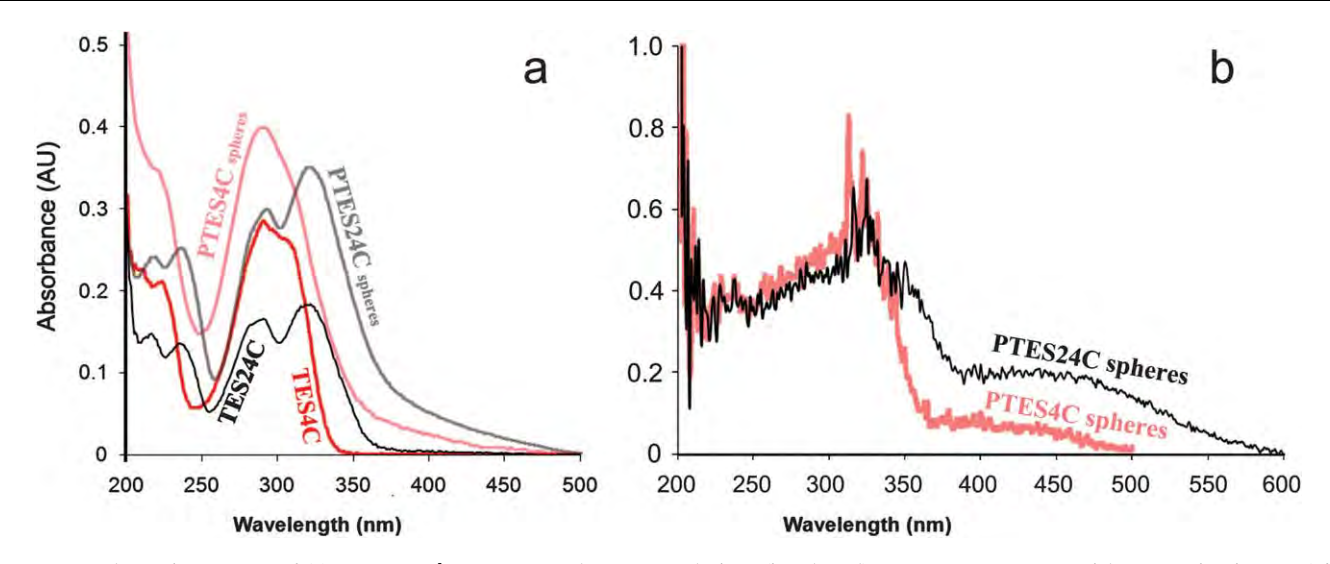


Fig. 3 UV absorption spectra of (a)  $1.28 \times 10^{-5}$  M TES4C and TES24C solutions (in ethanol), 120 ppm PTES4C particle suspension in 20% (v/v) aqueous ethanol, and 80 ppm PTES24C particle suspension in 20% (v/v) aqueous ethanol, and (b) dry PTES4C and PTES24C spherical solids.

This was likely to be due to the light scattering effect caused by the (230 nm diameter) PTES24C spheres.

The better UV filtering efficiency of the PTES4C over the PTES24C spheres could also be explained through a more effective light scattering of the bigger PTES4C spheres (560 nm) compared to the smaller PTES24C spheres (230 nm).

Usually, when the organic UV absorptive chromophore is in the solution state (normal organic UV filter), the UV filtering mechanism involves the absorption of UV radiation by the ground state electrons (electrons in their highest occupied molecular orbital, HOMO), the jumping of those electrons to the higher energy levels (the excited state which usually is the lowest unoccupied molecular orbital, LUMO), the return of the excited electrons to the ground state energy levels ideally via non-radiative pathways (e.g. vibrational relaxation and internal conversion which usually are accompanied with the release of infrared radiation). The energy gap between the excited and ground states determine the absorption wavelength of that particular filter. In the case of the hybrid organic-inorganic UV filtering particles, the particulate nature of the materials will cause light scattering, while the organic chromophores in the siloxane network structure will absorb photons of the right energy (here the energy will be in the UVB and UVA regions). Therefore, the particulate nature of the hybrid UV filtering spheres acts synergistically with the cinnamoyl chromophores by scattering the photons around, resulting in an increased chance for any given photon to be absorbed by the organic chromophores of the spheres. In other words, the particulate nature of the hybrid UV filtering spheres increases the time and path-length of each photon in the gel layer,

thus increasing their probability of being absorbed by the organic chromophores. This rationalization helps explain the high SPF and UVA-PF values of the PTES24C spheres despite the low molar extinction coefficient of their chromophore.

It should be noted here that the two cinnamoyl moieties, 4-methoxycinnamoyl and 2,4-dimethoxycinnamoyl, were chosen as the organic chromophoric part of the hybrid filters based on not only their UV absorption wavelengths, but also their appropriate photochemical and photophysical properties, *e.g.*, short lived excited state, low barrier for non-radiative decay and low fluorescent quantum yield.<sup>34,35</sup>

In addition to their good UV filtering property and easy preparation, the two hybrid UV filtering nanospheres could disperse well in water, contributed no oiliness to the personal formulations and did not act as photocatalyst, therefore, applications in personal care and cosmetic products should be possible.

#### PTES4C as carrier for controlled release of citronellal

PTES4C spheres were evaluated for their role as a suitable carrier for the controlled release of the volatile fragrant citronellal. Encapsulation of the citronellal was carried out at a TES4C: citronellal (w/w) ratio of 2:1 and 1:1. Assuming complete polycondensation (80% by wt TES4C and 20% by wt APTES) and 100% citronellal entrapment, the 1:1 and 1:2 citronellal-loaded PTES4C (citro-PTES4C-1 and citro-PTES4C-2, respectively) would possess a citronellal loading of 39 and 56% (w/w), which corresponds to a mole ratio between the cinnamoyl

Table 2 The solar protection factor (SPF) and UVA protection factor (UVA-PF) values of a polyacrylic acid gel containing PTES4C, PTES24C and EHMC

UV Filters	[UV Filter] (g 100 ml <sup>-1</sup> )	[Chromophore] (M)	$\varepsilon$ of the chromophore (M $^{-1}$ cm $^{-1}$ )	SPF (mean $\pm$ SD) <sup>a</sup>	UVA-PF (mean $\pm$ SD) <sup>a</sup>		
PTES4C PTES24C EHMC	10.8 11.9 10.0	0.0345 0.0345 0.0345	24 000 14 000 24 000	$22.0 \pm 1.5$ $14.4 \pm 1.4$ $19.8 \pm 1.4$	$7.9 \pm 0.8$ $5.5 \pm 0.5$ $7.3 \pm 1.2$		
<sup>a</sup> obtained from at least five measurements							

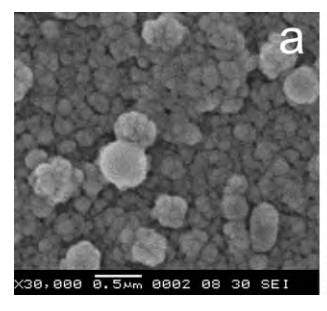
moiety: citronellal of 1.00: 0.96 and 1.00: 1.91, respectively. Analyzing the two encapsulated products gave an actual citronellal loading of slightly less than the theoretical level at 35% (w/w) (citro-PTES4C-1) and 48% (w/w) (citro-PTES4C-2), which corresponded to the mole ratio of the cinnamoyl moiety: citronellal at 1.00: 0.81 and 1.00: 1.40, respectively. This high loading level indicated that during the *in situ* hydrolysis—polycondensation of the TES4C monomers in the presence of citronellal molecules, the hydrophobic citronellal molecules delocalized themselves away from the increasing polar water medium, towards the forming nanospheres where they would have good hydrophobic interactions with the cinnamoyl moieties in the siloxane network structure.

With higher citronellal loadings, the spheres became smaller and more aggregated (Fig. 4). It was speculated that at high loading levels, more citronellal would be displaced to the particle's surface, therefore, causing more aggregation of the spheres. The presence of citronellal moieties at the particle's surface also prevented the contact between the growing particles and the new incoming TES4C monomer resulting in spheres of a smaller size.

Citronellal-loaded PTES4C spheres showed a clear controlled release property compared to the free citronellal at the same concentration (Fig. 5). The polysilsesquioxane spheres (sizes of approximately  $115 \pm 20$  and  $100 \pm 10$  nm for citro-PTES4C-1 and citro-PTES4C-2, respectively) certainly acted as a physical barrier, slowing down the diffusion of citronellal molecules. The hydrophobic interaction between citronellal molecules and the cinnamoyl moieties of the silica network structure probably helped retard the release of the volatile citronellal molecules, resulting in an obvious slower release of citronellal from both the citro-PTES4C-1 and citro-PTES4C-2 spheres. However, the fast initial release observed on the first day may in part be due to the burst release of citronellal located at the surface of citro-PTES4C-1 and the citro-PTES4C-2 nanoparticles, in addition to any concentration dependent release kinetics.

#### **Conclusions**

PTES4C and PTES24C nanospheres with UVB and UVA/B absorption properties, respectively, were prepared successfully from TES4C and TES24C hybrid monomers using a hydrolysis—polycondensation reaction. The catalyst type (acid, base or self-catalysis), the concentration of the ethanol (solvent of monomer) and the respective monomer used during the particle formation and the presence of the non-ionic surfactant Triton X-100, all



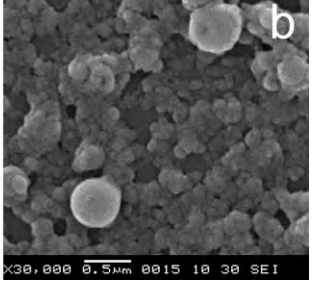


**Fig. 4** SEM images of (a) **citro-PTES4C-1** (35% (w/w) citronellal-loaded **PTES4C** spheres) and (b) **citro-PTES4C-2** (48% (w/w) citronellal-loaded **PTES4C** spheres).

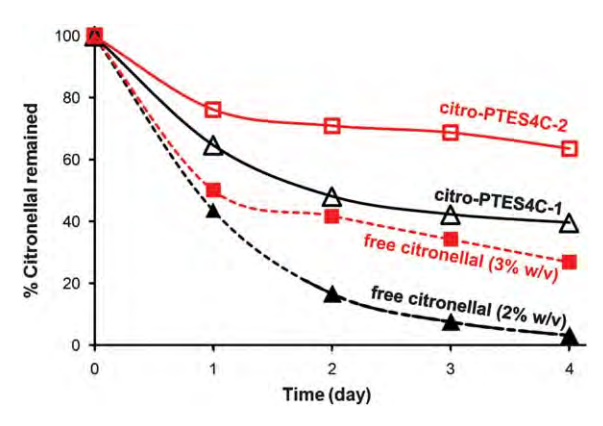


**Fig. 5** Release profiles of citronellal from **citro-PTES4C-1** (35% (w/w) citronellal loading) and **citro-PTES4C-2** (48% citronellal loading) in aqueous suspensions at a final citronellal concentration of 2% and 3% (w/v) for **citro-PTES4C-1** and **citro-PTES4C-2**, respectively. The profiles are displayed as % citronellal remaining. Releases of free citronellal at the same concentrations are also shown. The release experiment was conducted at 45 °C. The data are shown as the mean derived from two repeats.

affected the particle size and product yield. Optimization led to a mild self-catalysis process that gave PTES4C and PTES24C products with a high yield (71 and 73%, respectively) and acceptable nanoparticle size (~400 nm PTES4C and ~200 nm PTES24C). Both PTES4C and PTES24C spheres gave acceptable SPF and UVA-PF values despite the fact that the molar extinction coefficient value of the 2,4-dimethoxycinnamoyl chromophore in PTES24C was 1.71-fold lower than that for the 4-methoxycinnamoyl chromophore in PTES4C. A synergistic effect between the UV absorption of the cinnamovl chromophore in the siloxane network and the light scattering caused by the particulate nature of the UV filtering spheres was likely to be responsible for the good UV filtering efficiency of the obtained materials. Encapsulation of volatile citronellal into PTES4C nanoparticles could be carried out successfully by in situ polycondensation under self-catalysis conditions. The citronellal-loaded PTES4C spheres with a loading of 35% (w/w) (citro-PTES4C-1) and 48% (w/w) (citro-PTES4C-2) showed sustained release characteristics.

#### Materials and methods

APTES, 4-methoxycinnamic acid and 2,4-dimethoxy benzaldehyde were purchased from Acros Organics (Geel, Belgium). EHMC (Eusolex 2292) was obtained from Merck (Darmstadt, Germany). All other chemicals were reagent grade and were used without additional purification.

FT-IR analysis was carried out using a Nicolet Fourier transform Infrared spectrophotometer: Impact 410 (Nicolet Instruments Technologies, Inc., Madison, WI, USA). <sup>1</sup>H- and <sup>13</sup>C-NMR analyses were carried out using a Varian Mercury spectrometer which was operated at 400.00 MHz for <sup>1</sup>H and 100.00 MHz for <sup>13</sup>C nuclei (Varian Company, Palo Alto, CA, USA). UV analysis was done with the aid of a UV 2500 UV-Vis spectrophotometer (Shimadzu Corporation, Kyoto, Japan), using a quartz cell with a 1 cm pathlength. Transmission Electron

Microscopy (TEM) was carried out using a JEM-2100 (Jeol, Ltd., Japan) and Scanning Electron Microscopy (SEM) was performed on a JEM-6400 (Jeol, Ltd., Japan). The hydrodynamic particle sizes of the nanoparticle suspensions were determined without prefiltering on a Zetasizer nanoseries (Mulvern Instruments, Worcestershire, UK).

#### Synthesis of hybrid monomers

2,4-Dimethoxycinnamic acid was synthesized using Knoevenagel-Doebner condensation between 2,4-dimethoxybenzaldehyde and malonic acid.36 TES4C and TES24C were obtained from a condensation reaction between APTES and 4-methoxycinnamic acid and 2,4-dimethoxy cinnamic acid (via acid chloride), respectively (Scheme 1). 4-Methoxycinnamoyl chloride (or 2,4dimethoxycinnamoyl chloride) was first prepared by reacting 4methoxycinnamic acid (or 2,4-dimethoxycinnamic acid) with thionyl chloride (2.5 folds) in 200 ml of dry toluene. The mixture was refluxed for 6 h under an N<sub>2</sub> atmosphere. Then, the solvent and excess thionyl chloride were removed by vacuum pump. Finally, toluene (5 ml) was added to remove the trace amount of thionyl chloride by rotary evaporation under reduced pressure. The obtained 4-methoxycinnamoyl chloride (or 2,4-dimethoxycinnamoyl chloride) (0.1 mol) was dissolved in 250 ml of dry toluene. Then, 0.1 mol APTES and 0.1 mol triethylamine (TEA) were added. The mixture was refluxed for 3 h under N2 atmosphere. The solid salt of TEA-HCl was separated by suction filtration. The solvent and TEA were removed by rotary evaporation under reduced pressure. The obtained viscous liquid product was dried under vacuum to constant weight. NMR and IR spectra of the products are shown in the ESI.†

*TES4C*: Red-brown oil. Yield: 96.5%. FT-IR (cm $^{-1}$ ): 3276 (N–H stretching), 2966 (C–H stretching), 1655 (C=O stretching), 1602 (C=C Ar stretching), 1545 (N–H bending), 1509 (C=C Ar stretching), 1061 (C–O stretching) and 947 (Ar bending).  $^{1}$ H-NMR (400 MHz, CDCl<sub>3</sub>, δ, ppm): 7.56 (d, J=15.6 Hz, 1H, Ar–CH=), 7.42 (d, J=8.4 Hz, 1H, Ar–H), 6.88 (d, J=8.8 Hz, 1H, Ar–H), 6.24 (d, J=15.6 Hz, 1H, =CH–CONH), 5.91 (br, s, 1H, –CONH), 3.83 (m, 2H, –OCH<sub>2</sub>–CH<sub>3</sub>), 3.82 (s, 3H, –OCH<sub>3</sub>), 3.38 (m, 2H, –NH–CH<sub>2</sub>–CH<sub>2</sub>–), 1.69 (m, 2H, –CH<sub>2</sub>–CH<sub>2</sub>–CH<sub>2</sub>), 1.21 (m, 3H, –OCH<sub>2</sub>–CH<sub>3</sub>) and 0.68 (m, 2H, –CH<sub>2</sub>–CH<sub>2</sub>–Si–).

*TES24C*: Yellow-brown oil. Yield: 95.0%. FT-IR (cm<sup>-1</sup>): 3259 (N–H stretching), 2965 (C–H stretching), 1649 (C=O stretching), 1601 (C=C Ar stretching), 1562 (N–H bending), 1502 (C=C Ar stretching), 1079 (C–O stretching) and 836 (Ar bending). <sup>1</sup>H-NMR (400 MHz, CDCl<sub>3</sub>, δ, ppm): 7.74 (d, J = 16 Hz, 1H, Ar–CH=), 7.38 (d, J = 8.4 Hz, 1H, Ar–H), 6.47 (d, J = 8.8 Hz, 1H, Ar–H) 6.44 (s, 1H, Ar–H), 6.41 (d, J = 16.4 Hz, 1H, =CH–CONH), 5.86 (br, s, 1H, -CONH), 3.84, 3.82 (s, 2 × 3H, 2 × OCH<sub>3</sub>), 3.82 (m, 2H, -OCH<sub>2</sub>-CH<sub>3</sub>), 3.37 (m, 2H, -NH-CH<sub>2</sub>-CH<sub>2</sub>-), 1.68 (m, 2H, -CH<sub>2</sub>-CH<sub>2</sub>-CH<sub>2</sub>), 1.22 (m, 3H, -OCH<sub>2</sub>-CH<sub>3</sub>) and 0.67 (m, 2H, -CH<sub>2</sub>-CH<sub>2</sub>-Si-).

#### Polycondensation and particle formation

Hydrolysis coupled with polycondensation and particle formation were carried out simultaneously. Three external catalyst systems, acid catalysis with 0.1% (v/v) HCl, base catalysis with 3% or 5% (v/v) NH<sub>4</sub>OH<sup>37,31</sup> and self-catalysis<sup>38</sup> were compared.

Reactions were carried out with various percentages of ethanol solvent (Table 1). In addition, the effect of surfactant on the sphere formation was investigated.

# Acid and base catalyst (0.1% (v/v) HCl, 3% and 5% (w/w) NH<sub>4</sub>OH)

PTES4C spheres were prepared from the hydrolysis–polycondensation of TES4C in the presence of 20, 30 and 40% (v/v) of ethanol. TES4C (0.4 g) was dissolved in 4, 6 or 8 ml of ethanol and the obtained clear solution was dropped slowly (1 ml min<sup>-1</sup>) into stirred (700 rpm) water (16, 14 or 12 ml) containing the appropriate acid or base catalyst. The obtained suspension was further stirred at room temperature to complete the condensation. Completion of the reaction was checked by confirming that the obtained spheres were not soluble in ethanol. The PTES4C spherical suspension was then dialyzed against 20% (v/v) aqueous ethanol to remove residual monomers and catalyst, followed by dialysis against water. The suspension product was dried under vacuum to a constant weight and the synthesis yield was evaluated.

PTES24C spheres were prepared in a similar manner to PTES4C spheres with slight modification, from the hydrolysis—polycondensation of TES24C in the presence of 10, 20 or 30% (v/v) of ethanol. The hybrid monomer TES24C was dissolved in ethanol (2, 4 or 6 ml) to obtain a clear solution. The appropriate volume (18, 16 or 14 ml) of water was then dropped slowly (1 ml min<sup>-1</sup>) into the obtained TES24C solution whilst stirring at 700 rpm, and thereafter stirred at room temperature (see Table 1 for times and amounts of TES24C used). Residual monomers and catalysts were then removed by the same dialysis process used in the PTES4C preparation and the dry product was also obtained similarly.

#### Self-catalysis

PTES4C and PTES24C self-catalysed polymerization was carried out as above (acid/base catalysis) except that 1) APTES was mixed with the monomer at 20% (w/w) and 2) the water phase contained neither HCl nor NH<sub>4</sub>OH.

#### Surfactant

Polymerization of TES4C and TES24C by self-catalysis was also carried out in a presence of 5% (v/v) of the non-ionic surfactant, Triton X-100. The reaction was carried out with no added ethanol. Monomer (0.40 g for TES4C or 0.20 g for TES24C) was added to 1.0 ml of Triton X-100 and then stirred. Then the same procedure as described above was used except that the amount of water used was 19 ml and the monomer solution in the surfactant was used in placed of the monomer solution in ethanol. The residual monomer and surfactant residues were removed from the product by dialysis against 20% (v/v) aqueous ethanol, and then water. The obtained product was dried under vacuum to a constant weight and the synthesis yield was evaluated.

#### Encapsulation

Citronellal was encapsulated into PTES4C nanospheres by the *in situ* polycondensation of TES4C in the presence of citronellal

using the method modified from the works of Lapidot<sup>20</sup> and Ahn.<sup>39</sup> The encapsulation was carried out at a 1:2 and 1:1 (w/w) ratio of citronellal: TES4C. For encapsulation, at (w/w) ratio of 1:2 citronellal: TES4C, citronellal (0.20 g), TES4C (0.40 g) and APTES (0.08 g) were co-dissolved in 4 ml ethanol. The obtained clear solution was dropped slowly (1 ml min<sup>-1</sup>) into the stirred water (16 ml, stirring rate ~700 rpm), and the suspension stirred for 24 h at room temperature, before being centrifugally filtered (MWCO 100,000, Amicon Ultra-15, Millipore, Ireland) to collect the citro-PTES4C-1 spheres. The obtained spheres were then redissolved in water to a final volume of 20 ml. Encapsulation at a citronellal: TES4C (w/w) ratio of 1:1 was carried out similarly, except that 0.40 g of citronellal was used instead of 0.20 g and the obtained product was called citro-PTES4C-2.

Citronellal loadings in citro-PTES4C-1 and citro-PTES4C-2 were determined by directly evaluating the amount of citronellal in the obtained particles following extraction of the encapsulated citronellal nanoparticles with hexane. Five ml of hexane was added to 1.0 ml of the obtained suspensions, vigorously shaken, sonicated for 30 min, and left at 30 °C for 12 h before the hexane layer was withdrawn and the amount of citronellal in the hexane layer was determined by UV absorption spectroscopy with the aid of a calibration curve. The loading capacities were then calculated as follows:

%Loading =  $\frac{\text{Weight of citronellal found spheres} \times 100}{\text{Weight of citronellal loaded spheres}}$ 

#### Release of citronellal

Five ml of the aqueous suspension of citro-PTES4C-1 spheres (0.286 g) at the final citronellal concentration of 2% or 3% (w/v) (or 0.313 g of citro-PTES4C-2), were loaded into a 20 ml flat bottom-headspace-vial (five vials). The vials were left uncovered at 45 °C. Due to water evaporation, water was added to each vial everyday to maintain a near constant volume throughout the 4day experiment. At the indicated times (0, 1, 2, 3 and 4 days), one of the five vials was filled with 15 ml of hexane, capped with headspace aluminium crimp caps with PTFE/silicone septa and then vigorously vortexed, sonicated, and left to stand at 30 °C for 12 h. The hexane layer was then subjected to citronellal quantification using UV-Vis spectroscopy with the aid of a calibration graph constructed from the freshly prepared citronellal solutions. Control vials (unencapsulated citronellal of similar concentration) were prepared using standard citronellal in 20% (v/v) aqueous ethanol, i.e., 0.1 g of citronellal at the final volume of 5 ml and 0.15 g of citronellal at the final volume of 5 ml. Each experiment was carried out in duplicate and the average values were reported.

# Sun protection factor (SPF) and UVA protection factor (UVA-PF)

Cosmedia SP gel, containing 10.8% (w/v) PTES4C, was prepared by dispersing the PTES4C in the gel (1% (w/v) sodium polyacrylate in water with 0.05% di-sodium EDTA) with stirring. The freshly prepared sample gel was then subjected to SPF and UVA-

PF measurement using an SPF Analyzer (Optometrics, SPF-290s, MA, USA). PTES24C and EHMC were also subjected to the same measurement using the same protocol (see Table 2 for the amount of PTES24C and EHMC used).

#### Acknowledgements

The authors thank the Ratchadaphisesomphot endowment fund, the Special Task force for Activating Research from the centernary academic development project, Chulalongkorn University, the Commission of Higher Education-Thailand Research Fund (BRG5280004), Thai Government Stimulus Package 2 (TKK2555), for financial support. The authors are also very grateful for the English corrections from Robert Butcher of the Publication Counseling Unit, Faculty of Science, Chulalongkorn University, and the SPF and UVA-PF measurements from the Institute of Beauty and Health Sciences Co., Ltd.

#### References

- L. Marrot and J. R. Meunier, J. Am. Acad. Dermatol., 2008, 58, S139–S148.
- 2 G. Vielhaber, S. Grether-Beck, O. Koch, W. Johncock and J. Krutmann, *Photochem. Photobiol. Sci.*, 2006, **5**, 275–282.
- 3 S. Lautenschlager, H. C. Wulf and M. R. Pittelkow, *Lancet*, 2007, **370**, 528–537.
- 4 M. D. Palm and M. N. O'Donoghue, *Dermatologic Therapy*, 2007, 20, 360–376.
- 5 I. J. Fletcher, J. Kaschig, G. Metzger, D. Reinehr and P. Hayoz, US Patent 6,919,454 B22005, 2005.
- 6 S. Pattanaargson, N. Hongchinnagorn, P. Hirunsupachot and Y. Sritana-anant, *Photochem. Photobiol.*, 2004, 80, 322–325.
- 7 S. Pattanaargson and P. Limphong, Int. J. Cosmet. Sci., 2001, 23, 153–160.
- 8 H. Richard and L.M., US Patent 6,517,742 B1, 2003.
- 9 R. Jiang, M. S. Roberts, D. M. Collins and H. A. E. Benson, *Br. J. Clin. Pharmacol.*, 1999, 48, 635–637.
- 10 P. Klinubol, P. Asawanonda and S. P. Wanichwecharungruang, Skin Pharmacol. Physiol., 2008, 21, 23–29.
- 11 V. Sarveiya, S. Risk and H. A. Benson, J. Am. Acad. Dermatol., 2004, 50 P75
- 12 M. Heneweer, M. Muusse, M. van den Berg and J. T. Sanderson, Toxicol. Appl. Pharmacol., 2005, 208, 170–177.
- 13 C. Schlecht, H. Klammer, H. Jarry and W. Wuttke, *Toxicology*, 2004, 205, 123–130.
- 14 M. Schlumpf, B. Cotton, M. Conscience, V. Haller, B. Steinmann and W. Lichtensteiger, *Environ. Health Perspect.*, 2001, 109, 239– 244
- S. Pattanaargson, T. Munhapol, P. Hirunsupachot and P. Luangthongaram, J. Photochem. Photobiol., A, 2004, 161, 269–274.
- 16 S. Sasiwilaskorn, P. Klinubol, A. Tachaprutinun, T. Udomsup and S. P. Wanichwecharungruang, J. Appl. Polym. Sci., 2008, 109, 3502–3510.
- 17 N. Anumansirikul, M. Wittayasuporn, P. Klinubol, A. Tachaprutinun and S. P. Wanichwecharungruang, Nanotechnology, 2008, 19, 205101.
- 18 Y. A. Gomaa, L. K. El-Khordagui, N. A. Boraei and I. A. Darwish, Carbohydr. Polym., 2010, 81, 234–242.
- M. Vettor, S. Bourgeois, H. Fessi, J. Pelletier, P. Perugini, F. Pavanetto and M. A. Bolzinger, *J. Microencapsulation*, 2010, 27, 253–262.
- 20 N. Lapidot, O. Gans, F. Biagini, L. Sosonkin and C. Rottman, J. Sol-Gel Sci. Technol., 2003, 26, 67–72.
- 21 M. Buchalska, G. Kras, M. Oszajca, W. Łasocha and W. MacYk, J. Photochem. Photobiol., A, 2010, 213, 158–163.
- 22 A. O. Gamer, E. Leibold and B. Van Ravenzwaay, *Toxicol. in Vitro*, 2006, 20, 301–307.
- 23 R. Hu, X. Gong, Y. Duan, N. Li, Y. Che, Y. Cui, M. Zhou, C. Liu, H. Wang and F. Hong, *Biomaterials*, 2010, 31, 8043–8050.

- 24 P. Kocbek, K. Teskač, M. E. Kreft and J. Kristl, Small, 2010, 6, 1908– 1917.
- 25 R. Landsiedel, L. Ma-Hock, B. Van Ravenzwaay, M. Schulz, K. Wiench, S. Champ, S. Schulte, W. Wohlleben and F. Oesch, *Nanotoxicology*, 2010, 4, 364–381.
- 26 J. Lekki, Z. Stachura, W. Dabroś, J. Stachura, F. Menzel, T. Reinert, T. Butz, J. Pallon, E. Gontier, M. D. Ynsa, P. Moretto, Z. Kertesz, Z. Szikszai and A. Z. Kiss, Nucl. Instrum. Methods Phys. Res., Sect. B, 2007, 260, 174–177.
- 27 M. D. Newman, M. Stotland and J. I. Ellis, J. Am. Acad. Dermatol., 2009, 61, 685–692.
- 28 J. P. Zou, L. Jiang, T. P. Nguyen and Y. Dan, *Polym. Adv. Technol.*, 2010, 21, 598–605.
- 29 T. Walenzyk, C. Carola, H. Buchholz and B. König, *Int. J. Cosmet. Sci.*, 2005, 27, 177–189.
- 30 Y. B. Kim and K. S. Yoon, NSTI Nanotechnology Conference and Trade Show NSTI Nanotech 2007, Santa Clara, California, USA. *Technical Proceedings* 4, pp. 254–256.

- 31 W. Stober, A. Fink and E. Bohn, *J. Colloid Interface Sci.*, 1968, 26, 62–69.
- 32 K. W. Jang, S. H. Choi, S. I. Pyun and M. S. Jhon, *Mol. Simul.*, 2001, **27**, 1–16.
- 33 S. Q. Liu, P. Cool, O. Collart, P. Van der Voort, E. F. Vansant, O. I. Lebedev, G. Van Tendeloo and M. H. Jiang, *J. Phys. Chem.* B, 2003, 107, 10405–10411.
- 34 T. M. Karpkird, S. Wanichweacharungruang and B. Albinsson, *Photochem. Photobiol. Sci.*, 2009, **8**, 1455–1460.
- 35 P. Morliere, O. Avice and T. E. Melo Sa, *Photochem. Photobiol.*, 1982, 36, 395–399.
- 36 T. Monhaphol, B. Albinsson and S. P. Wanichwecharungruang, *J. Pharm. Pharmacol.*, 2007, **59**, 279–288.
- 37 D. A. Loy and K. J. Shea, Chem. Rev., 1995, 95, 1431-1442.
- 38 R. M. Ottenbrite, J. S. Wall and J. A. Siddiqui, J. Am. Ceram. Soc., 2000, 83, 3214–3215.
- 39 B. Y. Ahn, S. I. Seok and I. C. Baek, *Mater. Sci. Eng.*, C, 2008, 28, 1183–1188.

### คำวิจารณ์ผลงานวิจัยของ ศุภศร ที่ลงในวารสาร Chemistry World 2011 April



A new smart sunscreen suggested by researchers in Thailand could simultaneously protect skin and deliver topical drugs.

June 19-22, 2011

FREE

colleagues at Chulalongkorn University in Bangkok have combined the advantages of both types of sunscreen by making a hybrid polysilsesquioxane (complex silicate) particle that contains organic chromophores as part of an inorganic structural network. The two components work synergistically as the organic chromophore absorbs UV light, which is then scattered h

The sunscreen combines the advantages of inorganic and organic formulas

particles. The resulti Supason Pattanaargson Wanichwecharungruang and ight without generation colleagues at Chulalongkorn much titanium dioxid the sticky feeling of ti bound to the inorgan absorbed into the cir combined the advantages of both In addition, because types of sunscreen by making a synergistically as the organic

SAMPLE

The sunscreen combines the advantages of inorganic and organic formulas

particles. The resulting nanospheres are more effective than commercial sunscreen at absorbing UV light.

with a fragrance or d

sunscreen at absort

☑ Email this to a friend

Add to del.icio.us

Share on Facebook Seed Newsvine

Digg this story

® Reddit this

Twitter this

isolation. He sugges into the system, for e increase the range o Carol Stanier

team tested their nar hybrid polysilsesquioxane (complex that the scent was pr that the scent was pr silicate) particle that contains the University of Nort used for delivery and organic chromophores as part of an him is that the two cc inorganic structural network. The two components work chromophore absorbs UV light, which is then scattered by the

# Aggregation Phenomena of Amphiphilic UVB Absorptive Oligoesters Containing *p*-Alkoxycinnamate and Poly(ethylene oxide) Blocks

#### P. Changhin, 1,2 S. P. Wanichwecharungruang, 3 C. Luadthong, 3 Y. Sritana-Anant 3

<sup>1</sup>Program of Petrochemistry and Polymer Science, Chulalongkorn University, Patumwan, Bangkok, Thailand <sup>2</sup>National Center of Petroleum, Petrochemicals, and Advanced Materials (NCE-PPAM), Chulalongkorn University, Bangkok, Thailand

<sup>3</sup>Department of Chemistry, Faculty of Science, Chulalongkorn University, Patumwan, Bangkok, Thailand

Received 26 October 2008; accepted 31 July 2009 DOI 10.1002/app.31196

Published online 7 October 2009 in Wiley InterScience (www.interscience.wiley.com).

**ABSTRACT:** The synthesis of new amphiphilic oligoesters containing a hydrophobic block based on *p*-alkoxycinnamate and hydrophobic poly(ethylene oxide) is reported. Two hydrophobic monomers, 1,2-(bis(4-(2-carboxyvinyl)phenoxy))ethane (**M2**) and 1,12-(bis(4-(2-carboxyvinyl)phenoxy))dodecane (**M12**), were synthesized. Four oligoesters, poly((1,2-(bis(4-(2-carboxyvinyl)phenoxy))ethane) -co-(poly(ethylene oxide)200)) (**P2-200**), poly((1,2-(bis(4-(2-carboxyvinyl)phenoxy))phenoxy)) dodecane)-co-(poly(ethylene oxide)400)) (**P12-400**), and poly((1,12-(bis(4-(2-carboxyvinyl)phenoxy))dodecane)-co-

(poly(ethylene oxide)1000)) (P12-1000) were then constructed by reacting the M2 or M12 with poly(ethylene oxide) (PEO) with lengths of  $\sim 4$  (PEO 200),  $\sim 10$  (PEO 400), or  $\sim 23$  (PEO1000) units using multiple esterifications. These oligoesters possess UVB absorption properties and show good solubility in various organic solvents. Self-assembly of the oligoesters into aqueous spherical colloids could be induced through an acetone to water solvent displacement technique. © 2009 Wiley Periodicals, Inc. J Appl Polym Sci 115: 1724–1731, 2010

Key words: alkoxycinnamate; oligoester; sunscreen; colloid

#### INTRODUCTION

Different varieties of amphiphilic polymeric materials, both block copolymers and grafted polymers, have been synthesized and formed into countless of nanoscale architectures.<sup>1-4</sup> Nanostructure formation of amphiphilic polymers can be explained by the thermodynamic incompatibility between the hydrophilic and hydrophobic blocks, which makes the polymer chains to self-organize in the way that the contact between similar and dissimilar blocks are maximized and minimized, respectively. Macrophase separation is prevented by the entropic forces stemming from the covalent bonds holding the hydrophilic and hydrophobic blocks together. The system, then, must reach a balance between mixing and separating<sup>6</sup> and this usually results in self-assembled structures, in which microphase separation is observed. It has been demonstrated that such balance is a function of several variables, such as the chemical structure of the

block copolymer, ions in the solvent, concentration, and solvent selectivity.<sup>7–9</sup> During the self-assembly of amphiphilic polymers in an aqueous system or other polar solvents, the hydrophilic blocks (solvent–soluble block) usually form the corona, which provides the stabilization, whilst the hydrophobic blocks (solvent–insoluble polymer block) produce the core isolating the nanoparticles from the solvent.

Esters of p-methoxycinnamic acid are among the popular UVB screening compounds used in various sunscreen products. The most widely used derivative in this group is the 2-ethylhexyl-p-methoxycinnamate (EHMC), which possesses a high molar absorption coefficient ( $\epsilon = 22,000-24000 \text{ M}^{-1} \text{ cm}^{-1} \text{ at } 310 \text{ nm}$ ), and shows only few allergic reactions to human skin. 10,11 Nevertheless, transdermal penetration of EHMC through human skin has been reported, leading to the reduction of UV filtering efficiency at the skin surface. 12,13 Attempts to increase the skin accumulation of organic UV absorbers include incorporations of the UV filters into delivery systems 14,15 and some alterations in the formulations. <sup>16</sup> In addition, a few novel polymeric sunscreens have been developed recently under the assumption that large molecules presumably will have very low transdermal absorption. 17-21 To overcome these transdermal penetration problems, we have synthesized block-type-macromolecular amphiphilic chromophores containing a

Journal of Applied Polymer Science, Vol. 115, 1724–1731 (2010) © 2009 Wiley Periodicals, Inc.

Correspondence to: S. P. Wanichwecharungruang (psupason@chula.ac.th).

Contract grant sponsors: Thailand Research Fund, Office of Commission for Higher Education, Chulalongkorn University Graduate Thesis Grant.

hydrophobic block based on *p*-alkoxycinnamate and hydrophilic poly(ethylene oxide). Studies of the self-assembly of the obtained oligoesters into nano/microspheres are also demonstrated and correlation between hydrophobicity to hydrophilicity ratio and particle sizes are presented.

#### **EXPERIMENTAL**

#### Materials

Solvents used in syntheses and spectroscopic works were reagent or analytical grades purchased from Labscan (Bangkok, Thailand) and Carlo Erba Reagents (Rodano, Italy). Solvents used for column chromatography were purified from commercial grade solvents before use by distillation. 4-Hydroxybenzaldehyde, 1,2-dibromoethane, 1,12-dibromododecane, malonic acid, all polyethylene glycol's ( $M_W =$ 200, 400, and 1000) were purchased from Acros Organics (Geel, Belgium). Potassium carbonate was purchased from Fluka Chemical Company (Buchs, Switzerland). Piperidine was purchased from Sigma Chemical Co. (Steinheirg, Germany). The membranes used for dialysis were CelluSep T4 dialysis tube (MWCO 12,000-14000, 75 mm flat width, 17.9 mL/cm volume capacity, Membrane Filtration Products, Seguin, TX, USA). Column chromatography was performed using silica gel (Merck Kieselgel 60 G) (Merck KgaA, Darmstadt, Germany). Molecular weights were determined at room temperature by gel permeation chromatography using Waters styragel HR low molecular weight column and Waters 600E Multisolvent Delivery System (Waters, MA, USA), with tetrahydrofuran as a mobile phase. The IR spectra were recorded on a Nicolet Fourier Transform Infrared spectrophotometer (FTIR) using an Impact 410 (Nicolet Instrument Technologies, Madison, WI, USA). <sup>1</sup>H and <sup>13</sup>C-nuclear magnetic resonance (NMR) spectra were obtained using a Varian Mercury spectrometer (Varian Company, Palo Alto, CA, USA). A thermogram of each sample was obtained by differential scanning calorimetry using a DSC 204 (Netzsch Group, Selb, Germany). UV spectra were obtained with the aid of UV 2550 UV/VIS spectrophotometer (Shimadzu Corporation, Kyoto, Japan). MALDI mass spectra were recorded on an Ultraflex MALDI-TOF mass spectrometer (Bruker Daltonics, Bremen, Germany) with either sinapinic acid (m/z = 224.07) or 2,5-dihydroxybenzoic acid (m/z = 154.03). ESI-MS analyses were performed with Waters Micromass Quattomicro API ESCi (Waters, MA, USA).

#### Synthesis of monomers

1,2-(Bis(4-(formylphenoxy))ethane) (1)

In a two-necked round bottom flask, attached with a condenser and purged with  $N_2$ , 4-hydroxybenzalde-

hyde (6.1 g, 0.05 moles) was dissolved in acetonitrile (70 mL). Potassium carbonate (10 g) and 1,2-dibromoethane (13.0 g) were added and the mixture was refluxed until no 4-hydroxybenzaldehyde could be detected by TLC. The reaction mixture was then evaporated and the residual solute dissolved in 100 mL dichloromethane, washed three times with water and dried with anhydrous sodium sulfate to remove the water. The crude product was then purified by column chromatography on silica gel using dichloromethane / hexane (40 : 60 (v/v)) as the eluent. The product was obtained as white solid: 68%.

 $R_f$ : 0.40 (SiO<sub>2</sub>, EtOAc/hexane, 1 : 1). <sup>1</sup>H-NMR (400 MHz, CDCl<sub>3</sub>,  $\delta$ , ppm): 9.91 (s, 2H, Ar—CHO), 7.87 (d, J = 8.58 Hz, 4H, Ar—H), 7.06 (d, J = 8.58 Hz, 4H, Ar—H), 4.45 (s, 4H, —CH<sub>2</sub>—O—Ar). MS (m/z): calculated for C<sub>16</sub>H<sub>12</sub>O<sub>4</sub>, 270; found, 270 [M]<sup>+</sup>.

#### 1,12-(Bis(4-(formylphenoxy))dodecane) (2)

1,12-(Bis(4-(formylphenoxy))dodecane) (2) was prepared using the same procedure mentioned earlier, except that 1,2-dibromoethane was replaced by 1,12-dibromododecane (4.7 g). Product obtained as white solid: 68%.

 $R_f$ : 0.70 (SiO<sub>2</sub>, EtOAc/hexane, 1 : 1). <sup>1</sup>H-NMR (400 MHz, CDCl<sub>3</sub>,  $\delta$ , ppm): 9.92 (s, 2H, Ar—CHO), 7.87 (d, J = 8.58 Hz, 4H, Ar—H), 7.03 (d, J = 8.58 Hz, 4H, Ar—H), 4.08 (s, 4H, —CH<sub>2</sub>—O—Ar), 1.85–1.34 (br, 20H, —CH<sub>2</sub>—). MS (m/z): calculated for C<sub>22</sub>H<sub>18</sub>O<sub>4</sub>, 410; found, 410 [M]<sup>+</sup>.

#### 1,2-(Bis(4-(2-carboxyvinyl)phenoxy))ethane (M2)

In a two-necked round bottom flask, attached with condenser, compound 1 (13.50 g, 0.05 mole) was dissolved in pyridine (50 mL) and then malonic acid (20.80 g, 0.20 mole) and piperidine (1 mL) were added. The mixture was heated at 78 – 80°C for 74 h. After being cooled, most of the solvent was removed and the mixture was acidified with 200 mL of 2 *M* HCl. The solid product separated by suction filtration and washed with water was white solid: 70%.

m.p.  $310\text{--}315^{\circ}\text{C}$ , UV-Vis  $(\lambda_{\text{max}})$ : 308 nm  $(\varepsilon_{\text{max}} = 44,000 \text{ M}^{-1}\text{cm}^{-1})$ , IR (KBr, thin film, cm $^{-1}$ ): 3200–2400, 1677, 1599, 1509, 1241,  $^{1}\text{H-NMR}$  (400 MHz, DMSO- $d_{6}$ ,  $\delta$ , ppm): 12.23 (s, 1H, —COOH), 7.58 (d, J = 8.58 Hz, 4H, Ar—H), 7.48 (d, J = 16.38 Hz, 2H, Ar—CH=), 6.96 (d, J = 8.58 Hz, 4H, Ar—H), 6.32 (d, J = 16.38 Hz, 2H, Ar—CH=), 4.31 (s, 4H, —CH<sub>2</sub>—O—Ar) ppm,  $^{13}\text{C-NMR}$  (100 MHz, DMSO- $d_{6}$ ,  $\delta$ , ppm): 168.3 (—COOH), 160.4 (—C—), 144.1 (Ar—CH=), 130.4 (aromatic carbons), 127.5 (—C—), 117.1 (=CH—COOH), 115.3 (aromatic carbons), 66.9 (—CH<sub>2</sub>—O—Ar). MS (m/z): calculated for C<sub>20</sub>H<sub>18</sub>O<sub>6</sub>, 354; found, 353 [M—H] $^-$ .

1726 CHANGHIN ET AL.

1,12-(Bis(4-(2-carboxyvinyl)phenoxy))dodecane (M12)

1,12-(Bis(4-(2-carboxyvinyl)phenoxy))dodecane (M12) was prepared from compound 2 using the same procedure as described earlier for the M2 preparation, except that compound 1 was replaced with compound 2 (20.50 g). The product was obtained as white solid: 60%.

m.p. 202–205°C. UV–Vis (dimethylformamide)  $\lambda_{\text{max}}$ , nm (ε): 308 (45,000). IR (KBr, thin film, cm<sup>-1</sup>): 3200–2400, 1671, 1593, 1511, 1246. <sup>1</sup>H-NMR (400 MHz, DMSO- $d_6$ ,  $\delta$ , ppm):  $\delta$ 7.58 (d, J=8.58 Hz, 4H, Ar–H,), 7.50 (d, J=16.38 Hz, 2H, Ar–CH=), 6.92 (d, J=8.58 Hz, 4H, Ar–H), 6.34 (d, J=16.38 Hz, 2H, Ar–CH=), 3.97 (s, 4H, –CH<sub>2</sub>–O–Ar), 1.68–1.24 (br, 20H, –CH<sub>2</sub>–). <sup>13</sup>C-NMR (100 MHz, DMSO- $d_6$ ,  $\delta$ , ppm): 168.3 (–COOH), 160.8 (–C–), 144.0 (Ar–CH=), 130.3 (aromatic carbons), 127.4 (–C–), 117.0 (=CH–COOH), 115.2 (aromatic carbons), 68.0 (–CH<sub>2</sub>–O–Ar), 29.4–25.9 (–CH<sub>2</sub>–). MS (m/z): calculated for C<sub>30</sub>H<sub>38</sub>O<sub>6</sub>, 494; found, 493 [M–H]<sup>-</sup>.

#### Synthesis of oligoesters

Poly((1,2-(bis(4-(2-carboxyvinyl)phenoxy))ethane)-co-(poly(ethylene oxide)200)) (P2-200)

A mixture of monomer **M2** (0.354 g, 1 mmol) and freshly distilled thionyl chloride (15 mL) was refluxed for 3 h in a two-necked round bottom flask attached with a condenser and a drying tube. Unreacted thionyl chloride was then removed by evaporation under reduced pressure resulting in 1,2-(bis(4-(2-chlorocarbonyl vinyl)phenoxy))ethane. Poly(ethylene oxide),  $\overline{M_n} = 200$ , (0.02 g, 1 mmol) and 20 mL acetonitrile were then added, and the mixture was refluxed for 28 h. The reaction mixture was cooled to room temperature, the solvent was removed by reduced pressure evaporation and the residual solute dissolved in 50 mL ethyl acetate, washed three times with water and then dried with anhydrous sodium sulfate. The product was yellowwax-like solid.

<sup>1</sup>H-NMR (400 MHz, CDCl<sub>3</sub>, δ, ppm): 7.65 (d, J = 15.60 Hz, Ar—CH=), 7.47 (d, J = 7.9 Hz, Ar—H), 6.95 (d, J = 8.0 Hz, Ar—H), 6.35 (d, J = 15.60 Hz, Ar—CH=), 4.36–4.34 (—CH<sub>2</sub>—O—Ar, —COO— CH<sub>2</sub>—), 3.78–3.63 (—CH<sub>2</sub>—O—). IR (NaCl, cm<sup>-1</sup>): 1705, 1599, 1510, 1244. UV–Vis (dimethylformamide)  $\lambda_{\text{max}}$ , nm (ε): 311 (51,000). DSC:  $T_g = -18.8$ °C,  $T_m = 91.1$ °C.

Poly((1,2-(bis(4-(2-carboxyvinyl)phenoxy))ethane)-co-(poly(ethylene oxide)400)) (P2-400), Poly((1,12-(bis(4-(2-carboxyvinyl)phenoxy))dodecane)-co-(poly(ethylene oxide)400)) (P12-400), and Poly((1,12-(bis(4-(2-carboxyvinyl)phenoxy)) dodecane)-co-(poly(ethylene oxide)1000)) (P12-1000)

Poly((1,2-(bis(4-(2-carboxyvinyl)phenoxy))ethane)-co-(poly(ethylene oxide)400)) (**P2-400**) (yellow-oil)

poly((1,12-(bis(4-(2-carboxyvinyl)phenoxy))dodecane)-co-(poly(ethylene oxide)400)) (P12-400) (yellow wax) were prepared from 1,2-(bis(4-(2-chlorocarbonylvinyl)phenoxy))ethane (M2) and 1,12-(bis(4-(2-chlorocarbonylvinyl)phenoxy)) dodecane (M12), respectively, using the same procedure as described earlier for the **P2-200** preparation, except that poly (ethylene oxide),  $\overline{M_n} = 200$  was replaced with poly(ethylene oxide),  $\overline{M_n} = 400$ , (0.04 g, 1 mmol). Poly((1,12-(bis(4-(2-carboxyvinyl)phenoxy))dodecane) -co-(poly(ethylene oxide)1000)) (**P12-1000**) (yellow wax) was prepared from 1,12-(bis(4-(2-chlorocarbonylvinyl)phenoxy)) dodecane (M12), using similar proceedure except that poly(ethylene oxide),  $\overline{M_n}$  = 400 was replaced with poly(ethylene oxide),  $\overline{M_n} =$ 1000, (0.10 g, 1 mmol).

Poly((1,2-(bis(4-(2-carboxyvinyl)phenoxy))ethane)-co-(poly(ethylene oxide)400))(P2-400). <sup>1</sup>H-NMR (400 MHz, CDCl<sub>3</sub>, δ, ppm): 7.66 (d, J = 15.60 Hz, Ar—CH=), 7.49 (d, J = 7.8 Hz, Ar—H), 6.95 (d, J = 7.8 Hz, Ar—H), 6.36 (d, J = 15.6 Hz, Ar—CH=), 4.36 (d, —CH<sub>2</sub>—O—Ar, —COO—CH<sub>2</sub>—), 3.79–3.60 (—CH<sub>2</sub>—O—). IR (neat, cm<sup>-1</sup>): 3700–3300, 1705, 1603, 1514, 1244. UV–Vis (dimethylformamide)  $\lambda_{max}$ , nm: 311. DSC:  $T_o = -20.1$ °C

*Poly*((1,12-(*bis*(4-(2-*carboxyviny*))*phenoxy*))*dodecane*)-*co*(*poly*(*ethylene oxide*)400))(*P12-400*). <sup>1</sup>H-NMR (400 MHz, CDCl<sub>3</sub>, δ, ppm): 7.66 (d, J = 15.60 Hz, Ar—CH=), 7.46 (d, J = 7.8 Hz, Ar—H), 6.89 (d, J = 7.8 Hz, Ar—H), 6.34 (d, J = 15.60 Hz, Ar—CH=), 4.35 (—CH<sub>2</sub>—O—Ar), 3.98 (—COO—CH<sub>2</sub>—), 3.70 (—CH<sub>2</sub>—O—), 1.8 (br, —CH<sub>2</sub>—). IR (NaCl, cm<sup>-1</sup>): 3700–3300, 1709, 1603, 1501, 1248. UV–Vis (dimethylformamide)  $\lambda_{\text{max}}$ , nm: 311. DSC:  $T_g = -50.7^{\circ}$ C,  $T_m = 79.0^{\circ}$ C.

*Poly*((1,12-(bis(4-(2-carboxyvinyl)phenoxy)))dodecane)-co-(poly(ethylene oxide)1000))(*P*12-1000). <sup>1</sup>H-NMR (400 MHz, CDCl<sub>3</sub>, δ, ppm): 7.66 (d, J = 15.60 Hz, Ar—CH=), 7.47 (d, J = 7.8 Hz, Ar—H), 6.86 (d, J = 7.8 Hz, Ar—H), 6.34 (d, J = 15.60 Hz, Ar—CH=), 4.36 (—CH<sub>2</sub>—O—Ar), 3.98 (—COO—CH<sub>2</sub>—), 3.70 (—CH<sub>2</sub>—O—), 1.76 (br, —CH<sub>2</sub>—). IR (NaCl, cm<sup>-1</sup>): 3700–3300, 1708, 1600, 1500, 1247. UV–Vis (dimethylformamide)  $\lambda_{\text{max}}$ , nm: 311. DSC:  $T_g = -58.7^{\circ}$ C.

Poly((1,2-(bis(4-(2-carboxyvinyl)phenoxy))ethane)-co-(poly(ethylene oxide)400)) at higher concentration (P2-400c)

1,2-(Bis(4-(2-chlorocarbonylvinyl)phenoxy))ethane was prepared as aforementioned. Polymerization was also carried out using the same procedure as described for P2-400 preparation except that only 5 mL of  $CH_3CN$  was used instead of 20 mL. the product obtained as yellow-oil.

<sup>1</sup>H-NMR (400 MHz, CDCl<sub>3</sub>, δ, ppm): 7.66 (d, J = 15.60 Hz, Ar—CH=), 7.49 (d, J = 7.8 Hz, Ar—H), 6.95

(d, J = 7.8 Hz, Ar—H), 6.36 (d, J = 15.6 Hz, Ar—CH=), 4.38–4.34 (—CH<sub>2</sub>—O—Ar, —COO—CH<sub>2</sub>—), 3.79–3.60 (—CH<sub>2</sub>—O—). UV–Vis (dimethylformamide)  $\lambda_{\text{max}}$ , nm: 311. DSC:  $T_g = -15.82$ °C

#### Particle formation

Preparation of the particles from P2-200, P2-400, P12-400, and P12-1000 was carried out by a solvent displacement technique. Twenty milligrams of the oligoester were dissolved in 5 mL acetone. The solution (4000 ppm) was dialyzed against deionized water (Milli- $Q^{\otimes}$ ).

# Particle size, zeta potential, SEM, and TEM analyses

transmission electron microscopic (TEM) photographs were acquired on a TEM (JEM-2100, JEOL, Japan) with an accelerating voltage of 100–120 kV in conjunction with selected area electron diffraction.

Scanning Electron Microscopic (SEM) photographs were obtained using SEM (JSM-6400, JEOL, Japan). A drop of the nanoparticle suspension was placed on a glass slide and dried over night. After mounting the slide on an aluminum pin, the sample was coated with a gold layer under vacuum at 15 kV for 90 sec. The coated sample was then mounted on a SEM stud for visualization. The accelerating voltage used was 15 kV.

The particle sizes of the particles in water were acquired by Zetasizer nanoseries (Mulvern Instruments, Worcestershire, UK) equipped with He-Ne laser beam at 632.8 nm (scattering angle of  $173^{\circ}$ ). The concentration of particles in water was diluted to about 0.1 mg/mL. Each measurement was repeated five times with the average value  $\pm 1$  S.D. being reported.

#### **RESULTS AND DISCUSSION**

1,2-(Bis(4-(formyl phenoxy))ethane) (1) and 1,12-(bis(4-(formyl phenoxy))dodecane) (2) were successfully synthesized by the S<sub>N</sub>2 reactions between 4hydroxybenzaldehyde and 1,2-dibromoethane or 1,12-dibromododecane. These dialdehydes were then reacted with malonic acid using the Knoevenagel condensation reaction to produce 1,2-(bis(4-(2-carboxyvinyl)phenoxy))ethane (M2) or 1,12-(bis(4-(2carboxyvinyl)phenoxy))dodecane (M12) (Scheme 1). The UV absorption spectra of M2 and M12 showed a maximum absorption peak at 308 nm ( $\epsilon_{308~nm}$  = 44,000 (M2) and 45,000 (M12)  $M^{-1}cm^{-1}$ . The  $\epsilon$  values of both monomers were essentially double the value of 2-ethylhexyl-p-methoxy cinnamic acid  $(22,000 \text{ M}^{-1}\text{cm}^{-1})$ , confirming that both M2 and M12 most likely contain two cinnamoyl moieties in their

**Scheme 1** Synthesis of **M2** (m=1), **M12** (m=6), **P2-200**  $(m=1, m'\sim 4)$ , **P2-400**  $(m=1, m'\sim 10)$ , **P12-400**  $(m=6, m'\sim 10)$ , and **P12-1000**  $(m=6, m'\sim 23)$ .

molecules. The monomers were found to be soluble in pyridine, DMF, and DMSO.

The poly((1,2-(bis(4-(2-carboxyvinyl)phenoxy))ethane)-co-(poly(ethylene oxide)200)) (**P2-200**), poly ((1,2-(bis(4-(2-carboxyvinyl)phenoxy))ethane)-co-(poly(ethylene oxide)400)) (P2-400), poly((1,12-(bis(4-(2carboxyvinyl)phenoxy))dodecane)-co-(poly(ethylene oxide)400)) (P12-400), and poly((1,12-(bis(4-(2-carboxyvinyl)phenoxy))dodecane)-co-(poly(ethylene oxide)1000)) (P12-1000) were prepared by copolymerizations between M2 or M12 with poly(ethylene oxide) that had a number-average molecular weight  $(\overline{M_n})$  of 200, 400 or 1000. While M2 and M12 themselves were not soluble in CH<sub>3</sub>CN, their acid chloride derivatives were, allowing the condensation polymerizations to take place in CH<sub>3</sub>CN. The FTIR spectra (Fig. 1) of all oligoesters showed the characteristic absorptions of conjugated ester groups to be around 1705-1709 cm<sup>-1</sup> and 1000-1300 cm<sup>-1</sup>. The <sup>1</sup>H-NMR spectra of **P2-200** and **P2-400** show  $-CH_2-O-$  resonance at  $\sim 3.7$  ppm, indicating the presence of polyethylene oxide (Fig. 2). The appearance of  $-COO-CH_2-$  resonance at  $\sim 4.3$  ppm also confirms the successful esterifications. The <sup>1</sup>H-NMR spectra of P12-400 and P12-1000 also show resonances at  $\sim$  3.7 ppm (-CH<sub>2</sub>-O-) and  $\sim$  3.9 ppm (-COO-CH<sub>2</sub>-), indicating polyethylene oxide chain

Progress of the polymerization reaction followed by analyzing the  $\overline{M_n}$  of the reaction mixture at various reaction times using gel permeation chromatography. The polymerization was completed within few hours and the  $\overline{M_n}$  for P2-200, P2-400P12-400,

1728 CHANGHIN ET AL.

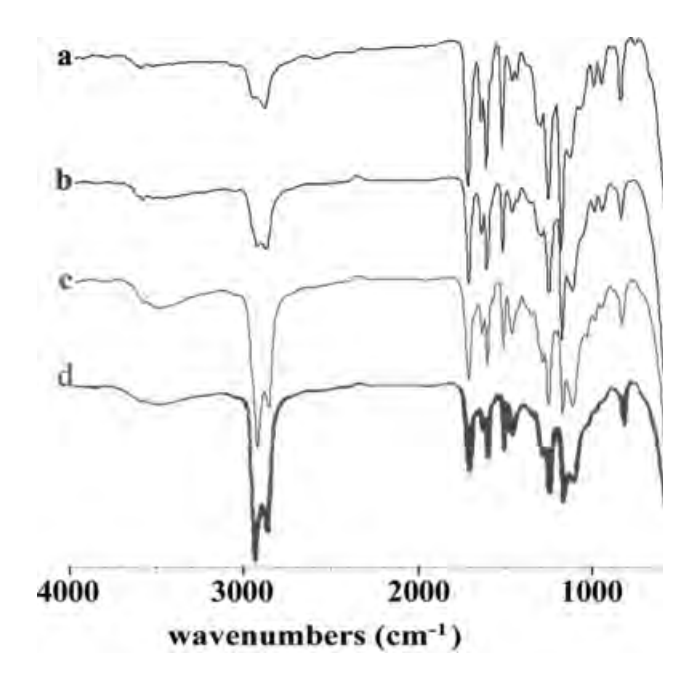


**Figure 1** FTIR spectra of a) P2-200, b) P2-400, c) P12-400, and d) P12-1000.

and **P12-1000** were found to be 2100, 2600, 2100, and 2600 Daltons, respectively (Fig. 3). It was speculated that the low  $\overline{M}_n$  values were the result of ring closure from intramolecular reactions between the two ends of the same chain. Therefore, polymeriza-

tion at a higher monomer concentration (P2-400c) was carried out and the oligomer so obtained (P2-**400c)** was found to possess an average  $\overline{M_n}$  of 4800, compared with the  $\overline{M_n}$  of 2600, obtained with a lower reaction concentration of the monomers (P2-400). This result supports the above speculation of intramolecular ring closure and indicated a possible mechanism (reactant concentration) for control of the size of the product. For further confirmation, the potentially cyclized products were analyzed by mass spectrometry. The MALDI-TOF MS spectra of the four oligomers gave m/z values of 688, 732, and 776 for P2-400, 828, 872, and 916 for P12-400, and finally 468, 512, and 556 for **P2-200**. Together with the lack of a broad absorption band around 2300–3600 cm<sup>-1</sup> (—COOH) in the FTIR spectra of the oligomers (Fig. 1), these data confirm the complete condensation reactions.

All oligoesters showed similar UV absorption wavelengths ( $\lambda_{max}$  of 310 nm in acetone) to their corresponding monomers and are soluble in many organic solvents such as acetonitrile, acetone, ethyl acetate, tetrahydrofuran, chloroform, and dichloromethane. This solubility is probably related to their low molecular weight, resulting from polymerization under dilute condition as stated above. Solubility of oligoesters in acetone enables self-assembly of these oligomers through the displacing of acetone with water as discussed below. Thus, no attempt was

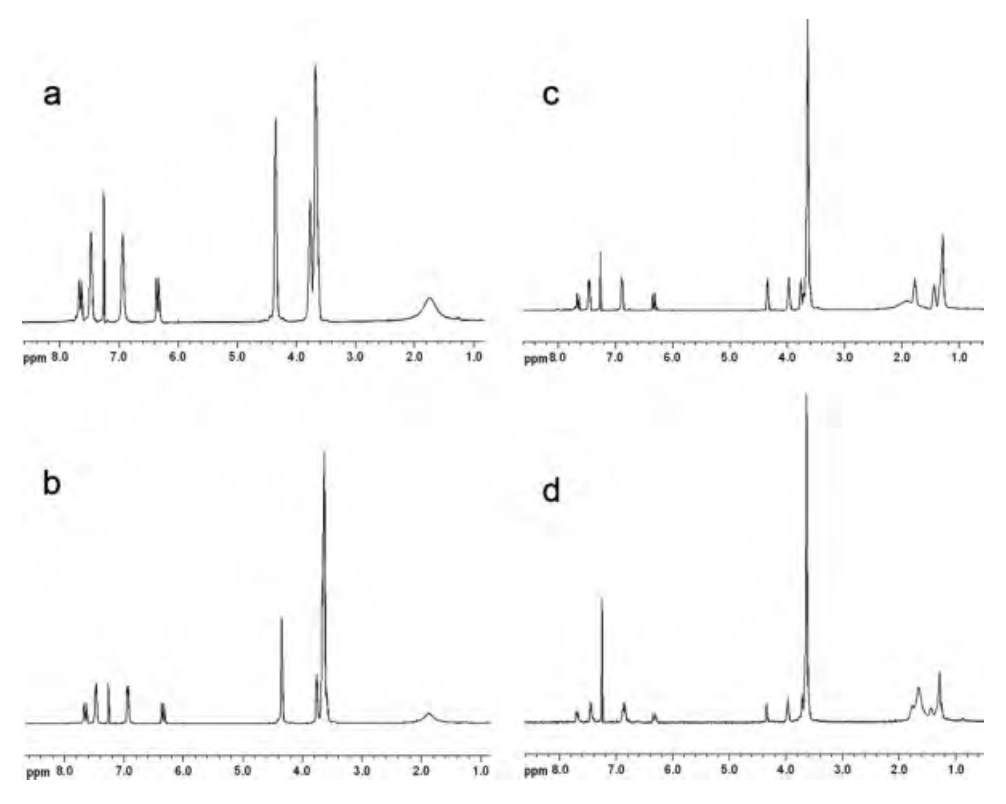


Figure 2 <sup>1</sup>H-NMR of a) P2-200, b) P2-400, c) P12-400, and d) P12-1000.

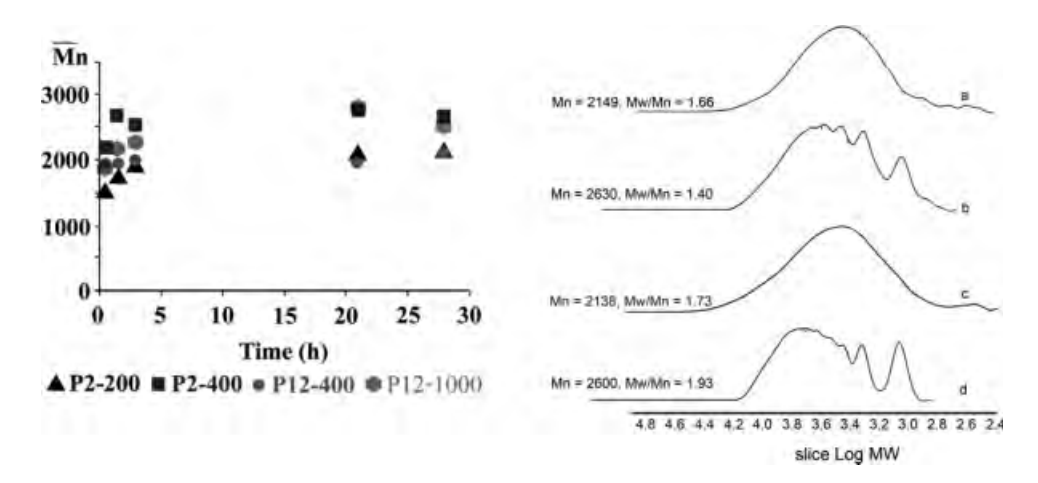
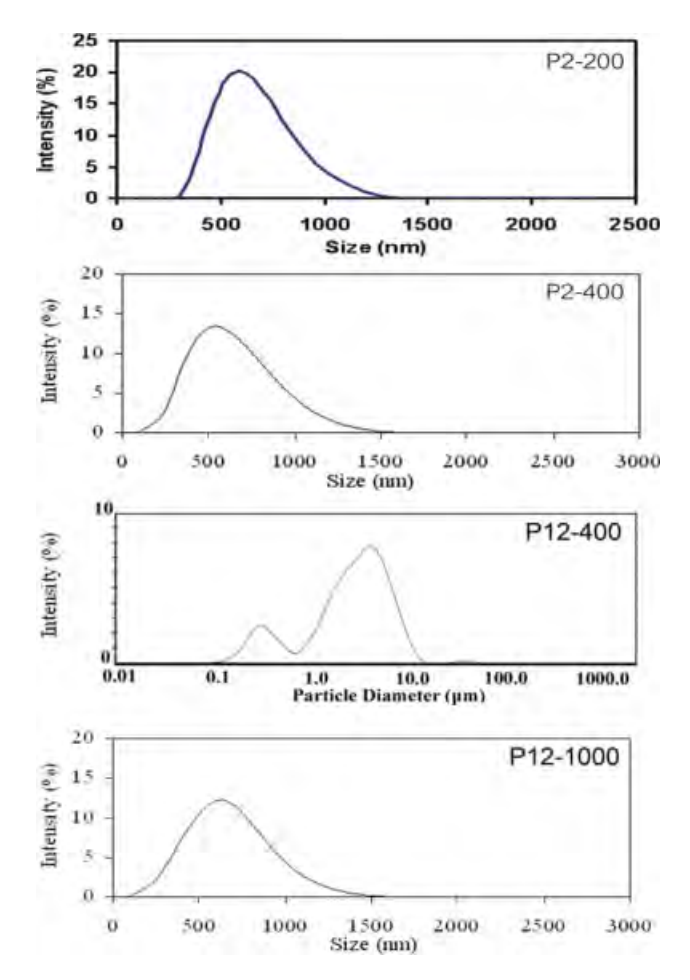


Figure 3 Molecular weight information of the synthesized oligoesters. Left: Number-average molecular weight  $(\overline{M_n})$  of oligoesters obtained at various reaction times. Right: Gel permeation chromatograms of a) P2-200, b) P2-400, c) P12-400, and d) P12-1000.

made to increase the molecular weight of the products. Instead, study was geared toward the formation of nano- and micro-spheres for application in cosmetics and pharmaceutical area.

The four synthesized oligoesters, P2-200, P2-400, P12-400, and P12-1000, could be self-assembled into submicron- / micron-size-particles by the solvent displacement technique (displacing acetone with water). The particles obtained at the concentration of 0.40% (w/v) oligoester were aqueous colloidal suspensions with mean hydrodynamic diameters of  $\sim 400$ –600 nm for **P2-200**, **P2-400**, and **P12-1000** (Fig. 4). Interestingly, P12-400 suspension showed microsize-particles ( $\sim$  3  $\mu m$ ). The SEM and TEM images indicate micelle-like-spherical architecture for all four self-assembled particulates (Fig. 5). These results agree well with the fact that all four oligomers possess hydrophilic weight fraction (f factor) of more than 40%.<sup>22</sup> Self-assembly of these oligomers in water should result in particles with hydrophobic p-alkoxycinnamate core and water soluble PEO corona. When the hydrophobic block was ethoxycinnamate or ((1,2-(bis(4-(2-carboxyvinyl)phenoxy))ethane), changing the PEO block length from  $\sim 4$  to  $\sim$  10 ethylene oxide units resulted in a slight decrease of the particle sizes (comparing P2-200 and P2-400 particles). A higher hydrophilic to hydrophobic ratio, or a longer hydrophilic block in P2-400, compared to P2-200, provides enough tethered PEO chains on the particles' surfaces to afford stability to the smaller particles. However, when the length of the hydrophobic block was increased to dodecoxycinnamate or ((1,12-(bis(4-(2-carboxyvinyl)phenoxy))dodecane), the length of PEO block was found to significantly affect the particle sizes. In the case of **P12-400**, in which the PEO block length is  $\sim 10$  ethylene oxide units, the hydrophilic to hydrophobic ratio is probably too low to provide enough of a PEO

corona for the stabilization of nano-size particles, thus the micron-size particles were observed. When the PEO block length increased to the average



**Figure 4** Size distribution profiles obtained from dynamic light scattering analysis of **P2-200**, **P2-400**, **P12-400**, and **P12-1000** particles. [Color figure can be viewed in the online issue, which is available at www.interscience. wiley.com.]

1730 CHANGHIN ET AL.

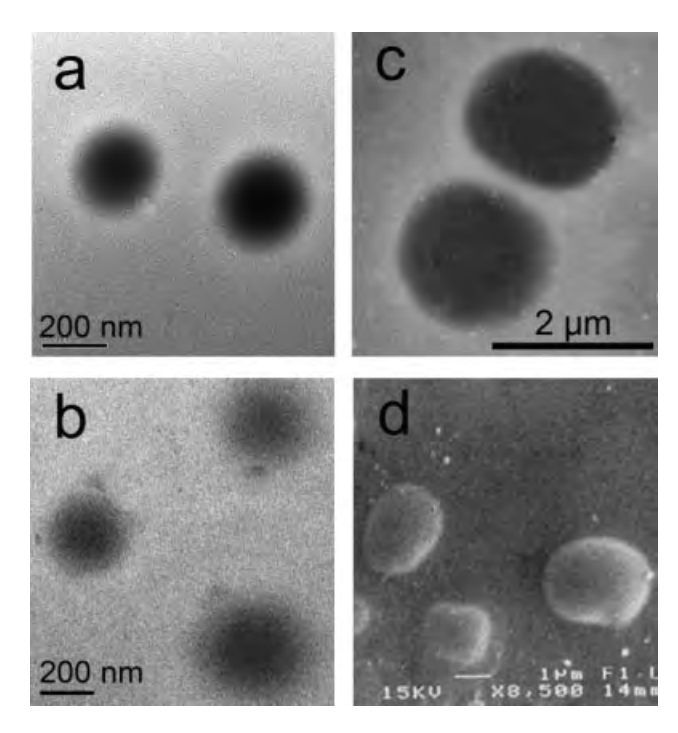


**Figure 5** TEM images of **P2-200** (a), **P2-400** (b), **P12-400** (c), and SEM image of **P12-400** (d) particles.

number of 23 ethylene oxide units in the **P12-1000**, the hydrophilic to hydrophobic ratio increased to a level, such that there were sufficient tethered PEO chains to cover the surface of the smaller size particles (500 nm) and stabilize them (model in Fig. 6).

The above explanation could be simplified using the length of the alkoxy group and the ethylene oxide unit (2 m and m' in scheme 1 and Table I) in each oligomeric structure. Higher 2 m/m' ratio in P12-400 (Table I) indicated not enough hydrophilic corona to stabilize small size particles, thus microsize particles were observed. In contrast, the smallest 2 m/m' ratio in P2-400 structure corresponded to enough PEO chains to cover surfaces of smaller par-

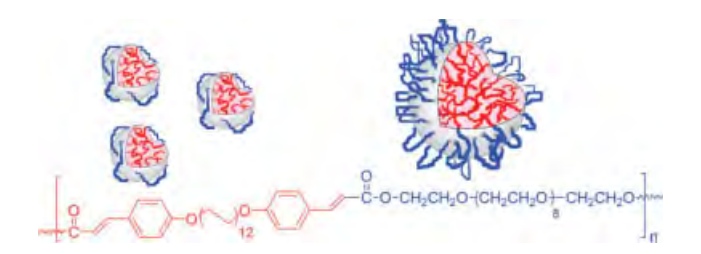


**Figure 6** Representative drawing explaining the formation of bigger spheres for **P12-400**; the unstable submicronsize particles without enough PEO on their surfaces (left) and the more stable micron-size sphere with enough PEO covering on the surface (right). The size of the spheres and the size of the oligoester chains are not in a real proportion. [Color figure can be viewed in the online issue, which is available at www.interscience.wiley.com.]

TABLE I
Particles' Size and the Ratio Between the Length of the
Alkoxy Group (2 m) and the Ethylene Oxide Unit (m') of
the Four Oligomers

	)-ot	CH <sub>2</sub> CH <sub>2</sub> O <del>) CH</del> <sub>2</sub> CH <sub>2</sub> O
Samples	2m/m′	Particle size
P2-200 P2-400 P12-400 P12-1000	0.5 0.2 1.2 0.5	$614.5 \pm 3.21$ $601.2 \pm 2.89$ $3260 \pm 29.2$ $631.1 \pm 2.90$

ticles. As a result, **P2-400** gave the smallest self-assembled spherical particles among the four oligomeric assemblies.

#### **CONCLUSIONS**

We have synthesized amphiphilic block oligoesters with various hydrophobic to hydrophilic ratios based on p-ethoxycinnamate and p-dodecoxycinnamate as the hydrophobic blocks and polyethylene oxide of various lengths as the hydrophilic block. Self-assembly of the obtained UVB absorptive oligomers into spherical structures were carried out by displacing acetone with water. The yellow-oil P2-400 and the yellow wax P2-200 and P12-1000 could self-assemble into spherical particles of submicron sizes whereas the yellow wax P12-400 could selfassemble into spherical microparticles. In addition, relationship between size of the self-assembled spheres and oligomeric structures was observed. Good water dispersibility of these UVB absorptive spheres should enable direct application in waterbase formulations, thus, these particles are potential UVB absorptive carriers for cosmetics and pharmaceutical applications.

#### References

- 1. Zhang, L. F.; Eisenberg, A. Science 1995, 268, 1728.
- 2. Yu, Y. S.; Eisenberg, A. J Am Chem Soc 1997, 119, 8383.
- 3. Cornelissen, J.; Fischer, M.; Sommerdijk, N.; Nolte, R. J. M. Science 1998, 280, 1427.
- Borsali, R.; Minatti, E.; Putaux, J. L.; Schappacher, M.; Deffieux, A.; Viville, P.; Lazzaroni, R.; Narayanan, T. Langmuir 2003, 19, 6.
- 5. Leibler, L. Macromolecules 1980, 13, 1602.
- Alexandridis, P.; Spontak, R. J. Curr Opin Colloid Interface Sci 1999, 4, 130.
- 7. Zhang, L.; Yu, K.; Eisenberg, A. Science 1995, 268, 1777.
- 8. Houga, C.; Giermanska, J.; Lecommandoux, S.; Borsali, R.; Taton, D.; Gnanou, Y.; Meins, J.-F. L. Biomacromolecules 2009,10, 32.
- 9. Rowan, S. J. Nat Mater 2009, 8, 89.
- 10. Kimura, K.; Katoh, T. Contact Derm 1995, 32, 304.

- 11. Schauder, S.; Ippen, H. Contact Derm 1997, 37, 221.
- 12. Jiang, R.; Roberts, M. S.; Collins D. M.; Benson, H. A. E. Br J Clin Pharmacol 1999, 4, 635.
- 13. Hany, J.; Nagel, R. Deutsche Lebensmittel-Rundschau 1995, 91, 341.
- 14. Yener, G.; Incegul, T.; Yener, N. Int J Pharm 2003, 258, 203.
- Calderilla-Fajardo, S. B.; Cazares-Delgadillo, J.; Villalobos-Garcia, R.; Quintanar-Guerrero, D.; Ganem-Quintanar, A. Drug Dev Ind Pharm 2006, 32, 107.
- 16. Chatelain, E.; Gabard, B.; Surber, C. Skin Pharmacol Appl Skin Physiol 2003, 16, 28.
- Mitchell, K.; Mitchnick, M. (SunSmart, Inc.). U.S. Pat. 5,587,148 (1996).
- 18. Pattanaargson, S.; Hongchinnagorn, N.; Hirunsupachot, P.; Sritana-anant, Y. Photochem Photobiol 2004, 80, 322.
- 19. Anumansirikul, N.; Wittayasuporn, M.; Klinubol, P.; Wanichwecharungruang, S. P. Nanotechnology 2008, 19, 205101.
- 20. Richard, H.; Ledue, M. (Societe L'Oreal S.A.). U.S. Pat. 6,080,880 (2000).
- Ledue, M.; Richard, H.; Lagrange, A. (Societe L'Oreal S.A.).
   U.S. Pat. 6,376,679 (2002).
- 22. Discher, D. E.; Eisenberg, A. Science 2002, 297, 967.

# สัญญาเลขที่ BRG5280004

# โครงการ: การปลดปล่อยน้ำหอมแบบควบคุม

# รายงานสรุปการเงินในรอบ 36 เดือน

ชื่อหัวหน้าโครงการวิจัยผู้รับทุน รศ.คร. ศุภศร วนิชเวชารุ่งเรื่อง รายงานในช่วงตั้งแต่ 1 มกราคม 2555 ถึงวันที่ 30 มิถุนายน 2555

รายจ่าย

หมวด	รายจ่ายสะสมจาก	ค่าใช้จ่ายในงวด	รวมรายจ่ายสะสม	งบประมาณ	คงเหลือ
(ตามสัญญา)	รายงานครั้งก่อน	ปัจจุบัน	จนถึงงวดปัจจุบัน	รวมทั้งโครงการ	(หรือเกิน)
1. ค่าตอบแทน	614,000	1	614,000	648,000	34,000
2. ค่าจ้าง	420,000	20,000	440,000	440,000	0
3. ค่าวัสคุ	362,000	1	362,000	362,000	0
4. ค่าใช้สอย	350,000	1	350,000	350,000	0
รวม	1,672,000	1	1,766,000	1,800,000	34,000

### จำนวนเงินที่ได้รับและจำนวนเงินคงเหลือ

### จำนวนเงินที่ได้รับ

งวดที่ 1	335,000	บาท	เมื่อ 29/07/09
คอกเบี้ยครั้งที่ 1	659.47	บาท	เมื่อ 19/12/09
งวคที่ 2	335,000	บาท	เมื่อ 08/04/10
คอกเบี้ยครั้งที่ 2	859.27	บาท	เมื่อ 19/06/10
งวคที่ 3	335,000	บาท	เมื่อ 17/09/10
งวดที่ 4	335,000	บาท	เมื่อ 22/09/10
คอกเบี้ยครั้งที่ 3	1,126	บาท	เมื่อ 18/12/10
งวดที่ 5	332,000	บาท	เมื่อ 14/01/11
คอกเบี้ยครั้งที่ 4	1,344	บาท	เมื่อ 18/06/11
งวดที่ 6	74,000	บาท	เมื่อ 23/09/11
คอกเบี้ยครั้งที่ 5	533.31	บาท	เมื่อ 24/12/11
คอกเบี้ยครั้งที่ 6	360.99	บาท	เมื่อ 23/06/12

รวม 1,750,883.04 บาท 🛈

### ค่าใช้จ่าย

งวดที่ 1 เป็นเงิน	335,000	บาท
งวดที่ 2 เป็นเงิน	335,000	บาท
งวดที่ 3 เป็นเงิน	670,000	บาท
งวดที่ 4 เป็นเงิน	332,000	บาท
งวดที่ 5 เป็นเงิน	74,000	บาท
งวคที่ 6 เป็นเงิน	20,000	บาท

รวม 1,766,000 บาท 2 จำนวนเงินคงเหลือ ① - 2 -15,116.96 บาท

ลงนามหัวหน้าโครงการวิจัยผู้รับทุน

ลงนามเจ้าหน้าที่การเงินโครงการ



Circulation: 200,000 Ad Rate: 720 

 Section: Digital Issue - First Section/ 

 วันที่: อังคาร 20 ธันวาคม 2554

 ปีที่: 13
 ฉบับที่: 3188

บท: 13 ฉบบท: 3188 Col.Inch: 18.43 Ad Value: 13,269.60

หัวข้อข่าว: คุมน้ำหอมติดทนนาน

**หน้า:** 28(บนซ้าย)

PRValue (x3): 39,808.80 คลิป: ขาว-ดำ

# คุมน้ำหอมติดทนนาน

กรุงเทพฯ : นักวิจัยจุฬาลง-กรณ์มหาวิทยาลัยเจ๋ง พัฒ-นาสารจากธรรมชาติคุมน้ำ หอมให้หอมได้ยาวนาน เอก-ชนรับถ่ายทอดเทคโนโลยี เพื่อนำเข้าตลาดแล้ว

รศ.ดร.ศุภศร วนิชเวชารุ่งเรื่อง จากคณะวิทยาศาสตร์
จุฬาลงกรณ์มหาวิทยาลัย โดยการ
สนับสนุนจากสำนักงานสนับสนุนการวิจัย (สกว.) ประสบ
ความสำเร็จในการพัฒนาสาร
จากธรรมชาติเพื่อใช้ห่อหุ้มน้ำ
หอมและคุมการปลดปล่อยให้
น้ำหอมคงความหอมได้ยาวนาน
เวลานี้บริษัท เวลเทค ไบโอเทคโนโลยี โปรดักส์ จำกัด โดย
น.สพ.วินัย โชติเธียรชัย ได้รับ
ถ่ายทอดเทคโนโลยีนำไปพัฒนา
ต่อยอดเป็นผลิตภัณฑ์สู่ตลาด

เอเชียต่อไป ซึ่งเมื่อเร็วๆนี้นำไป เปิดตัวในงาน In-Cosmetic Asia 2011 ณ ศูนย์แสดงสินค้าไบเทค บางนา

ผลิตภัณฑ์ดังกล่าวมีชื่อ ว่า Chitora® เป็นผลิตภัณฑ์นา โนเทคโนโลยีทำงานกักเก็บน้ำ หอมได้ด้วยกลไก 2 ระบบ ทำให้ เก็บน้ำหอมได้ทั้งกระบวนการทาง เคมีและกระบวนการทางกาย-ภาพอยู่ในรูปอนุภาคทรงกลม ขนาดเล็กระดับนาโนเมตร และ ปล่อยน้ำหอมที่กักเก็บไว้อย่าง ค่อยเป็นค่อยไปและต่อเนื่องจึง หอมได้ยาวนาน สามารถใช้กับ ผลิตภัณฑ์ได้หลายประเภท อาทิ เครื่องสำอาง อาหาร น้ำหอม ปรับอากาศ ผลิตภัณฑ์ที่ใช้ในครัว เรือน ผลิตภัณฑ์จากยางพารา ผลิตภัณฑ์สิ่งทอและเครื่องนุ่งห่ม และในอุตสาหกรรมต่างๆ

รหัสขาว: C-111220007048
iQNewsA/ert